Apport de la modélisation 3D et de la restauration structurale dans la compréhension des gisements de matières premières minérales

Pablo Eliécer Mejía Herrera

Apport de la modélisation 3D et de la restauration structurale dans la compréhension des gisements de matières premières minérales

THÈSE

présentée et soutenue publiquement le 16 Décembre de 2014
pour l'obtention du grade de

Docteur de l'Université de Lorraine

Spécialité Géosciences

par

Pablo-Eliécer Mejía-Herrera

Composition du jury :

Rapporteurs :	Helmut SCHAEBEN Mark JESSELL
Examinateurs :	Laurent AILLERES Jürgen HARTSCH Anne-Sylvie ANDRE-MAYER
Directeur de thèse :	Jean-Jacques ROYER

UMR 7359 - GeoRessources
Université de Lorraine - CNRS - CREGU
ENSG - Campus Brabois - TSA 70605
54518 Vandœuvre-lès-Nancy cedex - FRANCE

« Je donnerais tout ce que je sais pour la moitié de ce que j'ignore »
(*Daría todo lo que sé, por la mitad de lo que ignoro*)
René Descartes

Remerciements

Il s'avère que l'écriture des remerciements d'une thèse est une épreuve bien difficile, car d'une certaine manière il y a le risque d'oublier un grand nombre de personnes que je me dois de remercier et de ce fait, d'être injuste. Une thèse est une expérience très intense pour la personne qui l'a vécu, et pendant sa durée, un certains nombres de personnes y ont collaboré, de différentes manières et dans des moments distincts. Il devrait exister plusieurs sortes de remerciements : par exemple, un dédié à ceux qui m'ont aidé à trouver la bonne réponse à une question clé, ou lorsque leurs avis m'ont permis d'avancer dans un moment critique. Mais il devrait aussi exister un genre de remerciement pour ceux qui, grâce à leurs sourires ou leurs attentions chaleureuses envers moi, m'ont aidé à surmonter les moments difficiles, et qui de cette manière là, ont donc contribué à atteindre mon objectif d'obtenir le doctorat. Cependant, je pense avoir été chanceux, car à Nancy les personnes qui m'ont entouré, m'ont donné les deux c'est à dire des réponses et des sourires en même temps. C'est ainsi que ces mots sont dirigés envers ceux qui m'ont donné beaucoup plus de ce qu'ils ne peuvent l'imaginer, et pour cela je leur en serais toujours reconnaissant.

Je tiens d'abord à remercier à Jean-Jacques Royer de m'avoir partagé aussi bien sa sagesse que sa connaissance, et surtout d'avoir cru en moi en me donnant l'occasion de vivre cette aventure appelée thèse de doctorat. Merci à Guillaume Caumon, qui a également partagé avec moi ses connaissances, son amitié et aussi de m'avoir inspiré d'innombrables fois au cours de mon temps à Nancy. Merci à Pauline Collon de qui j'ai appris l'esprit critique et qui m'a donné le courage de poser des questions, car *l'entendement de quelque chose commence toujours par une question.* A Paul Cupillard par les discussions que nous avons échangé, même si elles portaient aussi bien sur les sciences, que sur le cinéma, la musique ou tout simplement sur la vie. Merci à Pierre Jacquemin et à Christophe Antoine pour leur immense coopération et patience avec moi. À cet égard, je tiens à remercier tout particulièrement Fatima Chtioui pour son soutien à chaque moment et circonstance. A Philippe Marion, Lev Philoppov et Alain Cheilletz, d'excellents professeurs et enseignants qui m'ont donné des leçons concernant ma vie professionnelle.

Je ressens énormément de gratitude pour mes amis et collègues de ma thèse : Gautier Laurent, François Bonneau, Jeanne Pellerin et Théophile Gentilhomme, qui ont été les premiers dans le groupe a m'accueillir chaleureusement, de qui je garde les meilleurs souvenirs pour tout ce que nous avons vécu, de m'avoir rendu heureux, et de m'avoir tant appris. À Charline Julio et à Jeremy Ruiu, mes camarades avec lesquels j'ai commencé l'odyssée de ma thèse et qui ont toujours été là pour me soutenir. À Arnaud Botella et Guillaume Rongier, pour qui j'éprouve une grande amitié mais aussi pour qui j'ai une grande admiration. À Christine Fay-Varnier, Marianne Conin, Benjamin Chauvin, Andrea Borghi et Anton Kusenko de m'avoir aidé à résoudre de nombreuses questions, mais aussi pour les discussions enrichissante que nous avons eu. À Marion Parquer, Gabriel Godefroy et Antoine Mazuyer avec qui j'ai eu la chance de partager la dernière année de ma thèse tout en passant d'agréables moments. Je dois remercier très vivement, mon ami, Jonathan Edwards pour tous les bons moments que nous avons vécus. Et enfin je tiens à remercier très fortement ma copine Aude pour sa patience, son soutien et pour m'avoir aimé sans conditions durant une période si difficile de ma vie.

Je tiens à remercier aux membres du jury de ma thèse : Helmut Schaeben, Mark Jessell, Laurent

Ailleres, Jürgen Hartsch Et Anne-Sylvie Andre-Mayer, pour leurs commentaires, leurs remarques et d'avoir apprécié et validé mon travail.

Je remercie ma famille, et particulièrement ma maman, qui en plus de m'avoir mis au monde, m'a par son courage et par sa volonté, donné l'envie de me dépasser et de toujours donner le meilleur de moi-même. Je remercie mes frères d'être toujours là pour moi, malgré la distance nous séparant. Et je remercie également mon papa, qui malgré son absence de ce monde, sera toujours là avec moi.

Merci aussi à tous ceux qui ont partagé avec moi quelque moment de leur vie mais qui ne sont pas mentionnés ici, par oubli, par manque de place, mais à qui je dois beaucoup.

Résumé

L'objectif de cette thèse est d'expliquer les avantages qu'offrent la reconstruction de l'architecture des unités géologiques, leurs déformations ainsi que leurs variations au cours du temps à l'exploration de ressources minérales, tout en appliquant des méthodes et outils de modélisation 3D et 4D. La modélisation et la restauration structurale sont utilisées ici pour estimer des attributs géologiques qui peuvent aider à la compréhension de la formation des gisements, et à l'identification des zones favorables aux minéralisations.

Cette thèse est axée sur l'application de la modélisation 3D et 4D à des cas réels pour trouver le lien entre une minéralisation et des processus géologiques tel que l'exhumation des terrains, l'activité des failles et la fracturation résultant d'un évènement de déformation. Ce mémoire est organisé en trois parties :

- la modélisation structurale ainsi que la restauration surfacique ont été appliquées au district minier de la Ceinture de Cuivre de Legnica-Głogów (sud-ouest de la Pologne), pour estimer les conditions favorables à la fracturation hydraulique. Cette fracturation est intervenue dans le nord de l'Europe lors d'une phase d'inversion à la fin du Crétacé et au début du Paléocène. Dans notre hypothèse de départ, la fracturation hydraulique développée au cours de cette période a joué un rôle important dans la distribution en cuivre observée aujourd'hui dans le district minier ;

- la courbure des surfaces triangulées, représentant les horizons stratigraphiques qui se trouvent dans la région des Sudètes polonaises, permet de mettre en évidence les systèmes de failles dans le socle. En particulier, des méthodes de restauration surfaciques ont été utilisées pour évaluer l'activité de des failles au cours du temps, en se basant sur la courbure des surfaces obtenues à chaque étape de la restauration. Les zones de fortes activités sont ici associées aux processus de minéralisation cuprifère de la région ;

- la restauration mécanique de la région de Mount Pleasant (Australie occidentale), a permis de simuler un évènement de raccourcissement apparu dans l'Archéen et qui est lié à un processus de minéralisation aurifère. La restauration mécanique est appliquée pour estimer le champ des déformations de la région au moment du raccourcissement. Avec ce champ de déformation, il est possible de calculer les paramètres d'endommagement de la masse rocheuse qui semblent liés aux zones aurifères situées hors des systèmes principaux de failles.

Cette thèse a ainsi permis de mettre en évidence l'aspect prometteur de la modélisation et de la restauration structurale pour identifier des zones potentiellement minéralisées, mettant en valeur leur utilisation pour pour l'exploration des gisements et des ressources minérales.

Table des matières

Remerciements iii

Résumé v

Introduction 1

1 Relations spatio-temporelles des gisements 9
1.1 Processus géologiques liés à la formation de gisements . . . 10
1.2 Relations spatio-temporelles . . . 11
1.2.1 Relations spatiales . . . 11
1.2.2 Relations temporelles . . . 12
1.3 Modélisation spatio-temporelle . . . 13
1.3.1 Échelle de la modélisation . . . 13
Intervalle d'échelle continentale . . . 15
Intervalle d'échelle régionale-locale . . . 15
1.3.2 Différentes approches dans la modélisation de gisements . . . 16
1.3.3 Avantages de la modélisation spatio-temporelle . . . 16
1.4 Méthodes et stratégies . . . 18

2 Late Cretaceous–Early Paleocene uplift and inversion in northern Europe: implications for the Kupferschiefer-ore in the Legnica-Głogów Copper Belt, Poland 21
2.1 Introduction . . . 22
2.2 Geologic setting and Mineralization . . . 24
2.2.1 Main aspects . . . 24
2.2.2 Sulfide mineralization . . . 26
2.3 Surface model and restoration of the LGCB . . . 26
2.3.1 3D model . . . 26
2.3.2 Surface-restoration . . . 26
2.3.3 Decompaction . . . 28
2.3.4 Simulating the pre-uplifting Upper Cretaceous conditions . . . 30
2.4 Hydro-fracturing and Mineralization . . . 33
2.5 Hydro-fracturing and Cu content . . . 34
2.6 Discussion . . . 36
2.7 Conclusions . . . 37

3 Curvature Attribute from Surface-Restoration as Predictor Variable in Kupferschiefer Copper Potentials: An Example from the Fore-Sudetic Region 41
3.1 Introduction . . . 42
3.2 General geology . . . 43
3.2.1 Geologic settings of the FSM . . . 43
3.2.2 Mineralization . . . 44
3.3 Modeling the Fore-Sudetic Monocline . . . 44

3.3.1 Modeling Outlines . . . 44
3.3.2 Outcome FSM 3D Model . . . 45
3.4 Detecting Fault Activity from Restoration . . . 45
3.4.1 Restoration Goals . . . 45
3.4.2 Surface Restoration . . . 45
3.4.3 Iterative Restoration . . . 47
3.4.4 Internal Deformation and Fault Activity . . . 49
3.4.5 Continuous-Surface Representation . . . 49
3.4.6 Restored Models . . . 49
3.4.7 Restoration Outputs . . . 51
3.5 Curvature and Cu Assessments . . . 53
3.5.1 Potentials Assessments and Predictors Variables . . . 53
3.5.2 Cu Potentials and Selected Predictors . . . 53
3.5.3 LR Models by Predictor . . . 54
3.5.4 Predictive Model and Conditional Independence . . . 54
3.6 Perspectives . . . 54
3.7 Discussion . . . 58
3.8 Conclusions . . . 58

4 Using strain parameters from 3D restoration to estimate distant off-fault gold potentials, Mount Pleasant Area, Western Australia 61
4.1 Introduction . . . 62
4.2 Evolution of Rocks Properties . . . 62
4.3 Mount Pleasant Gold System . . . 64
4.3.1 Geological Settings . . . 64
4.3.2 Mineralization . . . 65
4.4 3D Mechanical Restoration . . . 65
4.4.1 Mount Pleasant Region Modeling . . . 65
4.4.2 3D Geomechanical Restoration . . . 65
4.5 Gold Occurrences and Distant Off-fault Damage . . . 69
4.6 Discussion . . . 69

Conclusion générale 75

Annexes 93

Introduction

Que ce soit avec un approche scientifique ou économique, les modélisations 3D et 4D sont utilisées en tant qu'outils pour mieux comprendre les ressources minérales. Plusieurs logiciels sont disponibles pour le traitement de l'ensemble des données acquises au cours d'études géologiques, environnementales, d'exploration et d'exploitation des gisements ou des hydrocarbures. Le but de ces logiciels, tels que les *SIG 3D* et les *géomodeleurs* [Apel, 2006, Mallet, 2002], est de fournir un ensemble d'applications nécessaires pour représenter le sous-sol à partir d'informations directes ou indirectes. Les modèles 3D servent à : représenter la géologie structurale, évaluer et estimer les réserves, planifier les opérations minières, interpréter des données géophysiques, analyser des données géochimiques, évaluer les risques géotechniques et géotectoniques, entre autres.

Divers logiciels ont été créés spécifiquement pour la modélisation 3D, et pour résoudre des tâches complémentaires souvent utilisées dans les géosciences. Quelques exemples sont : *Geomodeler, Leapfrog, Micromine, Vulcan, Surfer, Surpac, Pétrel, Move* et *Gocad-Skua*. Bien que les géomodeleurs servent à un but commun, ils différent par les concepts mathématiques de base qu'ils utilisent et par leurs codes informatiques. En revanche, les notions et les concepts de géomodélisation, ainsi que leur application aux cas réels, ne dépendent pas du géomodeleur utilisé. Malgré certains aspects déterminés par le logiciel et sa technologie, la *géomodélisation* est un ensemble de connaissances, de méthodes et de techniques utilisées pour représenter un domaine géologique de façon simple et réaliste [Caumon et al., 2009, Jessell, 2001].

Modélisation 3D

Du point de vue numérique, la géomodélisation est un terme apparu dans les années 90 pour désigner les techniques informatiques utilisées dans la construction de modèles 3D dans le domaine des géosciences [Mallet, 2002]. Les concepts primordiaux compris dans la modélisation 3D correspondent à *les éléments géométriques* de base, *la topologie*, la notion de *propriétés* et la notion de *région*. Ces concepts sont présentés ci-dessous :

Éléments géométriques : Les éléments géométriques correspondent aux objets simples utilisés dans la géomodélisation. Ils sont :
- *Des nœuds* : des emplacements définis par des coordonnées (x, y, z).
- *Des courbes* : de points reliés par des segments. Ils peuvent contenir plusieurs composants.
- *Des triangles* : formés à partir de trois points reliés entre eux. Un ensemble de triangles adjacents forme une surface triangulée qui peut avoir aussi plusieurs composantes.
- *Des tétraèdres* : formés à partir de quatre points reliés entre eux qui délimitent un volume élémentaire appelé tétraèdre. Un ensemble de tétraèdres forme un maillage non structuré délimitant un volume.
- *Des prismes* rectangulaires (ou voxels) : un cube peut être déformés de façon à former une cellule élémentaire hexaédrique. Lorsque les cellules sont toutes identiques (mêmes dimen-

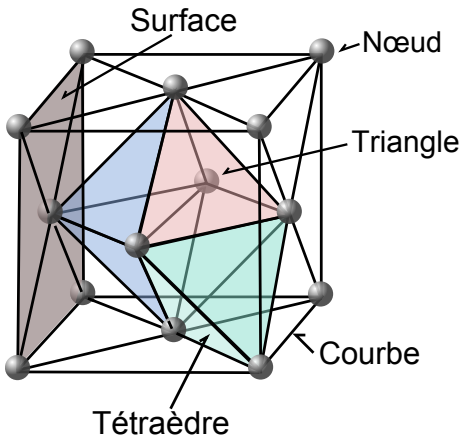

FIGURE 1 – Quelques éléments géométriques de base utilisés dans la modélisation 3D.

sions) et adjacentes ils peuvent délimiter un maillage cartésien régulier. Les prismes peuvent également être déformés pour s'adapter aux formations stratigraphiques plissées.
- *Des cellules polyédriques* : cellules irrégulières dont la juxtaposition forme des maillages non structurés.

La topologie : La topologie concerne les connexions, les interactions et la configuration relative entre les composants d'un modèle. Elle se réfère à des propriétés qui sont préservées sous des transformations continues (y compris l'étirement et la flexion mais pas le déchirement) [Kinsey, 1993]. Par exemple, en simulant un épisode tectonique avec un modèle structural surfacique, la topologie reste constante si le nombre de failles et leur connectivité reste le également.

Les propriétés : La géomodélisation doit traiter des attributs qualitatifs (types de roches, types d'altération, type de faciès,...) et des attributs quantitatifs (la teneur en métaux, la profondeur, l'épaisseur, la courbure...). Ces attributs sont représentés en tant que propriétés dans les géomodèles. Dans les modèles discrétisés (modèles mailles dans la fig. 2), les propriétés sont stockés sur les nœuds ou au centre des cellules.

Les régions : En géosciences, il est important d'être en mesure de manipuler les domaines et sous-domaines d'un modèle. Les régions correspondant à ces domaines et sous-domaines sont souvent formalisées par un indicateur, par lequel un point ou une cellule appartient à une région si la valeur de l'indicateur est égale à **1**, est à l'extérieur de la région si l'indicateur est égale à **0**. Les régions peuvent être définies en fonction de critères liés à la géométrie de l'objet (e.x. la courbure d'une surface triangulée), à l'aide d'une propriété assignée (p. ex. la teneur d'un élément dans un nuage de points), ou en utilisant un indicateur (p. ex. les faciès présents dans une séquence sédimentaire).

Approches utilisés dans la création de géomodèles

Deux différentes approches sont couramment utilisés pour représenter les entités géologiques du sous-sol : la représentation *surfacique* et la représentation *volumique* [Caumon, 2010]. Dans le premier cas, sont générés les interfaces géologiques contenues dans le sous-sol, tandis que dans le second sont crées les volumes et sous-volumes qui représentent les entités géologiques volumiques. Une façon de représenter les interfaces géologiques dans l'approche surfacique consiste à utiliser des polygones avec de nœuds reliés, dans le but de former de *surfaces polygonales*. Un exemple typique d'une surface polygonale est une surface triangulée (fig. 2a), où le triangle est l'élément de base pour créer la surface [Mallet, 2002]. Une autre méthode

appliquée dans l'approche surfacique consiste à représenter les interfaces géologiques en utilisant des fonctions rationnelles ou polynomiales pour décrire la géométrie de la surface avec des coordonnées paramétriques (u,v) (*surfaces paramétriques*) (fig. 2b). Les surfaces créées à partir de *NURBS*, par exemple, appartiennent à ce genre de surfaces paramétriques [Les and Wayne, 1997].

Dans l'approche volumique, l'espace 3D est représenté soit avec une grille soit par les surfaces marquant les frontières du modèle. Dans ce premier cas, quelques exemples de grilles sont :
- *grille cartésienne* : Cellules prismatiques régulières sans prise en compte de la géométrie des interfaces géologiques (fig. 2c) ;
- *grille stratigraphique* : Cellules prismatiques adaptées aux géométries des interfaces géologiques (fig. 2d) ;
- *grille tétraédrique* : Cellules formées avec des tétraèdres capables de s'adapter facilement aux interfaces géologiques en modifiant leur forme et taille (fig. 2f).

Dans la représentation par frontières, les surfaces qui représentent les interfaces géologiques, en addition aux surfaces limitant le modèle, enveloppent les sous-domaines de l'espace 3D (fig. 2g).

Modélisation 4D

Un certain nombre de significations peuvent être donnés au terme *modélisation 4D*. Dans cette thèse, la modélisation 4D fait référence à la restauration structurale d'un modèle 3D. La modélisation géologique 4D est un outil développé dans le domaine de la géologie structurale, principalement pour l'exploration d'hydrocarbures. Les résultats de modèles 4D sont utilisés pour déchiffrer l'évolution structurale d'une région et mieux prévoir la localisation des roches mères, les chemins de migration du gaz et de l'huile et la localisation ainsi que la configuration des roches réservoirs.

Les techniques de restauration géométrique ou géomécanique permettent l'intégration du temps dans les analyses numériques structurales pour obtenir des modèles avec une cohérence géométrique et cinématique. Ces modèles aident à comprendre les différentes relations entre les processus tectoniques et sédimentaires et à prévoir l'évolution d'un bassin prenant en compte les paléo- structures [Massot, 2002, Durand-Riard, 2010]. Malgré le nombre de cas où la restauration structurale numérique a été appliquée à l'exploration d'hydrocarbures, ces outils sont moins bien connus dans le cas des ressources minérales, plus particulièrement dans les gisements métalliques.

Vue d'ensemble de la restauration structurale

Les roches situées dans la croûte terrestre sont déformées à travers le temps géologique par différents évènements tectoniques, qui se superposent sur les empreintes lithologiques et sédimentaires. Le volume ou la forme des unités lithologiques changent sous l'effet de contraintes selon la nature des roches et leurs propriétés géomécaniques. Les évènements tectoniques sont ainsi indirectement enregistrés dans la configuration actuelle des unités lithologiques. Autrement dit, l'histoire tectonique d'une région est observable dans les roches déformées. Sur ce principe, la reconstitution de la géométrie initiale des roches est possible en se basant sur les déformations observées aujourd'hui (fig. 3). Une telle reconstitution est une opération appelée restauration structurale. La restauration peut être utilisée pour : valider un modèle géologique, réduire les incertitudes dans les zones des structures complexes, estimer les déformations, les

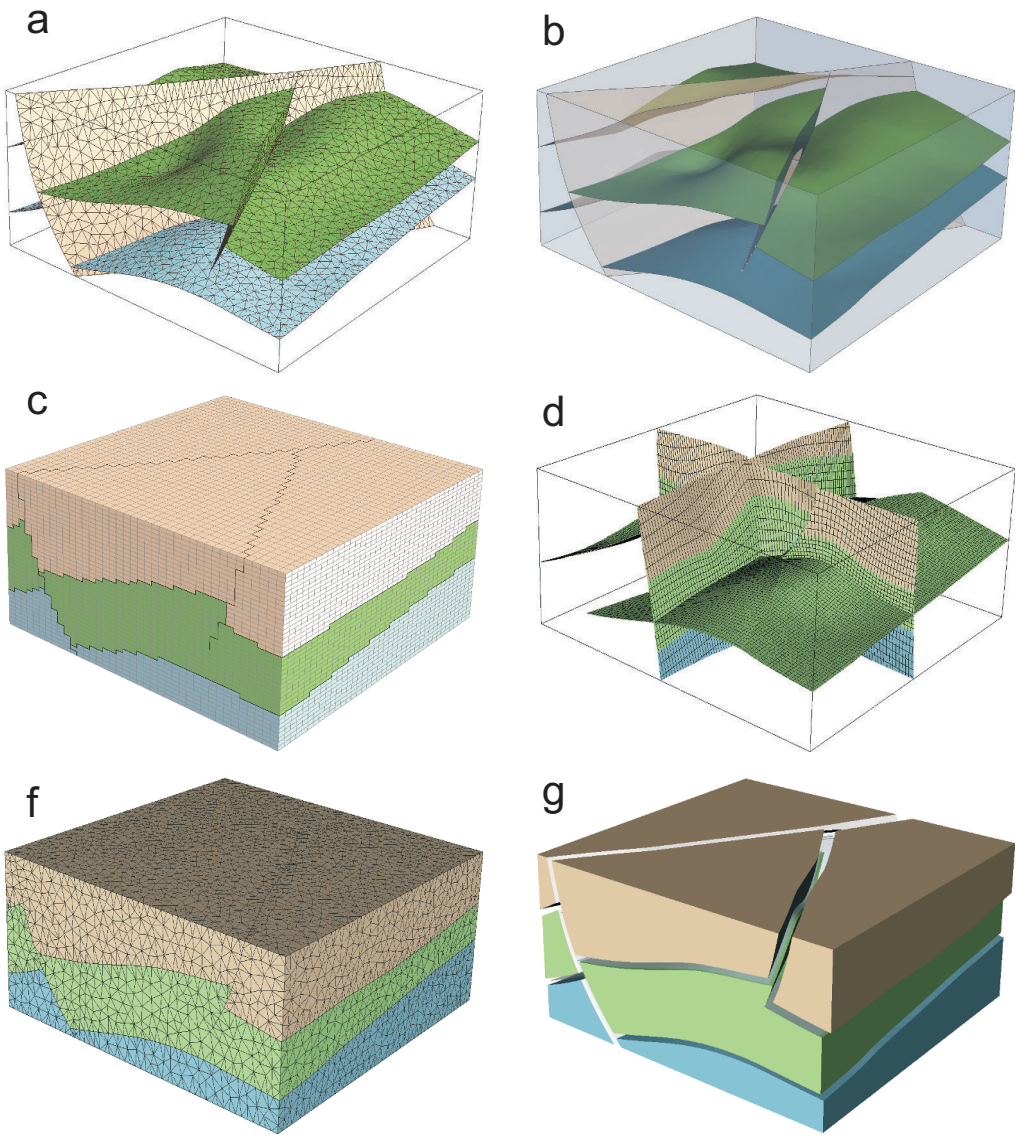

FIGURE 2 – Six différents types de représentations appliquées dans la modélisation 3D. a. et b. : Modèles créés avec un approche *surfacique*. c. à f. : Modèles créés avec une approche *volumique* en utilisant une grille. f. Modèle avec une représentation par frontières.

contraintes et leurs directions, prédire les zones de fracturation, déduire la paléo-géométries et également pour tester la cohérence des données [Groshong, 2006, Moretti, 2008, Durand-Riard et al., 2013].

La restauration ne se limite pas à la géométrie des structures géologiques, mais comprend également la cohérence entre les contraintes et le temps au cours duquel se produisent les déformations. La restauration des structures en tant qu'outil de modélisation 3D est disponible dans plusieurs logiciels commerciaux (p. ex. *Move, Igeoss, Kine3D dans Gocad-Skua,* ...). Ces logiciels de restauration fonctionnent en 1D (courbes), 2D (coupes verticales), 2.5 (modèles surfaciques) et en 3D (modèles volumiques). La plupart d'entre eux se basent sur des considérations géométriques en supposant différents contextes tectoniques, mais aussi sur des considérations géomécaniques pour le cas de la restauration 3D.

Un modèle restaurable est un modèle capable d'être déplié et déformé jusqu'à sa géométrie initiale de pré-déformation. Un tel modèle est topologiquement et géométriquement consistant. Une structure non restaurable est topologiquement impossible et, pourtant, géologiquement improbable [Dahlstrom, 1969]. Les premiers travaux sur la restauration structurale ont été publiés par Chamberlin [1910], qui a été un pionnier dans la restauration des sections géologiques en utilisant le principe de la conservation de la surface. Plus tard, ce concept a été étendu à la conservation des volumes constants par Dahlstrom [1969]. Avec les avancées informatiques dans le domaine de la géomécanique, il est aujourd'hui possible d'intégrer les propriétés des roches dans la modélisation structurale [Frantz, 2010]. Cette dernière permet d'avancer dans la compréhension de phénomènes tels que la fracturation dans la masse rocheuse, phénomène clé pour les systèmes minéralisés.

Démarche appliquée dans cette thèse

La démarche repose sur la construction de modèles structuraux 3D régionaux comprenant le gisement à étudier. Pendant leurs constructions ont été intégrés l'évolution géodynamique de la région ainsi que les principaux évènements tectoniques. De la même façon, ont été considérés : le changement des conditions physico-chimiques (altération de la roche, maturité de la matière organique, changements de phases, etc.), des facteurs physiques (variation de pression et température) et la déformation (inélastique ou élastique). Le but a été d'introduire dans le modèle tous les phénomènes et processus géologiques observés ou supposés dans la la région, même s'ils ne sont pas liés d'une façon évidente à la minéralisation étudiée. Les méthodes de restauration sont ensuite appliquées sur le modèle 3D pour obtenir une représentation de la configuration géologique dans un état passé. Des évidences géologiques expliquant la minéralisation sont ainsi obtenues. Ces évidences sont ensuite utilisées dans l'estimation de zones mineralisées potentiels dans la région étudiée.

Publications associées à cette thèse

La liste suivante des publications ont été présentées dans le cadre de cette thèse mais ne sont pas inclus dans les chapitres (voir Annexe) :

P. Mejia-Herrera, C. Le Breton, and A. Botella. Solving non-linear PDEs on Gocad models using *escript*. In *Proc. 34th Gocad Meeting*, p. 1–6, 2014.

M. Le Mesnil, P. Collon-Drouaillet, L. Dewaide, P. Mejia-Herrera, G. Rongier, and V. Hallet. Karst conduit generation: the Furfooz area case study (Belgium). In *Proc. 34th Gocad Meeting,*

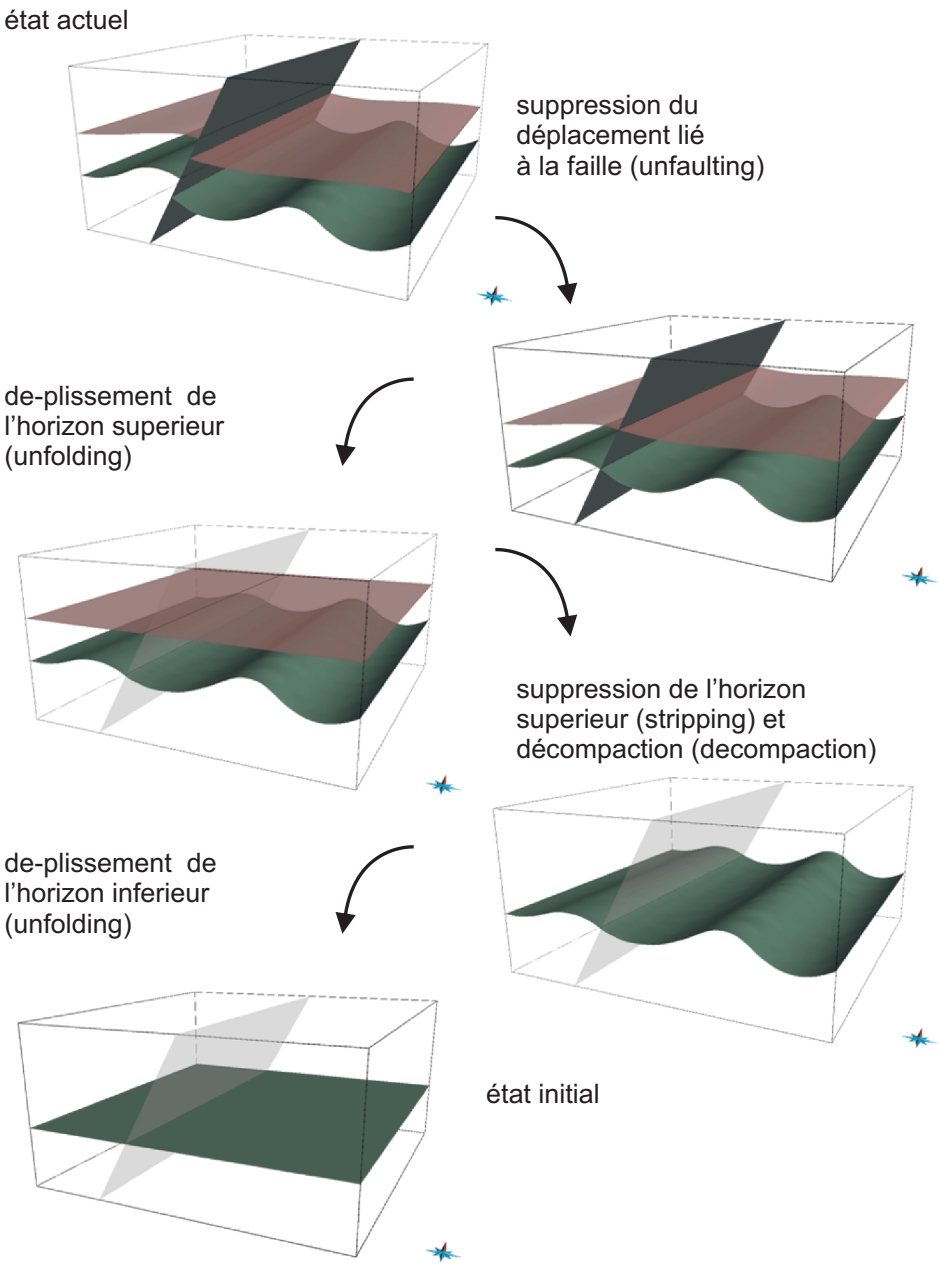

FIGURE 3 – Application de la restauration structurale d'un modèle surfacique dans un cas hypothétique. Le modèle a été restauré en utilisant la méthode de *flexural slip* avec Kine3D-2.

Nancy, France, p. 1–19, 2014.

P. Mejia-Herrera and J.-J. Royer. Cu potentials in the Fore-Sudetic Monocline using 4D modeling data. In *Proc. 33rd Gocad Meeting*, p. 1–12, 2013.

J. Pellerin, G. Caumon, C. Julio, P. Mejia-Herrera, and A. Botella. Elements for measuring the complexity of 3D structural models : topology and geometry. In *Proc. 33rd Gocad Meeting*, 2013.

P. Mejia-Herrera, J.-J. Royer, J. Hartsch, and P. Hielscher. Enhancing copper predictions at the base of Zechstein with 4D modelling. In *Proc. of the 12th SGA Biennial Meeting*, 2013.

J.-J. Royer, P. Mejia-Herrera, G. Caumon, and P. Collon-Drouaillet. 3 & 4D geomodeling applied to mineral exploration. In *Proc. of the 12th SGA Biennial Meeting*, 2013.

Chapitre 1

Relations spatio-temporelles des gisements

Sommaire

1.1 Processus géologiques liés à la formation de gisements 10
1.2 Relations spatio-temporelles 11
1.2.1 Relations spatiales 11
1.2.2 Relations temporelles 12
1.3 Modélisation spatio-temporelle 13
1.3.1 Échelle de la modélisation 13
Intervalle d'échelle continentale 15
Intervalle d'échelle régionale-locale 15
1.3.2 Différentes approches dans la modélisation de gisements 16
1.3.3 Avantages de la modélisation spatio-temporelle 16
1.4 Méthodes et stratégies 18

Cette thèse se focalise sur la modélisation structurale des ressources minérales non énergétiques (sauf pour le cas de l'uranium ou similaires), en essayant de coupler les approches scientifiques et économiques liées à la notion de gisement et de gîte minéral. Du point de vue scientifique, les modélisations 3D et 4D de gisements complètent les outils qui servent à expliquer leur distribution, leur genèse et leurs caractéristiques. Du point du vue économique, elle sert à estimer leur potentiel et les besoins techniques pour leur exploitation. Les matériaux de carrières ne sont pas considérés ici du fait de leur identification directe liée à des entités des roches sédimentaires, métamorphiques ou ignées, sans la présence explicite d'un phénomène de concentration particulière.

Dans ce chapitre sont introduits les concepts de base de la modélisation des gisements, qui permettront de comprendre ses objectifs, ses méthodes, la portée de ses résultats mais aussi ses limites. Dans une première réflexion seront expliqués les différents processus géologiques liés à la formation des gisements (section 1.1). Ensuite, nous décrirons les relations spatio-temporelles liées à la formation, la position et la distribution des gîtes minéraux (section 1.2). Postérieurement seront énumérés les éléments à prendre en compte au moment de réaliser la modélisation (section 1.3). Pour conclure, nous discuterons des stratégies de modélisation selon le gîte minéral, basées sur les outils techniques et informatiques disponibles aujourd'hui (section 1.4).

1.1 Processus géologiques liés à la formation de gisements

Des termes tels que *minéralisation*, *gîte minéral* et *gisement* sont couramment utilisés en géologie économique. Ils indiquent la présence d'une substance, ou d'un ensemble de substances, naturellement déposée avec une concentration plus élevée que dans la croûte terrestre. Bien que ces termes soient généraux et parfois même vagues, ils sont différenciés par des facteurs économiques intrinsèques plutôt que par les phénomènes qui les ont créés. Sans entrer dans le détail de leur équivalence dans différentes langues (notamment l'anglais ou l'espagnol), ou leur signification dans les différents codes miniers disponibles dans le monde (p.ex. JORC [2012]), nous pouvons dire qu'une minéralisation correspond globalement à une substance naturelle inorganique avec une concentration *in-situ* élevée. Un gîte minéral correspond à une minéralisation susceptible d'être exploitée à des fins économiques ou stratégiques, tandis qu'un gisement est un gîte où les conditions de son exploitation sont données [Jébrak and Marcoux, 2008]. Tout au long de ce mémoire, nous allons utiliser ces termes de façon interchangeable comme indication d'une concentration naturelle supérieure à la moyenne d'une substance donnée, sauf dans les cas où l'application d'une définition rigoureuse est nécessaire.

Les processus géologiques qui créent les gisements ne sont pas différents de ceux impliqués dans la formation des roches. Cependant, la formation d'un gisement est un évènement exceptionnel dans lequel se sont présentées des conditions bien particulières. Trois facteurs sont essentiels dans leur formation : (*i*) la source de la substance, (*ii*) les moyens et les conditions de transport et (*iii*) les mécanismes de dépôt et de concentration. Bien que le rôle et l'importance de chacun de ces facteurs soient inhérents d'un gisement à l'autre, plusieurs similitudes se trouvent entre les dépôts d'un même type ou d'une même classification. Un exemple de cette similitude se trouve dans la morphologie des gisements hydrothermaux, qui est normalement définie par les chemins qu'ont suivi les fluides minéralisateurs. Ainsi la source, le transport et le dépôt font partie d'un système encadré par les paramètres physiques et chimiques donnés dans l'environnement géotectonique au moment de la minéralisation.

De façon générale, un gîte ne se forme pas en même temps que la roche qui le contient. Initialement, les éléments qui forment la minéralisation se trouvent dispersés dans les roches de la croûte ou dans le manteau. En revanche, certains phénomènes de minéralisation sont différents. Dans de rares cas, le gîte se forme dans une des diverses étapes qui se succèdent lors de la création de la roche encaissante. C'est ainsi le cas de quelques gisements magmatiques exceptionnels d'Uranium. À cause de sa très forte incompatibilité, l'uranium est préférentiellement fractionné dans des silicates fondus lors de la fusion partielle et de la cristallisation fractionnée au moment de la formation d'un granite (ou syénite) peralcalin [Cuney, 2014]. Malgré l'existence de ces exemples pour l'Uranium, ou pour n'importe quel autre type d'élément ou composant, la source des éléments et l'endroit où la concentration finale a lieu sont le plus souvent éloignés.

Le mécanisme de transport fait partie des conditions essentielles dans la formation d'un gîte, car il contrôle la migration des éléments de la minéralisation depuis leur position initiale jusqu'à l'endroit où le gîte est finalement formé. Bien que les mécanismes de transport des éléments depuis la source soient particuliers pour chaque type de gisements, il est possible de citer quelques conditions communes : (*i*) la présence d'une phase fluide ; (*ii*) l'addition d'énergie dans le système pour démarrer et soutenir le mécanisme de transport ; et (*iii*) l'existence de conduits ou chemins depuis la source jusqu'au dépôt [McQueen, 2005]. Les structures telles que les failles, les fractures, les strates perméables, les interfaces entre les roches, etc., font partie des entités impliquées dans la genèse de gisements en tant qu'éléments régulateurs de ce processus de transport.

Si les conditions chimiques sont appropriées, le dépôt et la concentration qui donnent lieu à la minéralisation se produisent lorsque l'énergie existante pendant le transport est diminuée ou devient insuffisante pour continuer à mobiliser les éléments nécessaires dans la création d'un gîte. Le même phénomène peut avoir lieu lors qu'il y a une variation dans l'état du système de transport, donné pour des conditions externes ou internes dans ce système, et que ce changement est favorable pour provoquer la précipitation ou le dépôt de la substance cible [Guilbert and Park Jr, 2007, Jébrak and Marcoux, 2008].

le magmatisme, le métamorphisme, la sédimentation, la météorisation et l'érosion sont les processus majeurs responsables de la génération de gisements [McQueen, 2005]. Pour chaque grand groupe de processus il existe plusieurs types de minéralisation particuliers. Cependant, ces processus sont aussi des processus modificateurs d'un gisement de la même façon que pour les roches. Ainsi, certains dépôts sont le résultat de plusieurs processus qui se chevauchent. Une première approche dans la compréhension de la genèse et de la distribution d'un gisement consiste à identifier les processus qui ont permis sa création et sa modification ultérieure. Par ailleurs, bien que cette identification soit une tâche facile pour des gisements récents, cette tâche est beaucoup plus complexe pour des terrains anciens . Dans ce cas, il est nécessaire de comprendre la nature des relations spatio-temporelles entre la minéralisation, les roches encaissantes et le contexte géodynamique dans lequel le gisement se trouve.

1.2 Relations spatio-temporelles

Dans cette section, nous présentons de façon générale les principales relations spatiales et temporelles entre gîtes minéraux, leurs encaissants, la proximité de la surface et les structures qui jouent un rôle dans le processus de minéralisation.

1.2.1 Relations spatiales

Il existe différentes relations spatiales associées aux minéralisations. La relation spatiale la plus importante correspond sûrement à la localisation de la minéralisation par rapport à la surface de la Terre. Le lien entre une minéralisation et sa profondeur de formation exprime des facteurs physiques (p.ex. pression et température) ainsi que des facteurs chimiques (p.ex. les types de fluides présents pendant la phase de transport de la substance concentrée) nécessaires au moment de la création du gîte minéral. D'autres relations qui dépendent de la profondeur se trouvent dans les propriétés du milieu encaissant, comme par exemple la variation de la porosité dans les roches détritiques, ou la réponse du milieu face à une exigence tectonique (rhéologie du milieu).

Au début du *20ème* siècle, la profondeur de formation d'une minéralisation est considérée comme l'un des aspects les plus importants pour sa classification. La pression, la température et la nature de l'eau (météorique ou magmatique) sont considérées comme les principaux éléments régulateurs dans la genèse d'un gisement [Lindgren, 1922]. Ainsi, les premiers systèmes de classification sont basés sur la profondeur de formation. Par exemple, les termes *épithermal*, *mésothermal* et *hypothermal* (par analogie aux zones métamorphiques de Grubenmann [1910]) ont donné le cadre physique et chimique en fonction de la profondeur pour les minéralisations hydrothermales.

Un demi siècle plus tard, avec l'arrivée de la nouvelle théorie de la tectonique de plaques, le nombre d'éléments régulateurs dans la genèse des gîtes minéraux s'est précisé. La localisation d'une minéralisation par rapport aux limites d'une plaque tectonique est considérée comme

un facteur inéluctable dans la compréhension de sa genèse. À cette époque, non seulement la profondeur est importante dans le processus de minéralisation mais aussi la proximité du manteau et son interaction avec la croûte. Le manteau est considéré comme la source de chaleur et de nouveaux matériaux qui s'ajoutent à la surface terrestre. Son importance dans les hypothèses métallogéniques est telle que sa proximité à un gisement est considérée comme clé dans la compréhension de sa genèse.

Les découvertes de minéralisations de fer dans la Mer Rouge (ride océanique) [Miller et al., 1966], la localisation de gîtes de porphyres dans des marges continentales ainsi que des arcs d'îles océaniques [Sillitoe, 1972], et la position des gîtes sulfurés au niveau global [Sawkins, 1972] ont montré à l'époque le besoin de trouver un lien entre la localisation d'une minéralisation, par rapport à la géodynamique de la plaque correspondante, et sa genèse. C'est à partir des années 80 que l'environnement tectonique, ou cadre géotectonique, a commencé à être pris en compte dans les systèmes de groupement de gisements [Sawkins, 1984].

Aujourd'hui, le contexte géotectonique (convergent, divergent ou anorogénique) est un facteur prépondérant dans l'exploration d'un gîte en particulier [Groves et al., 2005]. Parfois, le rapport entre le type de minéralisation et le cadre géotectonique est tellement important que l'évolution géologique d'une région du globe peut être mieux comprise en fonction des gisements qu'il contient [Groves and Bierlein, 2007]. Cependant, la nature changeante d'une plaque ajoute un élément d'incertitude quant au moment de la formation de la minéralisation et des conditions géotectoniques à cette époque. Enfin, les relations spatiales entre un gîte et son environnement devraient être considérées de façon dynamique, ce qui rend indispensable l'intégration de la composante temporelle dans le système des relations entre un gîte et son environnement.

1.2.2 Relations temporelles

De façon similaire aux relations spatiales, le concept de relations temporelles d'un système minéralisé a changé au fil du temps. La relation la plus simple entre une minéralisation et sa roche encaissante correspond à leur simultanéité, c'est-à-dire si la minéralisation a eu lieu après la formation de la roche ou si les deux sont le résultat du même phénomène. Des termes utilisés dans la définition des gisements tels que *syngénétique* et *épigénétique* indiquent ce rapport temporel [Lindgren, 1933]. Bien qu'il soit habituel de discuter la classification de certains gîtes, il est possible de distinguer les types de relation temporelle avec l'aide de techniques de datation avancées (e.g. datation isotopique [Stein et al., 2001]) ou avec l'analyse des textures qui peuvent caractériser le gîte [Craig et al., 1981]. Les amas de sulfures massifs pour le cas syngénétique, et les gisements du type de la Vallée du Mississippi entre autres pour le cas épigénétique (fig. 1.1) sont des exemples notables.

Certains gisements sont cependant le résultat d'un certain nombre de processus superposés spatialement mais éloignés dans le temps. L'enrichissement d'un ou plusieurs éléments, ou la substitution d'un élément par un autre, survenus dans le lieu de la minéralisation sont des évènements courants dans la constitution finale d'un gîte. Par exemple, les gisements de minéraux sulfurés classés en tant que supergénétiques (fig. 1.1) se sont formés à partir de l'altération et de la destruction de la minéralisation originale dues aux des conditions oxydantes proche de la surface, à la migration postérieure des éléments libérés et à leur concentration finale dans des conditions chimiques et mécaniques favorables [Guilbert and Park Jr, 2007] .

Un autre aspect de la temporalité dans la formation des gisements correspond à leur distribution dans l'histoire géologique. Même si les conditions de formation de plusieurs gisements

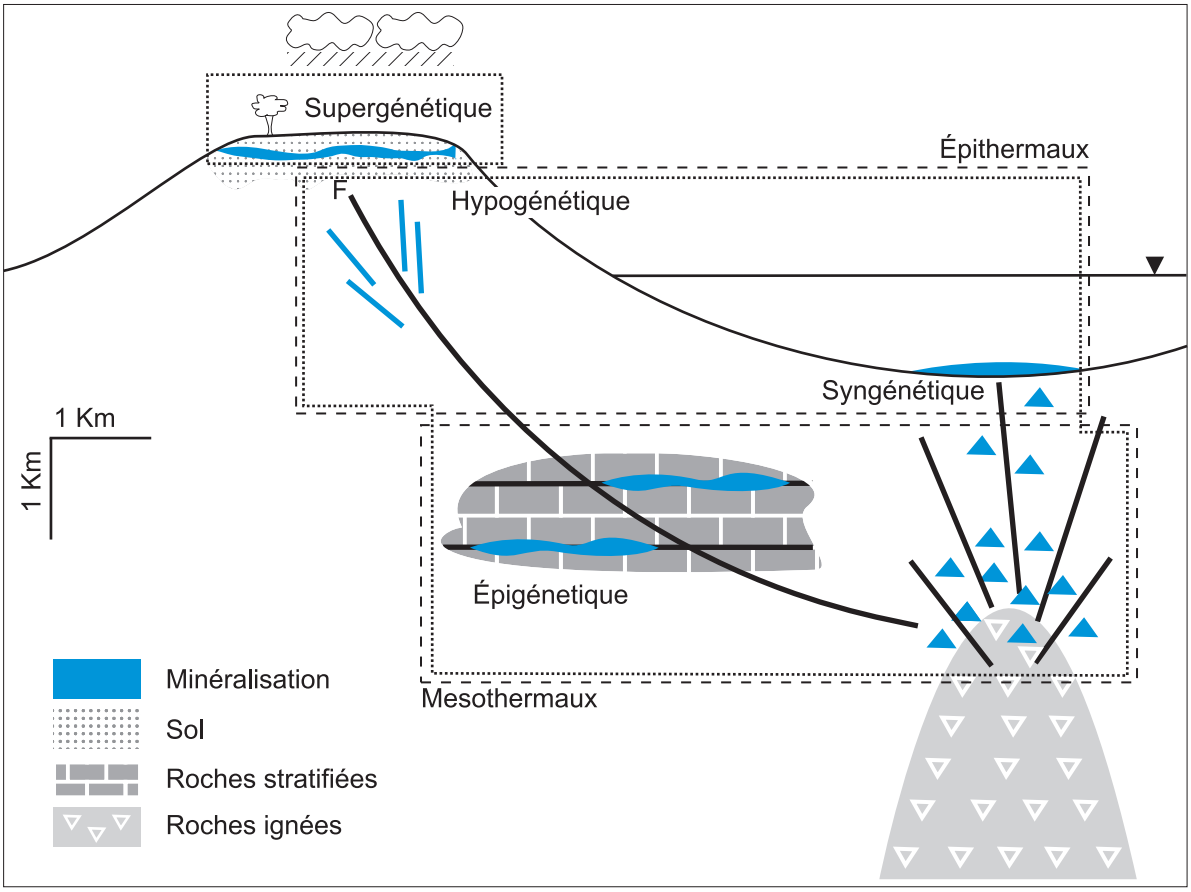

FIGURE 1.1 – Quelques relations spatiales et temporelles dans les gisements hydrothermaux. Dans la figure sont considérés les profondeurs de formation de quelques gisements liés au magmatisme (épithermaux et mesothermaux), ainsi que le temps de leur emplacement par rapport à la formation de la roche encaissante (syngénétique et épigénétique), et au processus de météorisation (supergénétique et hypogénétique).

localisés dans une même région de la Terre peuvent être différentes, un lien temporel entre eux peut se manifester comme le résultat d'un processus géologique à grande échelle [Meyer, 1988, Barley and Groves, 1992]. Au début du *20ème* siècle, Lindgren [1909] avait déjà commenté et re-groupé en époques métallogéniques diverses minéralisations observées dans des provinces représentatives de certaines périodes géologiques en l'Amérique du Nord. Des travaux similaires ont été réalisés en Europe notamment par Launay [1913].

Les gîtes d'origines diverses mais liés temporellement sont la manifestation de processus géodynamiques singuliers existants au moment de la formation d'un système minéralisé [Groves and Bierlein, 2007]. En outre, un type de gisement peut manifester un caractère limité dans le temps (fig. 1.2). En d'autres termes, il y a des périodes dans l'histoire de la Terre durant lesquelles certains types de gîtes sont absents, des moments où ces gîtes sont présents mais rares, d'autres où ils sont abondants, et d'autres encore pendant lesquels les données conservées sont insuffisantes [Goldfarb et al., 2010].

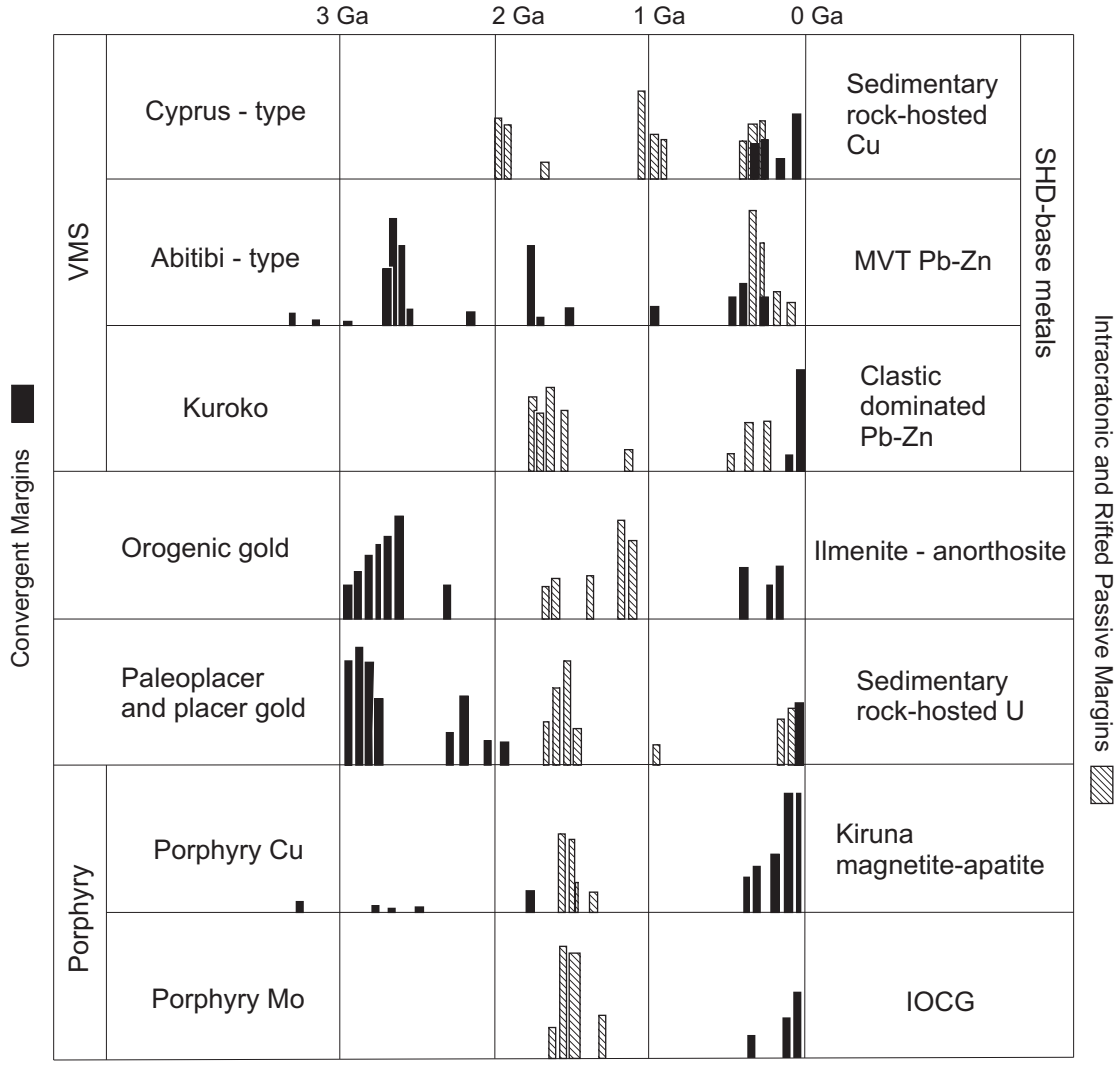

FIGURE 1.2 – Relation temporelle de quelques gisements à l'échelle globale. Distribution temporelle selon le contexte géodynamique d'après Goldfarb et al. [2010]. SHD : sediment hosted deposit, VMS : volcanogenic massive sulfides, MVT : Mississippi valley type, IOCG : iron-oxide copper gold.

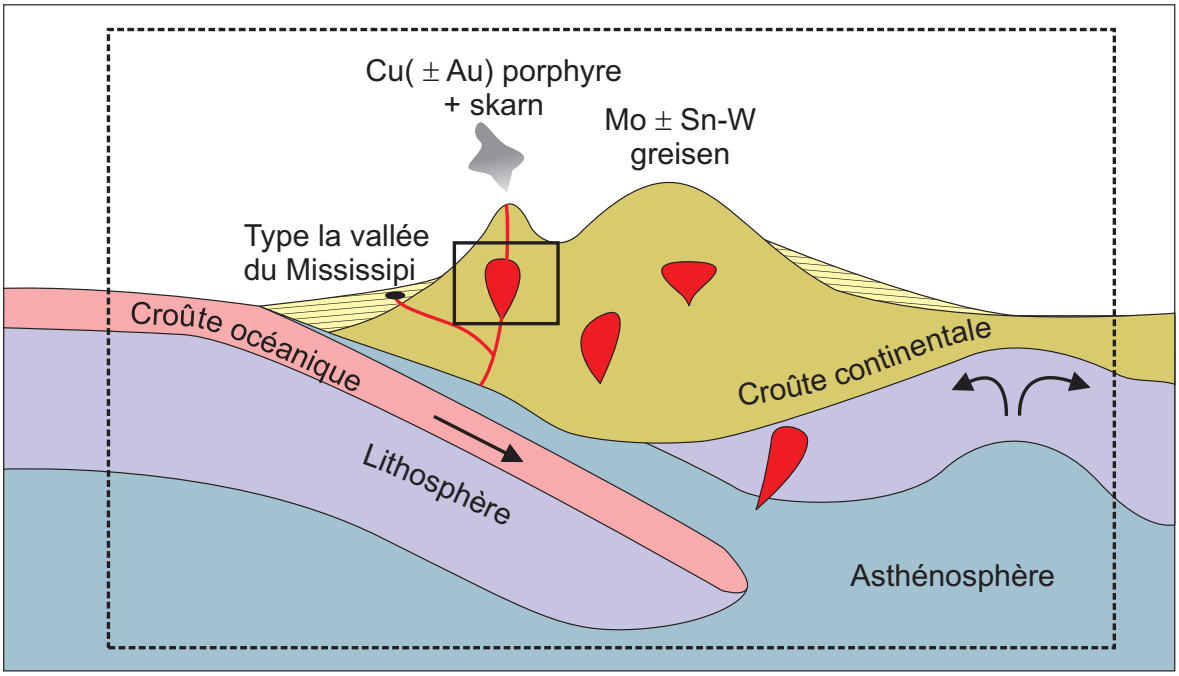

FIGURE 1.3 – Principales échelles dans la modélisation des gisements et des phénomènes géologiques liés à leur formation. La ligne en trait continu symbolise l'échelle de modélisation régionale-locale, tandis que la ligne en trait discontinu indique l'échelle continentale. L'image correspond au schéma des gisements formés dans une marge continentale convergente de type Andin (d'après Groves and Bierlein [2007].

1.3 Modélisation spatio-temporelle

1.3.1 Échelle de la modélisation

En raison de la diversité et de la grande extension de phénomènes géologiques liés à la création et au développement de systèmes minéralisés, la modélisation spatio-temporelle des gisements peut être considérée comme une tâche à multiples échelles. En revanche, deux grands intervalles d'échelles sont dominants : l'intervalle d'échelle continentale et l'intervalle d'échelle régionale-locale. Bien qu'il n'existe pas une séparation concrète entre ces deux intervalles, on peut dire de façon générale que dans le premier sont pris en compte les phénomènes existants du manteau supérieur de la Terre jusqu'à la croûte, tandis que dans le second sont considérés uniquement les phénomènes géologiques liés à la formation et distribution de gisements qui se limitent à la lithosphère (fig. 1.3).

Intervalle d'échelle continentale

La modélisation des gisements à cette échelle est abordée avec la reconstruction paléotectonique et la simulation des phénomènes résultants de l'interaction entre les différentes couches qui composent la Terre depuis le noyau jusqu'à la croûte. Ici, la modélisation est conçue à partir de la cinématique des plaques, de la dynamique du manteau, et de la remontée vers la surface des matériaux en profondeur. En utilisant des modèles conceptuels ou bien avec la simulation de ces processus cinématiques et dynamiques sont abordées les questions sur la genèse, l'emplacement, la morphologie et la distribution des gisements. Quelques exemples et

contributions dans la modélisation de gisements à cette échelle sont détaillés dans Bertrand et al. [2014], Muchez et al. [2005], Richards [2003], entre autres.

Intervalle d'échelle régionale-locale

Dans cet intervalle d'échelle sont réalisés la plupart des modèles des gisements à des fins d'exploration et d'exploitation. Sans être complètement détachée des processus géologiques à une échelle plus large, la modélisation spatio-temporelle dans cet ordre de grandeur joue un rôle majeur dans la détermination de plusieurs facteurs impliqués dans la formation d'un gisement, que sont en premier lieu l'architecture et sa taille [Wang et al., 2011], en second lieu la chimie, la source des métaux et les mécanismes de transport [Rawling et al., 2006], et en dernier lieu la géodynamique [Liu et al., 2005].

1.3.2 Différentes approches dans la modélisation de gisements

La modélisation des gisements a plusieurs approches. Le choix d'une des ces approches est le plus souvent défini par le point de vue d'un individu plutôt qu'en fonction de la minéralisation. Cependant, certaines minéralisations sont classiquement traitées avec une approche particulière :

- approche géométrique : les gîtes considérés comme une seule entité sont généralement modélisés avec une approche géométrique. En utilisant des éléments structuraux et morphologiques, il est possible d'établir la limite de séparation entre le domaine minéralisé et le domaine stérile (fig. 1.4a). Un corps d'amas sulfuré non faillé ou non démembré est un exemple de minéralisation qui peut être modélisé avec une approche géométrique. Quand il y a suffisamment d'informations disponibles, la surface qui enveloppe le corps minéralisé peut être construite avec des critères géométriques et structuraux [Hillier et al., 2014, Sprague and de Kemp, 2005, Lemon and Jones, 2003, Mallet, 2002] ;
- approche stochastique : les minéralisations disséminées avec une distribution de teneur variable sont modélisées avec une approche stochastique. Dans ce cas, l'objectif est de trouver et de délimiter les zones riches avec des méthodes probabilistes (fig. 1.4b). Par exemple, les gisements de type porphyre sont souvent modélisés avec une approche stochastique, dans lesquels l'interpolation par krigeage ou par simulation gaussienne séquentielle sont fréquemment utilisées dans la définition de zones économiques ou exploitables [Chiles and Delfiner, 2009, Ortiz and Emery, 2006, Ortiz and Deutsch, 2004] ;
- approche physique : finalement, certaines minéralisations sont modélisées en simulant les processus physico-chimiques, ainsi que les propriétés pétrophysiques qui ont permis la formation du gisement (fig. 1.4c). De façon générale, ces méthodes sont basées sur l'obtention d'une solution réaliste du modèle mathématique qui simule l'ensemble de phénomènes physico-chimiques primordiaux au moment de la formation d'un gisement en particulier. Dans l'application de ces méthodes sont ajustées les variables physico-chimiques du système ainsi que les valeurs pétrophysiques pour avoir un accord entre la géométrie et la distribution de la minéralisation [Ingebritsen and Appold, 2012, Gross et al., 2009, Hobbs et al., 2000].

Bien qu'il y ait une différence très marquée dans l'utilisation et l'objectif poursuivi pour chaque méthode, cela ne signifie pas que la modélisation d'un gisement doive être limitée à une seule de ces approches. La connaissance finale d'une gisement, ainsi que la définition de son potentiel économique, a besoin de la combinaison de ces approches. Dans de nombreuses

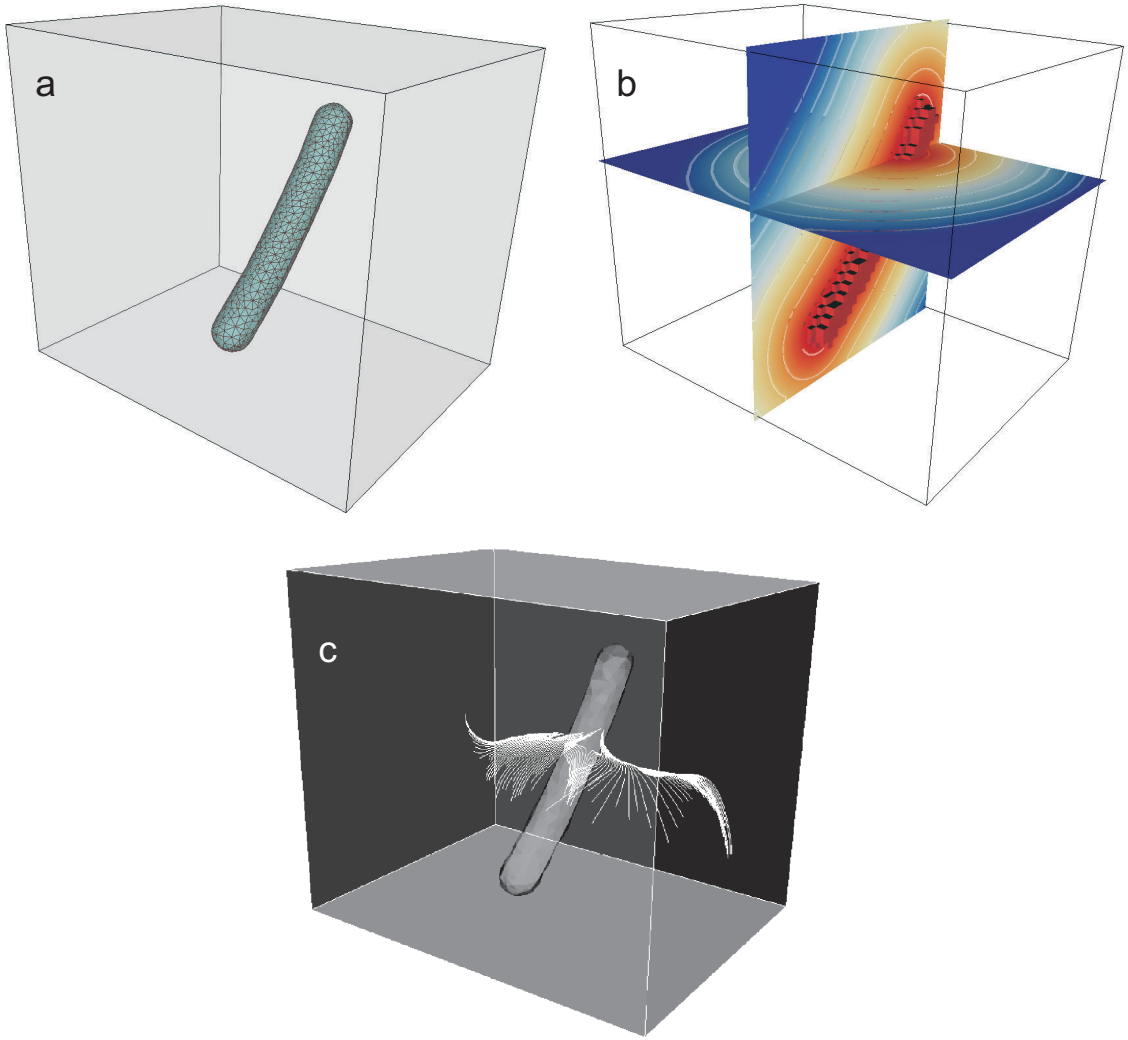

FIGURE 1.4 – Exemples simplistes des différentes approches dans la modélisation de gisements. **a** : Corps minéralisé représenté par une surface fermée. **b** : Corps minéralisé défini par une simulation gaussienne. **c** : Simulation d'écoulement où les lignes de courant contournent le corps minéralisé comme conséquence du contraste de perméabilité entre le corps et la roche encaissante.

situations, une approche est complémentaire d'une autre afin de fournir un modèle le plus représentatif possible.

1.3.3 Avantages de la modélisation spatio-temporelle

Indépendamment de l'approche choisie, l'intégration de la dimension temporelle dans la modélisation structurale des gisements a plusieurs avantages. Un des avantages consiste en l'amélioration de la prédiction par rapport aux zones minéralisées. La reconstruction de la configuration structurale d'une région dans un état antérieur (ou restauration) est d'ailleurs une méthode courante de validation de résultats dans la modélisation structurale [Durand-Riard, 2010, Titeux, 2009, Muron, 2005]. Pour les gisements, la restauration aide non seulement à mieux comprendre la position des corps minéralisés ou la distribution des zones riches, point recherché dans la prospection de ressources, mais aussi à faciliter la recherche de l'ensemble des variables liées à leur genèse, en contribuant ainsi au développement d'hypothèses métallogéniques (fig. 1.5).

1.4 Méthodes et stratégies

La modélisation structurale d'un gisement commence par la reconstruction de l'histoire géologique de la zone d'étude. Il s'agit d'intégrer les phénomènes impliqués dans son évolution, à une échelle supérieure et inférieure à l'échelle définie pour le domaine d'étude. La reconstruction de l'histoire géologique ne prend pas seulement en compte les différentes contraintes appliquées dans le volume analysé, mais aussi la modification des matériaux en fonction du temps grâce aux changements des conditions physiques (principalement de pression et de température), ou l'addition ou soustraction de matériaux (formation ou érosion de roches). Cet aspect sera traité au chapitre 2, où l'exhumation apparue à la fin de Crétacé dans le nord de l'Europe a donné les conditions pour la redistribution de la minéralisation dans la Ceinture de Cuivre de Legnica-Głogów, au sud-ouest de la Pologne.

À partir de l'analyse de l'histoire géologique et de l'évolution structurale il est possible de définir les évènements qui ont permis la formation du gisement ou qui ont modifié sa configuration finale. Pour résumer, il s'agit d'établir les relations spatio-temporelles entre la minéralisation et le volume encaissant dans le domaine d'étude. Encore une fois, les questions de source, de transport et de dépôt de l'élément cible se posent, mais, en ajoutant la modification postérieure à la minéralisation suite à un évènement de déformation. Se pose egalment la question de la création ou de la destruction des matériaux originaux. Un telle situation sera traitée dans le chapitre 3, avec une analyse de la probabilité de trouver une zone minéralisée avec les éléments géométriques liés à la modification des horizons pendant l'évolution du basin des Sudètes polonais.

Un modèle 3D du gisement construit avec une analyse stratigraphique et structurale de ses éléments à l'état actuel est le point de départ pour l'établissement des différentes relations spatiales, tandis que l'analyse géochronologique entre ces mêmes éléments permet d'établir le cadre des relations temporelles dans lequel les relations spatiales sont données. Fréquemment, les relations temporelles sont déduites de façon conceptuelle et pas de manière concrète comme le résultat de la limite de la perception du continuum temporel pour les évènements antérieurs à notre existence. Souvent, un phénomène géologique ou physique connu est extrapolé, comme par exemple le taux de subsidence d'un bassin, la vitesse de déplacement d'une plaque tectonique, ou le plissement des horizons lors d'un évènement de raccourcissement.

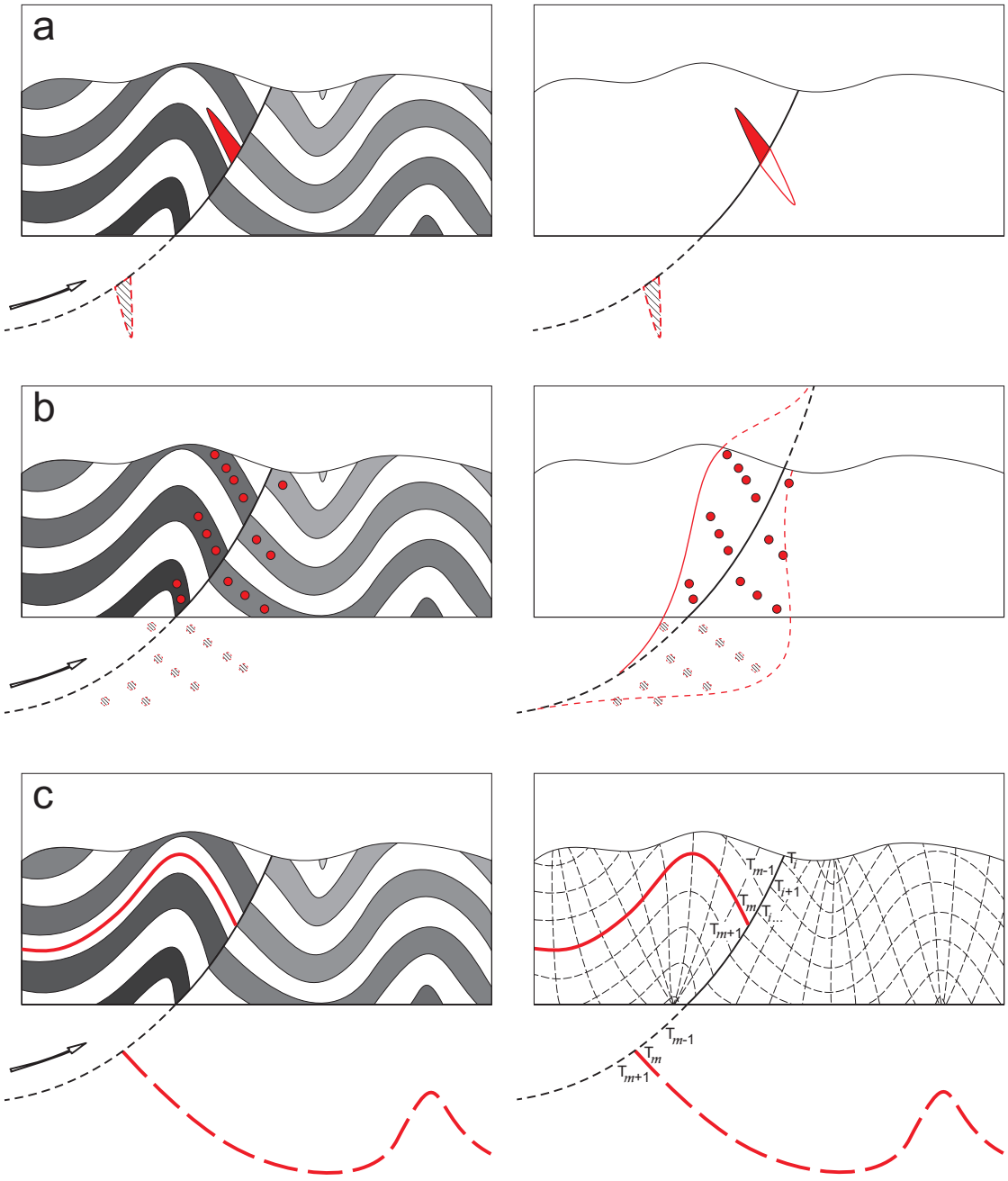

FIGURE 1.5 – Exemple schématique des différentes approches dans la modélisation spatio-temporelle de gisements. **a** : Corps minéralisé coupé par une faille inverse. **b** : Minéralisation disséminée avec une distribution gaussienne le long de la faille, où la distribution est décalée de chaque côté de la faille dû au mouvement inverse. **c** : Minéralisation stratiforme contrôlée par le gradient thermique. Les paléo-isothermes (parallèles à la stratification) sont marquées avec **T**.

Cette approche sera traitée dans le chapitre 4, où la dépendance de l'endommagement rocheux associé à un évènement de raccourcissement a permis d'estimer des zones aurifères hors failles dans le district minier de Mont Pleasant, Australie.

Les chapitres suivants présentent l'application de la modélisation et de la restauration structurale à des cas réels où l'intégration du temps se trouve dans la définition d'un état structural antérieur à l'état observé aujourd'hui. Cette approche offre des avantages car il permet de comprendre les éléments primordiaux dans le processus de minéralisation. La connaissance de ce processus donne la possibilité d'identifier les variables à utiliser dans la prédiction d'une région potentielle du point vue des ressources minérales. Enfin, une conclusion rependra les principaux points acquis dans ce travail.

Chapitre 2

Late Cretaceous–Early Paleocene uplift and inversion in northern Europe: implications for the Kupferschiefer-ore in the Legnica-Głogów Copper Belt, Poland

Sommaire

2.1 Introduction . . . 22
2.2 Geologic setting and Mineralization . . . 24
2.2.1 Main aspects . . . 24
2.2.2 Sulfide mineralization . . . 26
2.3 Surface model and restoration of the LGCB . . . 26
2.3.1 3D model . . . 26
2.3.2 Surface-restoration . . . 26
2.3.3 Decompaction . . . 28
2.3.4 Simulating the pre-uplifting Upper Cretaceous conditions . . . 30
2.4 Hydro-fracturing and Mineralization . . . 33
2.5 Hydro-fracturing and Cu content . . . 34
2.6 Discussion . . . 36
2.7 Conclusions . . . 37

A preliminary version of this research has been presented as a conference paper at the 32^{th} Gocad Meeting [Mejía-Herrera and Royer, 2012].

Abstract

The sediment-hosted polymetallic Kupferschiefer-ore in the Legnica-Głogów Copper Belt, in south west Poland, is one of the most important sources of Cu in present days. This world-class copper deposit combines several geological particularities such as the presence of organic matter, a thick evaporitic sequence covering the ore-series, and a location near to basement/cover unconformity. Previous works focusing on the mineralization process have showed that the Kupferschiefer-ore is the result of several mineralization events distanced in time. In this study, a sequential surface-restoration procedure from the Upper Permian

to Cenozoic was achieved in the Legnica-Głogów Copper Belt district, trying to identify the main structural changes during the tectonic evolution of the region. From the restoration step at Late Cretaceous–Early Paleocene, we estimated the pore pressure in the mineralized horizon as a function of depth assuming a closed system scenario. The calculated pore pressure shows the possibility of natural hydraulic-fracturing in the mineralized horizon caused by the tectonic inversion and uplifting occurred in the region at Late Cretaceous–Early Paleocene. The hydraulic-fractures may lead to the recirculation of fluids and metals during the uplifting, then taking part on the Cu sulfides distribution. A hydro-fracturing index is calculated from simulating the fluid overpressure during the Late Cretaceous uplifting, and seems to correlate with the Cu content distribution in the ore-series. These results are in agreement with an Early Paleocene dating on the Kupferschiefer-ore in the Sangerhausen district in Germany, which may represent the last stage of the Kupferschiefer mineralization. The correlation between the Cu distribution and the hydro-fracturing index could be used to consider favorable zones for a high Cu concentration.

2.1 Introduction

The polymetallic-sediment-hosted Kupferschiefer-ore is one of the most exploited Cu deposits in the world. It extends over 1.500 km in an east-westerly belt across north-central Europe, from north-westernmost Belorussia to northern Ireland [Ziegler, 1982, Vaughan et al., 1989, Jébrak and Marcoux, 2008] (fig. 2.1). The Kupferschiefer-ore was one of the main metalliferous source in Europe from Middle Age, but today it is mainly exploited in the Legnica-Głogów Copper Belt (LGCB) district, south west Poland (fig. 2.2), there being a world-class copper deposit. The production in the LGCB is focused on copper and silver, but lead, zinc, gold and PGE also have economic importance [KGHM Polska Miedź S.A., 2007].

The conjunction of diagenetic and hydrothermal events that have affected the Kupferschiefer [Vaughan et al., 1989, Speczik, 1995, Wagner et al., 2010] makes it difficult to propose a single understandable genetic model for explaining the present state of the mineralization. This last is partially confirmed by the different ages obtained in the works that tried to date the mineralization [Jowett et al., 1987, Bechtel et al., 1999, Symons et al., 2011]. Another aspect that limits a simplest approach for the genetic mineralization process consists of the different ways in which it manifests: the Cu-Ag stratabound mineralization is related to a reduced part of sediment pile, the Au-PGE stratabound mineralization is limited to the oxidized zone and the Cu, Co, Ni, Bi, Ag, and As vein-type mineralization cross cuts all the formations [Wagner et al., 2010]. Despite opposite ideas about the genetic models, multiple evidence suggesting different mineralization stages have become stronger the last decades [Speczik, 1995, Schmidt Mumm and Wolfgramm, 2004]. The multi-stage mineralization model can be summarized in three steps: (i) a first mineralization phase with syn-sedimentary to early diagenetic bacterial pyrite, followed by (ii) a replacement phase and the main formation of Cu (or Cu-Fe) sulfides related to hydrothermal fluids and, (iii) a final Au and other precious metals bearing hydrothermal stage [Piestrzyński and Wodzicki, 2000, Gouin, 2008].

The fracturing of the host rocks is one of the main factors that controls the distribution of metals in the Kupferschiefer [Jowett, 1986, Jowett et al., 1987, Jowett, 1992]. Fractures related to the ore-deposit have different origin and nature, and each fracture type has played a role by channeling the mineralizing fluids, facilitating the metals migration, the replacement of early bacterial pyrite and, finally, hosting the ore-sulfides (fig. 2.3). Several fracture types with various orientations exist in the Kupferschiefer Formation as result of the tectonic evolution of the basin. Its long time activity (since Upper-Permian) makes difficult to

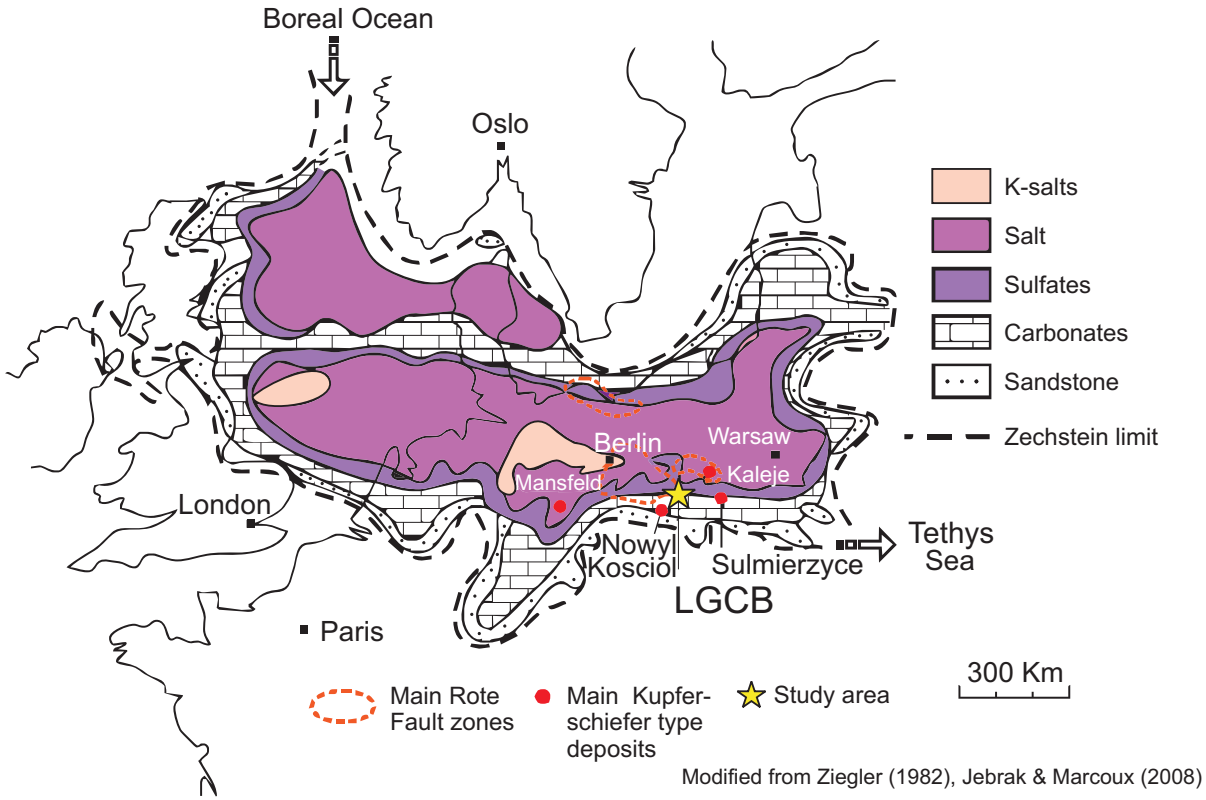

FIGURE 2.1 – Presente day distribution of the Zechstein Formation in Europe. The Kupferschiefer mineralization is located at the base of Zechstein. The Legnica-Głogów Copper Belt (LGCB) district is today one of the main sources of Cu in the World.

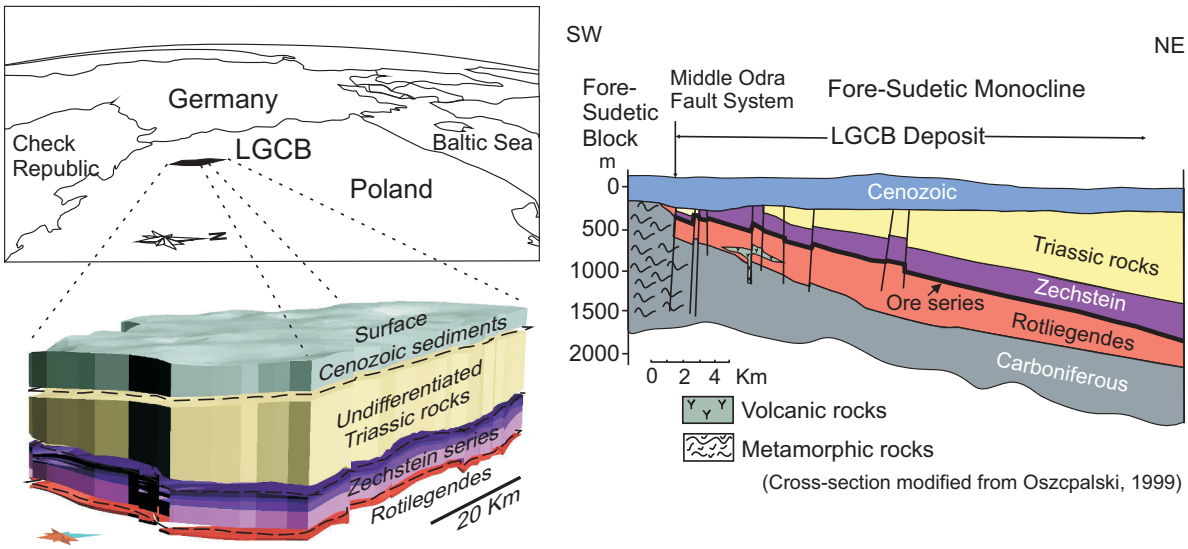

FIGURE 2.2 – Location and 3D model of the Legnica-Głogów Copper Belt district. The ore-series overlaying the Rotliegendes Formation and overlain the Zechstein Formation.

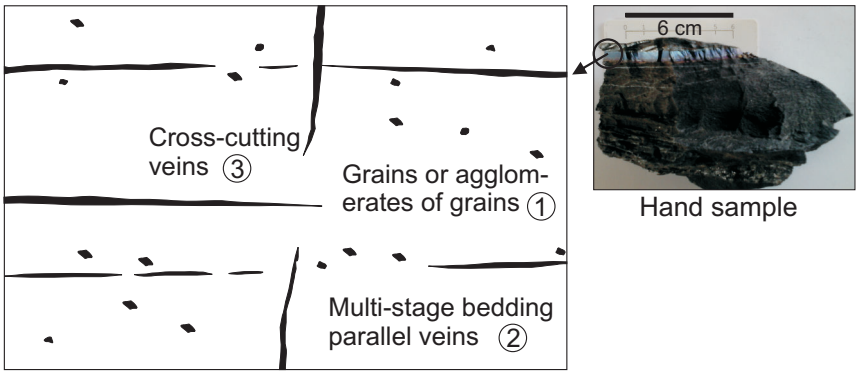

FIGURE 2.3 – Schematic representation of the Kupferschiefer mineralization. The hand sample corresponds to the exploited black shale in the study area. The sulfides in the hand sample within the bedding-parallel vein are mainly chalcopyrite, covellite and bornite.

decipher the mechanisms, development of fractures and the role played by them during the ore-deposit history. However, it seems possible that some of bedding-parallel veins are the result of fractures created during the regional uplifting that affected the whole of northern Europe during the Late Cretaceous–Early Paleocene [Resak et al., 2008, Mazur et al., 2010, Narkiewicz et al., 2010], which is one of the major tectonic events in Europe. This event may lead to favorable conditions for hydraulic-fracturing and mineralization. This work suggests a simple 3D restoration modeling procedure to evaluate the favorable conditions which could have caused to the hydraulic-fracturing of the host rocks during the inversion and uplifting at the end of Cretaceous time. Each layer has been restored, while a hydro-fracturing index was evaluated to estimate the hydro-fractures distribution. Our results show some matching between the spatial hydro-fracturing index and the emplacement of the Cu (Cu-Fe) sulfides exploited today in the LGCB region.

2.2 Geologic setting and Mineralization

2.2.1 Main aspects

The Kupferschiefer (copper slate), is a sedimentary formation created from the eustatic variations of the Zechstein Sea at the end of Permian, which extends over northern Europe on more than 600.000 km^2 [Blundell et al., 2003]. Sensu-strictu, it is a shale thin layer (<1 m) bearing on average about 7% organic matter, placed between the Lower Permian terrestrial/volcanic sediments (Rotliegend and Weissliegendes) and the Upper Permian marine sediments of Zechstein [Jowett, 1986, Oszczepalski, 1999, Blundell et al., 2003, Gouin, 2008] (fig. 2.4). The most part of the Upper Permian–Late Cretaceous history of the region was dominated by extensional tectonics and subsidence [Stephenson et al., 2003, Lamarche and Scheck-Wenderoth, 2005] leading to the creation of marine sedimentary rocks (Triassic and Jurassic) and sandstones, conglomerates and marls (Cretaceous). In many parts of Poland, as well as in the northern-Europe, the tectonic inversion at Late Cretaceous–Early Paleocene time caused the erosion of hundreds to thousands of meters of the Cretaceous sediment pile [Mazur et al., 2005, Scheck-Wenderoth and Lamarche, 2005, Resak et al., 2008, Narkiewicz et al., 2010]. For the LGCB region the uplifting has been estimated to at least 1.000 m [Stephenson et al., 2003] eroding the rocks from Triassic to Cretaceous. The pre-Cenozoic rocks were tilted 3° to 6° to the northeast, probably during the Alpine orogeny [Oszczepalski, 1999].

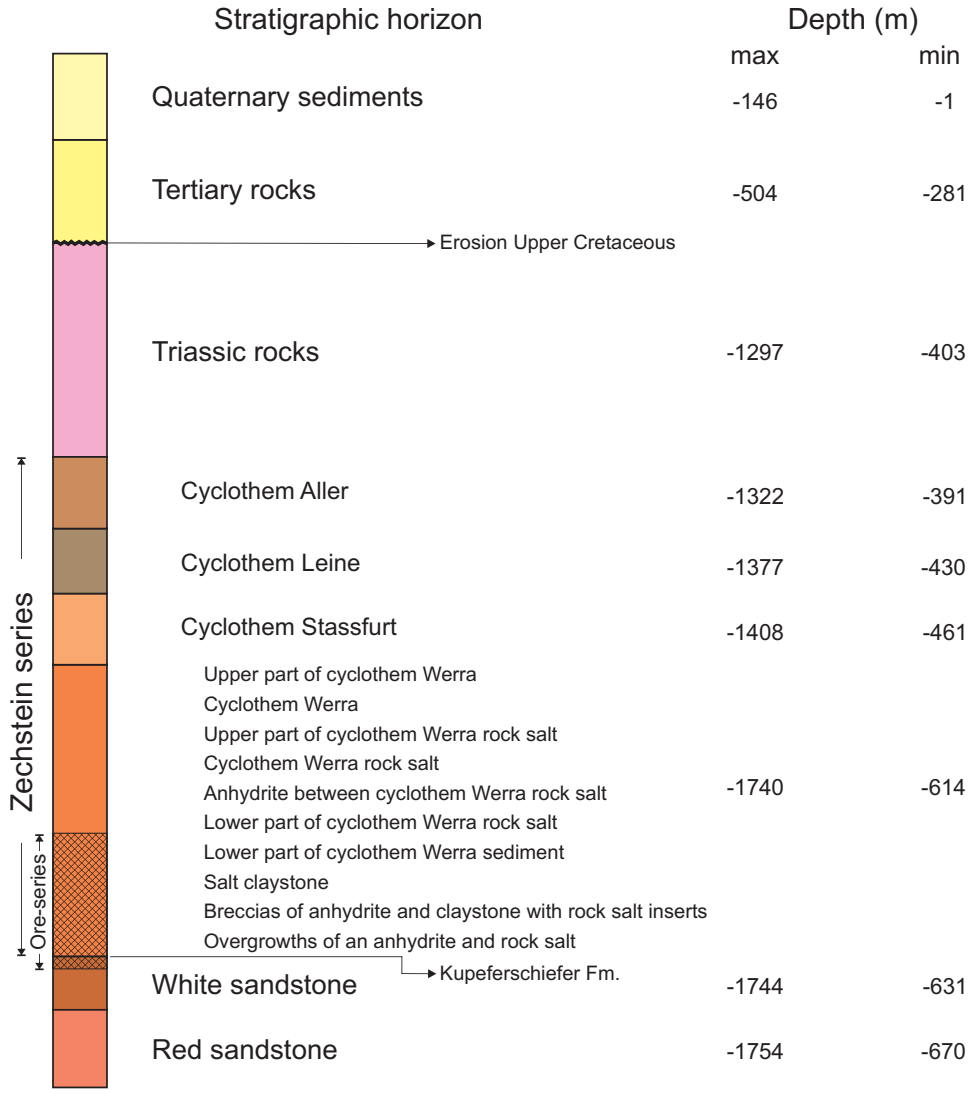

FIGURE 2.4 – Stratigraphic column of LGCB district based on exploration drill-holes. The depth values correspond to the maximum and minimum found in the 3D model of the study area.

2.2.2 Sulfide mineralization

There are three main mineralized sulfide levels within this shale both as grains, cross-cutting and bedding-parallel veinlets: a boundary dolomite (lower) level, a bituminous black shale (middle) level and a dolomite black shale (upper) level. In a broad sense, the word Kupferschiefer has a mining origin and refers to mineralized layers that involve the black shales but, also their rough limits with Rotliegend and Zechstein Formations [Oszczepalski, 1999, Piestrzyński and Sawlowicz, 1999]. The polymetallic Kupferschiefer-ore in the Fore-Sudetic Monocline has a large list of minerals. The major ore minerals are chalcocite, bornite, chalcopyrite, covellite, digenite, pyrite, galena, sphalerite, tennantite, native silver, stromeyerite, cobaltite and castaingite, with minor Cu, Ag, Fe, Ni, Co, Mo, Hg, Bi, Pt and Pd sulfides, arsenides, diarsenides, sulphosalts, thiosulphates, arsenates, and noble metals and alloys containing Au, Ag, Hg and Pb [Piestrzyński and Sawlowicz, 1999].

2.3 Surface model and restoration of the LGCB

2.3.1 3D model

The study area is located in the Legnica-Głogów Copper Belt mining district, south west Poland. The area extends over 700 km^2 and the maximum difference in height between the upper and lower layers is about 1.700 meters. The stratigraphic horizons comprise of the units of Cenozoic, Triassic and Upper Permian. The geological 3D model that represents each one of the stratigraphic horizons were built using: (i) maps showing the contours of the Zechstein and the stratigraphic layers units, (ii) map of fault traces without dip information, (iii) the markers of 288 geological wells available as Excel database with lithological descriptions. All data base was provided by KGHM Polska Miedź S.A. (fig. 2.5 a). The resulting 3D model was performed using the Structure & stratigraphic Workflow of *SKUA®-2011*. The fault blocks were considered having vertical dips, knowing that the faults in the area are mainly verticals or sub-verticals (fig. 2.5 b).

2.3.2 Surface-restoration

The *Simple-shear* method was used to sequentially restore the several horizons of the surfaced-based model of the study area. This method restores deformed horizons in a cross section as if it was constituted by an infinite number of planar slices that are free to slip on one to the other [1]. The simple shear is produced by slip on closely spaced, parallel planes with no length or thickness changes parallel or perpendicular to the slip planes. The shearing can be oriented in any direction of the space, along the depositional planes, oblique or perpendicular to it (fig. 2.6). The simple shear method preserves distances in the shear direction, but lengths, layer thicknesses and areas are not necessarily preserved [Moretti et al., 2007]. The method works sequentially from the younger to the older depositional surfaces. When the simple shearing is applied, a reference horizon at a given position is assumed to be the initial deposition surface, this assumption is a required step to perform the restoration. This implies vertical or oblique differential displacements of elementary blocks of a vertical cross section [Verrall, 1981]. The package *Kine3D-2* of *GOCAD-SKUA®-2011* was applied for performing the sequential restoration on the top of sedimentary horizons modeled as triangular surfaces. This procedure is called as *surface-restoration* or *2.5D-restoration*.

1. A good analogy is a pile of paper sheets that is bent and slipped.

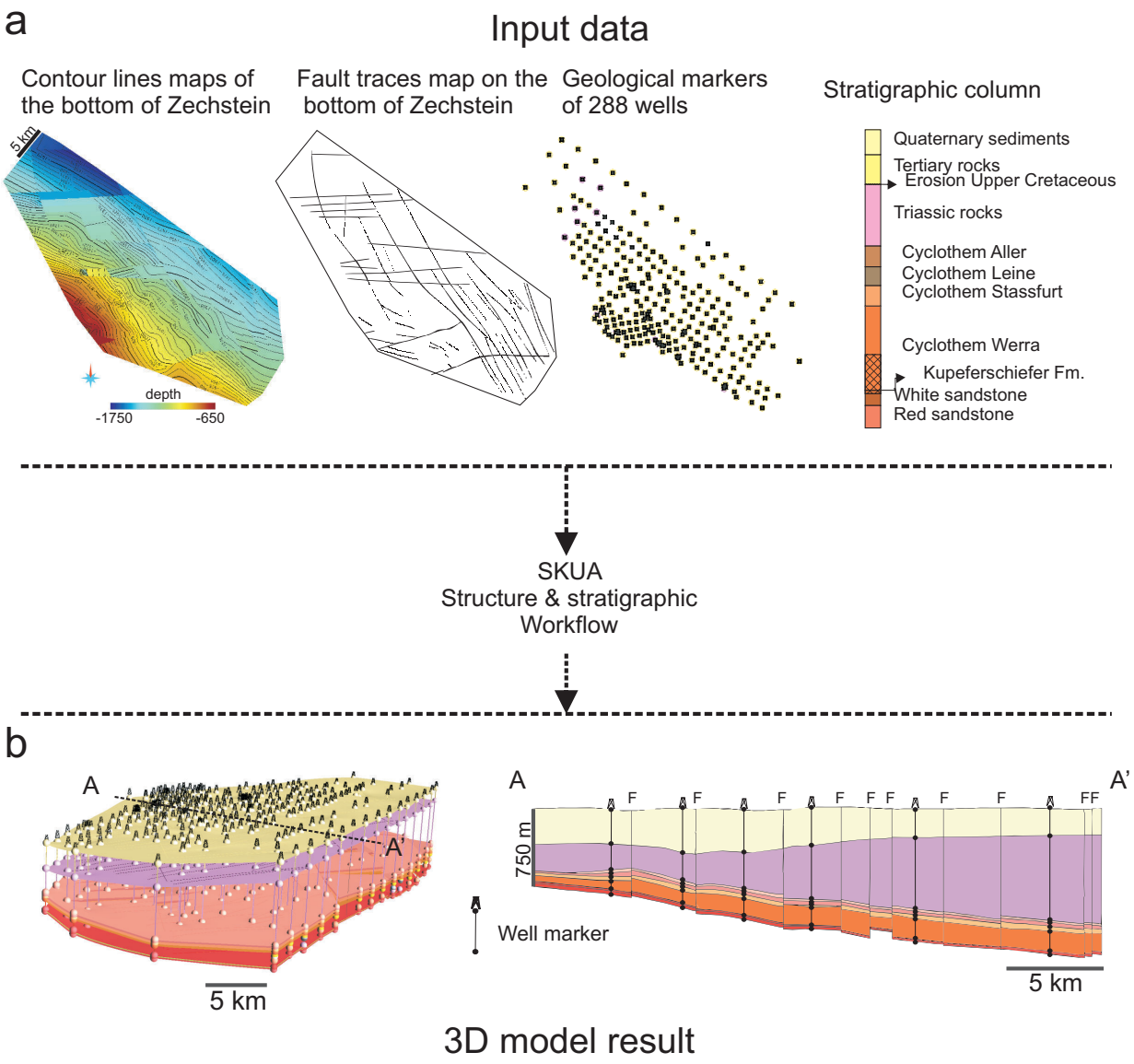

FIGURE 2.5 – Input data and resulting 3D model of the Legnica-Głogów Copper Belt district. More than 288 drill-holes have been used for building the implicit model of the region. The mineralized horizon is located at the base of the Zechstein series.

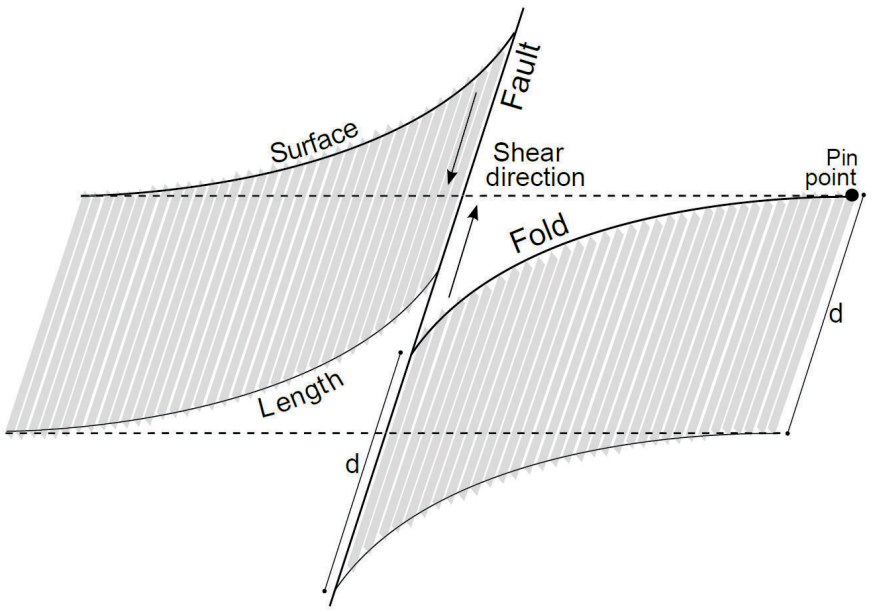

FIGURE 2.6 – Simple-shear restoration method. It is performed by slip on closely spaced, parallel planes with no length or thickness changes parallel or perpendicular to the slip planes. The horizons are restored as if they were constituted by an infinite number of planar slices. Simple shear preserves distances in the shear direction, but lengths, layer thicknesses and areas may change.

The surface-restoration, by flattening the top horizon and consequently propagating this flattening on the below surfaces, was reiterated on each sub-sequential horizon. After each restoration step, the upper surface was stripped and the process was reiterated with a new decompaction-restoration process on the remaining surfaces (sec. 2.3.3). During restoration, the surface inconsistencies were pointed out on unrealistic nearby horizon shapes, fault behavior or thickness variations. These inconsistencies were corrected by reshaping the initial surfaces modifying their continuity (suppression or addition of faults, forcing continuity, modifying the position in some unrecognized zones, etc.) but honoring all the available wells and faults map data. These corrections were applied prior to applying any new restoration step.

2.3.3 Decompaction

Decompaction is a necessary step during a restoration process that aims at removing the bed rocks loading effect on a sedimentary sequence. When a layer is placed on top of another layer, it is necessary to remove the compaction effect due to the weight of the upper bedded rocks. Commonly, the compaction impacts the pile at the horizon as a vertical movement and as a negative layer volume change. The decompaction can be calculated given the sedimentary layer properties (surface porosity, porosity deep factor), its present position and the bed rocks' thickness. The methodology described by Sclater and Christie [1980] was used. The equation governing the upward movement of the stratigraphic horizons is as follows:

$$\begin{aligned} z_2' - z_1' &= z_2 - z_1 - \frac{\phi_0}{c}\left(e^{-cz_1} - e^{-cz_2}\right) + \frac{\phi_0}{c}\left(e^{-cz_1'} - e^{-cz_2'}\right) \\ \delta z &= z_2' - z_1' \end{aligned} \tag{2.1}$$

Where z_i is the original position of the top layer before decompaction, z_i' is the top layer

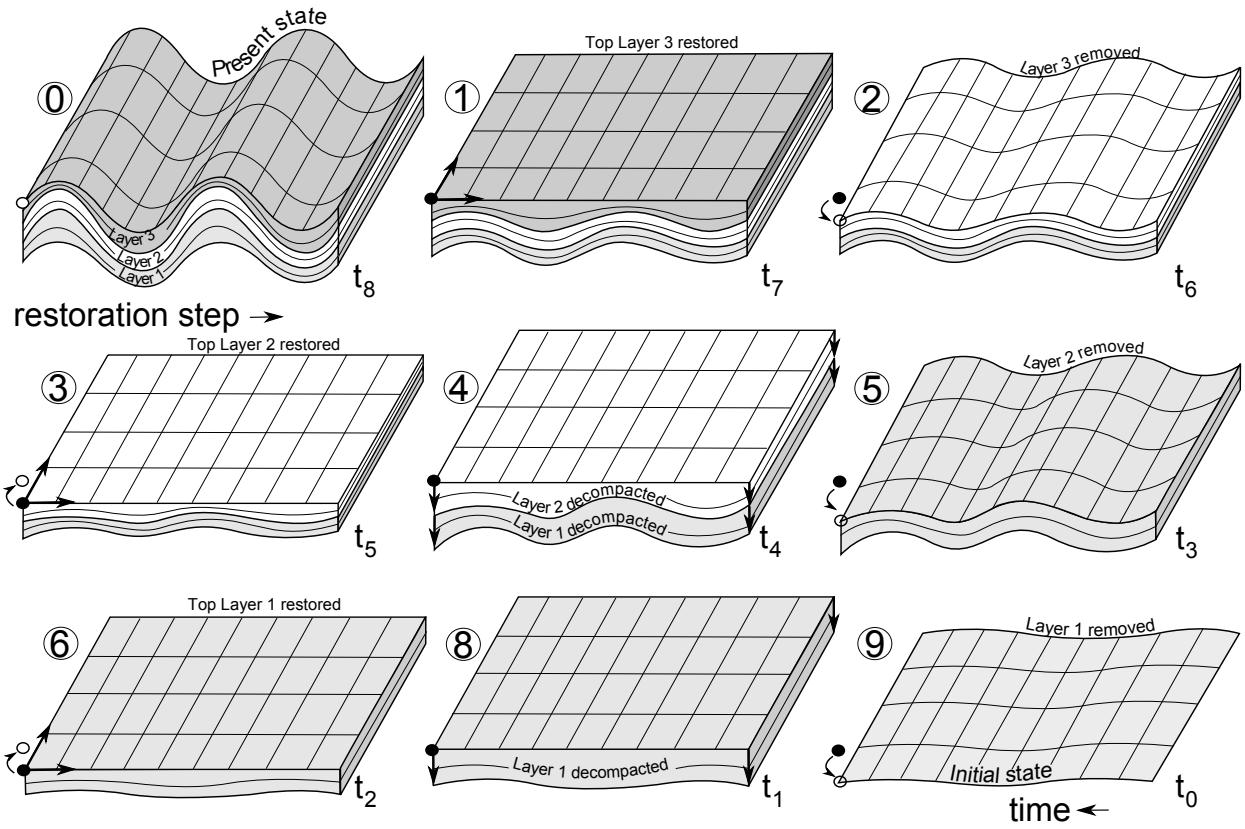

FIGURE 2.7 – Graphic illustrating an example of the steps involved in the decompaction-restoring algorithm for a syndepositional folding scenario without faulting. (1) the top of the upper horizon is restored in its original depositional state (here flattened) from the initial present model (0). (2) the first horizon is removed. (3) the top of the second layer is restored (flattened) and the pile moved to the reference sea-level $\bullet \rightarrow \circ$. (4) the layers of the sedimentary pile are decompacted iteratively using Scatler's equation 2.1. (5) the process is reiterated from step (2), the second layer is removed. (6) the third top layer is flattened and the pile moved to the reference sea-level as in step (3). (7) the layers of the pile are decompacted as in step (4). (8) the process is then reiterated with the last layer.

position after decompaction, ϕ_0 the surface porosity and **c** the porosity deep factor of sediments. The decompaction estimation is performed each time once the upper layer is removed and before restoring the horizon that is placed at the top of the sequence (see Annex). Fig. 2.7 resumes schematically the overall surface-restoration-decompaction workflow applied in an idealized scenario of syndepositional folding without faulting.

During decompaction the materials with natural porosity can change volume depending on the thickness variation according to eq. 2.1. By contrast, the volume of evaporite rocks does not vary during the decompaction because the natural porosity is very low and is therefore considered that the layer thickness remains constant throughout the restoration-decompaction process. However, the clastic sediment layers which are confined by the evaporites may or may not vary in volume depending on their ability of dewatering throughout the pile sediments history. We believe that during most of the formation of the sediment pile, the fluids confined by the evaporite rocks remains hydraulically isolated from the rest of the sediments overlying the evaporites and, therefore, the volume of the rocks below the Zechstein Formation remain almost constant. However, with a long history from over 200 Ma the fluids can eventually

TABLE 2.1 – Rock properties used for the modeled horizons of the LGCB area. ϕ_0 and **c** attributes according to Scheck-Wenderoth and Lamarche [2005] and Resak et al. [2008]). Horizons in *italic* were not eroded in the study area.

Rock type	**Lithology**[1]	**Thickness** (m)	ϕ_0 **- Initial Porosity** (%)	c- **Porosity depth factor** ($10^{-4} \cdot m^{-1}$)	T-**Tensile**[3] **Strength** ($inMPa$)
	Quaternary (Q)	44	0.51	6.2	3.5
	Tertiary (TR)	262	0.51	6.2	3.5
	Upper Cretaceous	411	0.48	5.0	-
	Lower Cretaceous	823	0.48	6.1	-
Clastic	Upper Jurassic	188	0.51	5.2	-
	Middle Jurassic	140	0.62	19.4	-
	Lower Jurassic	110	0.35	5.0	-
	Norian-Rhaetian	318	0.48	4.4	-
	Schilfsandstein +				
Evaporitic	Upper Gypsium Beds[2]	108	0.06	0.3	-
	Lower Gypsium Beds	34	0.06	0.3	-
	Lower Keuper	1,100	0.70	8.3	8.8
	Muschelkalk	450	0.53	5.6	8.8
Clastic	Upper Buntsandstein	450	0.62	19.4	3.6
	Middle Buntsandstein	200	0.35	5.0	3.6
	Lower Buntsandstein	200	0.62	19.4	3.6
	Triassic (T)	37	0.06	0.3	-
	Cyclothem Aller (PZ4)	43	0.06	0.3	6.9
Evaporitic	*Cyclothem Leine (PZ3)*	64	0.06	0.3	6.1
	Cyclothem Stassfurt (PZ2)	16	0.06	0.3	6.0
	Cyclothem Werra (PZ1)	204	0.06	0.3	6.2
	Rotliegend White sandstone (PCB)	18	0.51	6.2	0.8
Clastic	*Rotliegend Red sandstone (PCC)*	-	0.51	6.2	0.8

[1] Rock density assumed at $\rho = 2,670kg \cdot m^{-3}$ for each layer.
[2] This layer was eroded during the $221 - 214$ My time interval.
[3] Pondered tensile strength estimated from the values reported by Pytel [2003] in the LGCB district.

flow upwards by normal-fault–related earthquakes, then leading the compaction process and volume change within and below the Zechstein Formation. Fig. 2.8 shows the different depth of the Rotliegend Formation (PCB) considering the possibility of a compaction process and the opposite situation. Table 2.1 shows the compaction parameters ϕ_0 and **c** used in this work.

2.3.4 Simulating the pre-uplifting Upper Cretaceous conditions

In order to model the pre-uplifting structural state at Late Cretaceous, we used PetroMod 11.0 software to infer the basin evolution of the LGCB district. Using a 1D approach in a virtual well located in the modeled study area, we estimated the burial evolution and the eroded sediment stack for obtaining the depth of the Kupferschiefer Formation before the uplifting episode. Rock properties such as density, porosity, permeability, compressibility and thermal conductivity are defined by PetroMod using its rock type libraries. We used the rocks, thermal history and boundary conditions according to Resak et al. [2008] for his PetroMod 1D modeling of Polish Basin (fig. 2.9 and Table 2.2). For the basin evolution were considered the assumptions used by Lamarche and Scheck-Wenderoth [2005] for their structural model of Poland. The vitrinite reflectance data in the organic matter contained in the Kupferschiefer Formation for the study area [Gouin, 2008] registers a burial history minimal temperature of 120°C (a similar value was reported by Bechtel et al. [2001b] in the Sangerhausen mining district, Germany) that corresponds to almost 2.300 of burial depth for the Kupferschiefer in the LGCB, where almost 1.000 m of overlying sediments that have been eroded during the Late Cretaceous–Early Paleocene time (fig. 2.10). The results match the amount of inversion calculated by Dadlez et al. [1997] in his structural reconstruction of the region from seismic data.

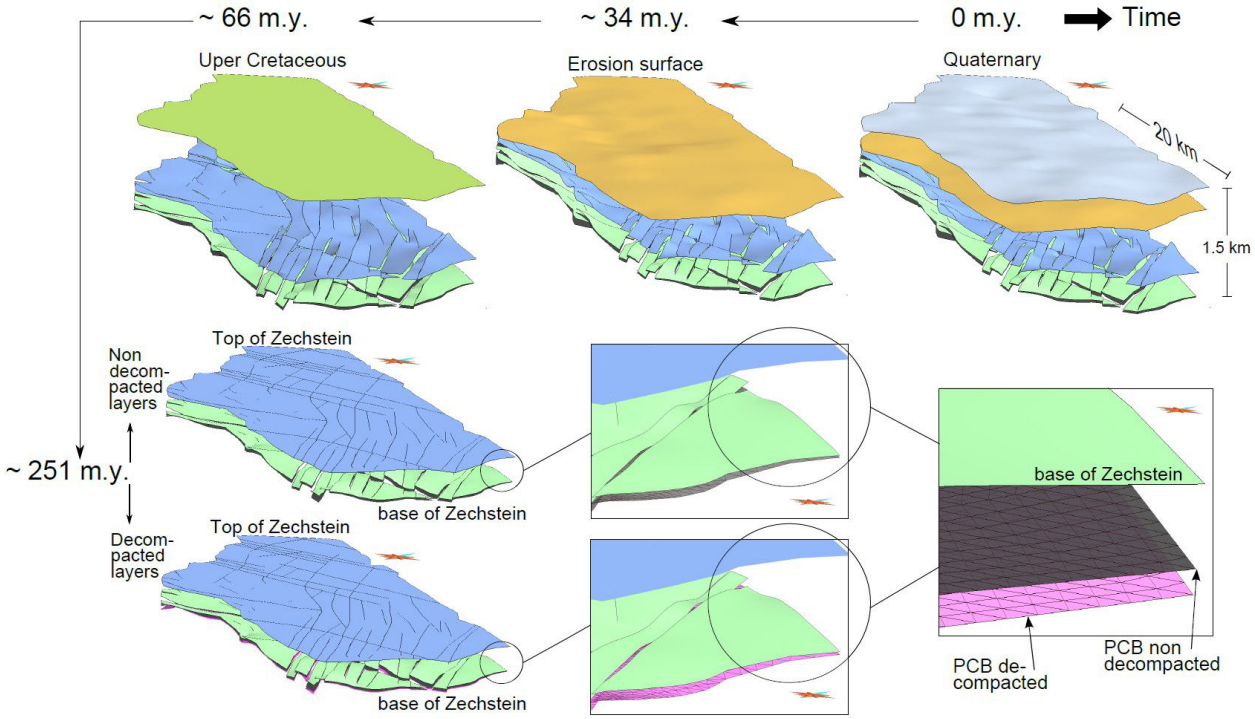

FIGURE 2.8 – 3D models from the restoration of the LGCB region showing the restored top of the Rotliegend Formation with the compaction effects. The figure shows the decompacted and non-decompacted surfaces at the Triassic restoration step. The PCB layer represents the Upper top of the Rotliegend Formation and also the approximated location of the Kupferschiefer deposit. The thickness variation of the Zechstein series is practically null because they are mainly constituted by evaporites rocks and hence the porosity remain almost constant (vertical exaggeration $x5$).

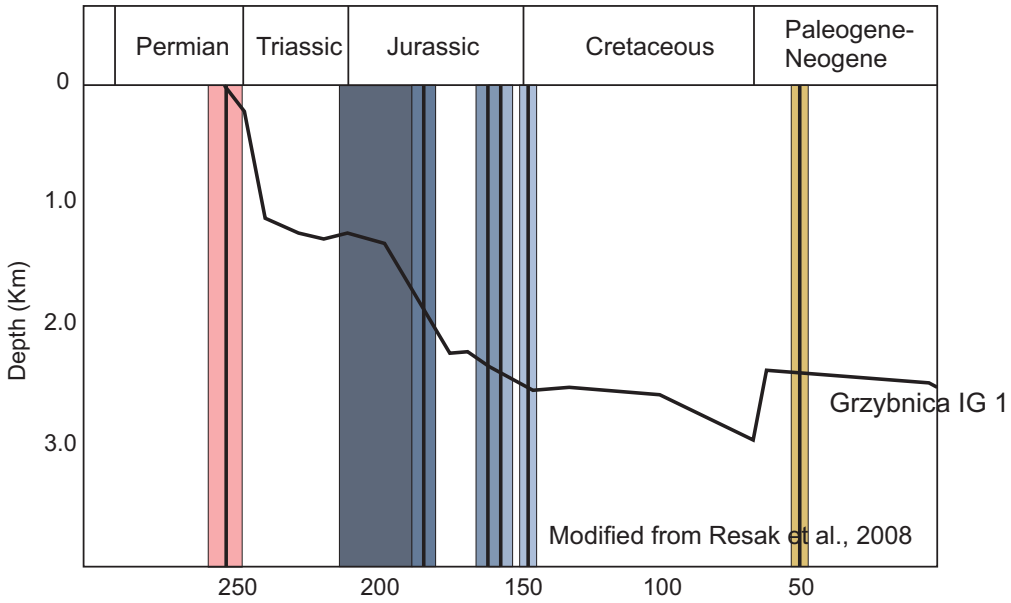

Age	Method
▲ **256 ± 6** Jowett and Parce (1987)	Paleom.
▲ **190 to 216** Bechtel et al. (1999)	K–Ar Illite
186.2 ± 4.2, 163.7 ± ▲ 3.8, 158.8 ± 3.6 Michalik (1997)	K–Ar Illite
△ **149 ± 3, 53 ± 3** Symons et al. (2011)	Paleom.

FIGURE 2.9 – 1D basin evolution and some datations of the Kupferschiefer mineralization in Germany and Poland. The basin simulation corresponds to *Grzybnica IG 1* study well according to Resak et al. [2008]. The ages grossly match with important subsidence and uplifting events marked in the simulation.

TABLE 2.2 – Input data used for the 1D simulation in PetroMod. Sequence of depositional and erosional events estimated in a virtual well located in the study area.

Layer	Thick (m)	Deposition age (Ma)		Erosion age (Ma)		SWIT*	Heat flow*
		from	to	from	to	(°C)	(mW/m^2)
Quaternary	281	1.80	0.00			7.38	56.4
Tertiary	132	33.90	1.80			21.18	55
Upper Cretaceous	-90	99.60	66.00	66.00	65.50	26.36	50
Lower Cretaceous	-90	145.50	99.60	65.50	65.30	25.16	50
Upper Jurassic	-204	161.20	145.50	65.30	64.80	23.61	50
Middle Juarassic	-204	175.60	161.20	64.80	64.00	21.85	50
Lower Jurassic	-516	199.00	175.60	64.00	61.70	21.78	50
Norian-Rhaetian	-48	199.60	199.00	61.70	61.50	24.14	50
Schilfsandstein + Upper Gypssium Beds	-90	229.00	221.00	221.0	214.0	25.17	50
Lower GypsiumBeds	-54	232.50	229.00	61.30	61.10	25.09	50
Lower Keuper	-51	235.00	232.50	61.10	59.90	25.06	50
Muschelkalk	-63	243.00	235.00	59.90	59.70	25.00	50
Upper Buntsandstein	-84	244.05	243.00	59.70	59.40	25.00	50
Middle Bundstain	337	248.70	244.05			24.69	50
Lower Bundstain	168	251.00	248.70			24.50	50
Top Zechstein	43	252.06	251.00			24.60	50
Cyclothem Aller	34	252.78	252.06			24.32	50
Cyclothem Leine	115	254.50	252.78			23.97	50
Cyclothem Stassfurt	70	256.69	254.50			23.85	50
Cyclothem Werra	81	257.99	256.69			23.50	50
Kupferschiefer	1	258.00	257.99			23.49	50
Upper Rotliengend	10	258.10	258.00			22.69	50

* SWIT and heat flow after Resak et al. [2008].

2.4 Hydro-fracturing and Mineralization

As was mentioned before, one of the factors involved in the formation of the Kupferschiefer-ore in the LGCB district is the presence of fractures that concentrate the metals in sulfides [Jowett, 1986, Blundell et al., 2003, Gouin, 2008]. The hydraulic fracturing necessary to transport and enrich the base metals has been suggested by Jowett [1986], Jowett et al. [1987]. According to Cosgrove [2001], the common condition for tensile failure by hydraulic fracturing along any plane is that the fluid pressure (P_f) must be equal to or greater than the tensile strength of the rock (T) normal to that plane and the normal stress (σ_n) acting across it., i.e.

$$P_f \geq T + \sigma_n \tag{2.2}$$

Thus, the hydraulic fracturing may occur either by increasing the fluid pressure P_f, or by reducing the tensile strength T of the rock (e.g. alteration), or by decreasing the normal stress σ_n. During subsidence, the normal stress will increase like the fluid pressure, while the tensile strength remains more or less constant, most of the time, it increases by expelling fluids and cementation of the rock. In this case, the only way to get a fluid overpressure is to increase P_f on the left side of eq. 2.2. This is the idea suggested by Jowett [1986], Jowett et al. [1987] who invoked an aquathermal pressuring mechanism due to the generation of water, CO_2 and CH_4 from the coaly material bearing in the Carboniferous rocks under the Kupferschiefer, the Zechstein Formation being known as a reservoir rock in many places in Europe.
Another possibility to obtain the same result is reducing the magnitude of the right side of eq. 2.2 by decreasing $T + \sigma_n$. As the tensile strength T is a factor that remains almost constant (depending of the rock type), the only way is to decrease the normal stress σ_n maintaining steady fluid pressure at the same time. For a given decreasing in σ_n, the favorable hydraulic fracturing conditions will be reached. This situation might occur during a tectonic inversion event. During a basin forming subsidence episode, the normal stress increases continuously and the fluid pressure remains between a lithostatic and hydrostatic pressure (fig. 2.11 right).

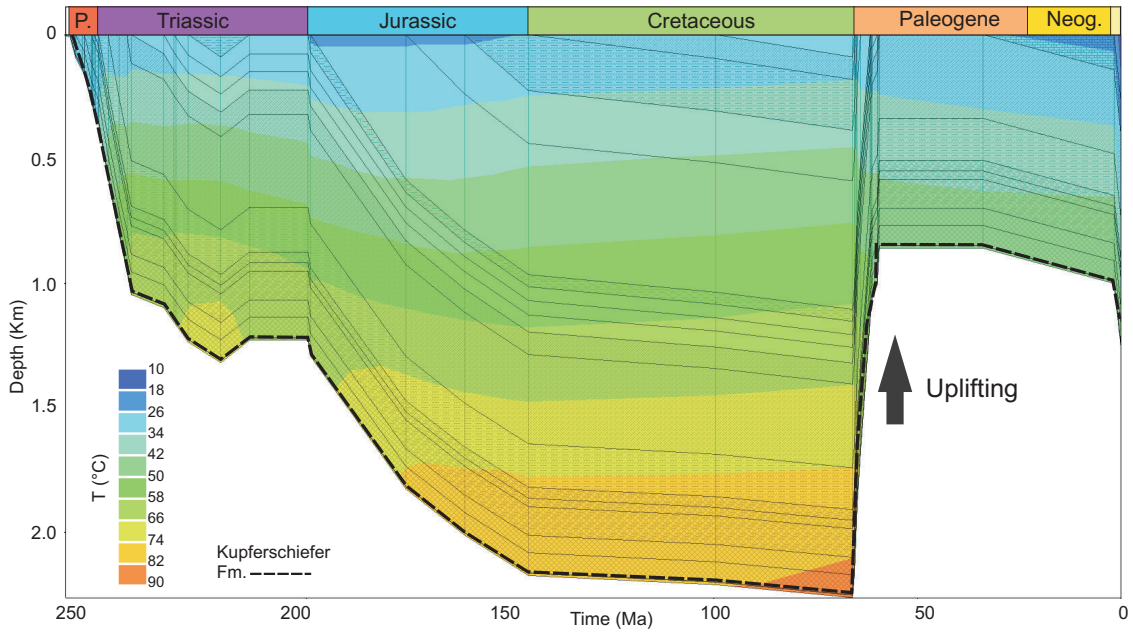

FIGURE 2.10 – Burial history from PetroMod 1D analysis in a virtual well located in the LGCB model. The temperatures were estimated from the vitrinite reflectance of the organic matter contained the Kupferschiefer Formation in the Lubin area, within the LGCB [Gouin, 2008].

When a tectonic inversion occurs, the normal stress decreases and the fluid pressure would decrease if hydrostatic conditions are reached. However, in the case of the Kupferschiefer ore-series, the fluids are trapped and confined below the Zechstein evaporite rocks, and are not able to escape through a normal dewatering process. Assuming correct this hypothesis, the fluid pressure can surpass the condition established in the eq. 2.2 leading to possible hydro-fracturing conditions. Under this condition, new bedding-parallel fractures can be formed or reactivated allowing an improvement of the rocks/fluids interaction and hence metals remobilization and redistribution of the enriched zones in the ore-deposit. Sibson [2003, 2004] have showed some examples about the link between the overpressured fluids and rocks, the tectonic regime changes and the orientation of fractures (fig. 2.11 left and center).

2.5 Hydro-fracturing and Cu content

From the 3D restoration since Permian to present time, it is possible to reconstitute a realistic geological model at the Late Cretaceous–Early Paleocene time in the LGB region. For each rock layer, the tensile strength is assigned according to the values reported by Pytel [2003] for the Rotliegend and Zechstein series in the mines within the LGCB district (Table 2.1). The lithostatic, hydrostatic and fluid pressures are calculated as a function of the depth. A Stratigraphic grid is built honoring the structural model. Rock properties and pressure values are assigned to the cell center of a regular grid (cells size being 200 x 200 x 10m). A hydro-fracturing index (HF) defined from eq. 2.3 as follows:

$$HF = P_f - (T + \sigma_n) \tag{2.3}$$

is calculated at each grid cell node of the 3D model at the Late Cretaceous–Early Paleocene

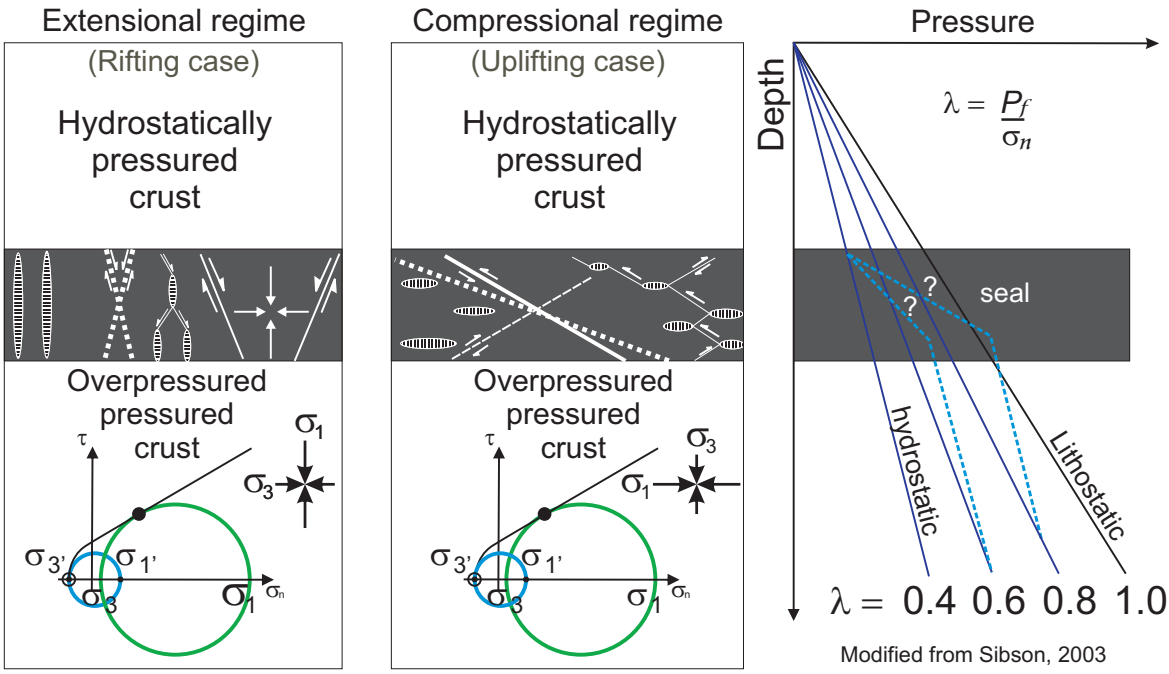

FIGURE 2.11 – Fluid pressure and hydraulic fracturing development under different tectonic regime conditions. Mohr–Coulomb and Griffith's criterion for fractures in opposite regimes. Under hidrostatically pressured crust conditions, the fluid pressure favors the development of fractures. Shear fractures will appear if the difference between σ_1 and σ_3 is superior to $4T$ (green circles). On the contrary, tensile fractures will be created (blue circles defined by σ_1' and σ_3'). The orientation of fractures depends on the stresses orientation and magnitude. The horizontal tendencies present in the current Cu sulfides veinlets style are compatible with hydraulic fractures developed in the uplifting case (see fig. 2.3). The empty points show the conditions to form tensile fractures, while the filled points correspond to the conditions to form shear fractures

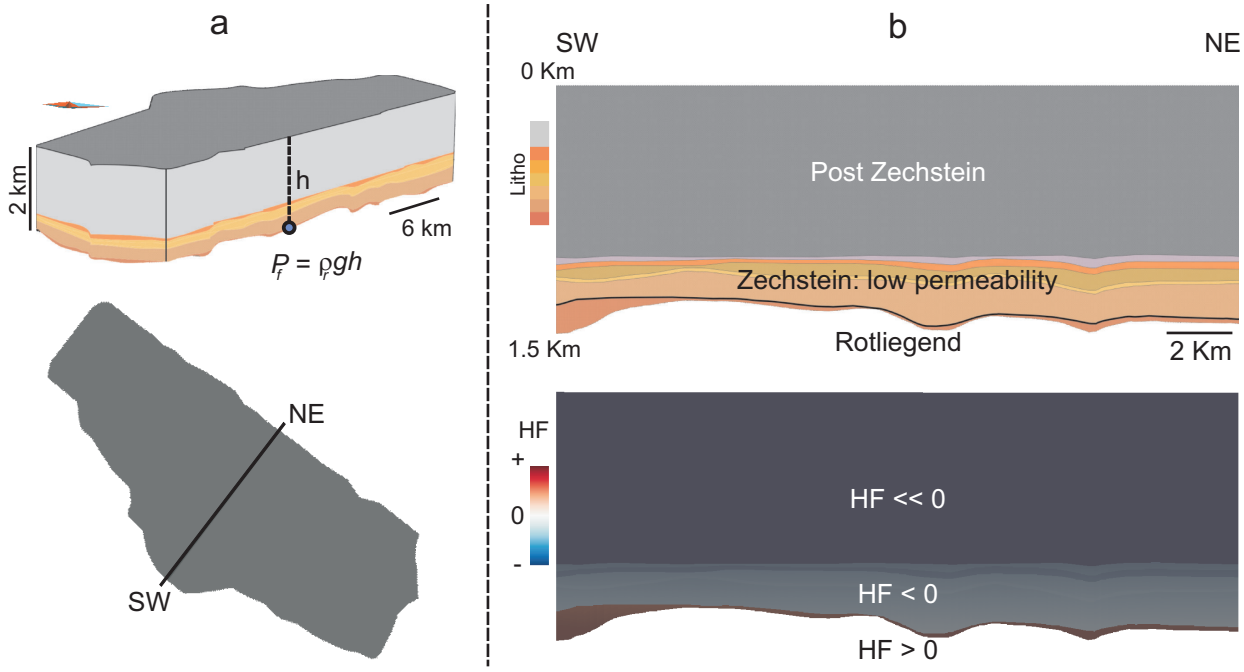

FIGURE 2.12 – Stratigraphical grid representing the LGCB 3D model at Late Cretaceous–Early Paleocene with HF estimations. **a**. The HF index is calculated from the parabolic-form Griffith criterion (eq. 2.3), performed from the P_f before the uplifting event and assuming an equilibrium state with the lithostatic pressure. **b**. The HF is estimated on the grid model for each corresponding horizon considering their depth and tensile strength (Table 2.1). The image points out favorable zones for a hydro-fracturing development ($HF > 0$). These zones, located below the sealing Zechstein salt horizons, are favorable for the re-circulation of mineralizing brines and the re-distribution of the Cu(Cu- Fe) sulfides.

period (fig. 2.12). Positive values of the hydro-fracturing index ($HF > 0$) means that the cell has reached conditions in which hydraulic fracturing might occur, while negative HF values indicate that hydraulic fracturing did not happened. The resulting HF distribution in the 3D model considering the uplifting conditions shows the possibility of fracturing in the Rotliegend Formation and in the low-tensile-strength rocks (shale and limestones) at the Zechstein base, while the HF in the upper Zechstein series are negatives. This is in agreement with the emplacement of the mineralization that occurs nearby the cover/basement interface, below the low-permeability series present within the Zechstein Formation. The overlaying rocks are not considered for the mineralization potential, because the low-permeability Zechstein materials have isolated the basement fluids and hence without possibility to interact with the post-Permian rocks (fig. 2.1 and fig. 2.12). The HF values of the basement/cover interface (Kupferschiefer and its rough contact with the Rotliegend and Zechstein Formations) were assigned on the nearest well-markers having Cu content.

2.6 Discussion

The Cu content cumulative frequency distribution for the HF values estimated in the ore-series shows the presence of Cu in regions with possibility to develop hydraulic-fracturing during the Last Cretaceous–Early Paleocene uplifting (fig. 2.13). However, there is no clear

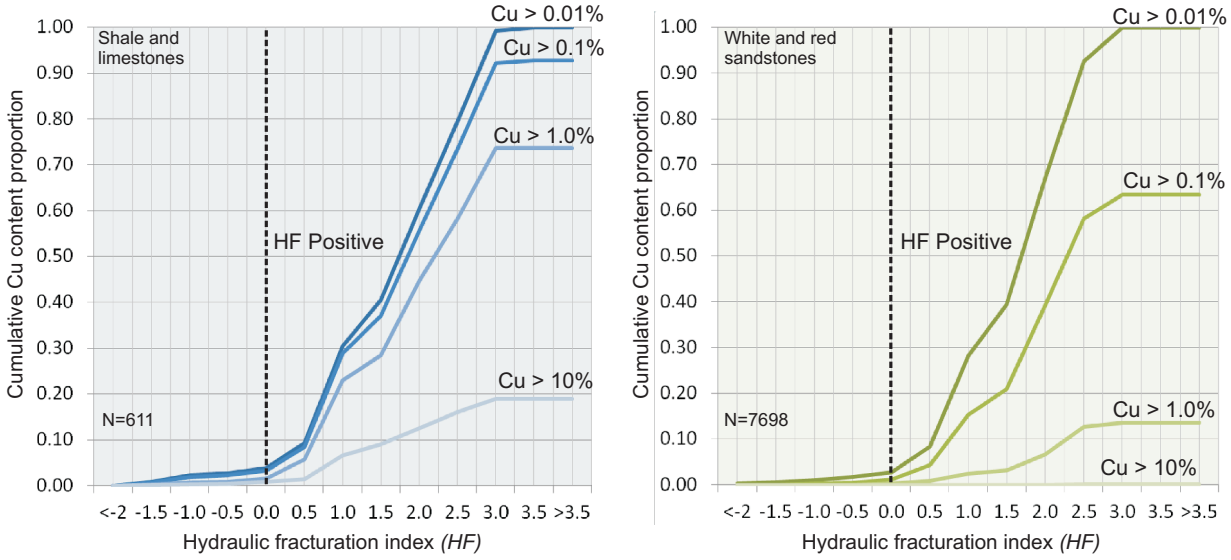

FIGURE 2.13 – Relationship between the Cu content and the hydro-fracturing index (HF). The Cu content rises abruptly when HF is positive. However, no clear association has been observed between HF and the Cu-grade in the ore-series (shales, limestones and Rotliegend/Weissliegend) horizons.

relationship between the fracture intensity (HF increasing at the side right) and the high Cu grades in the ore-series. Another point is that the Cu-content distribution is related to the rock type (Rotliegend-Weissliegend, shales and limestones) in zones with similar HF values. This different behavior would indicate the efficiency of the organic matter present in the black shales for precipitating the Cu (Cu-Fe) sulfides, or the positive role of the primary pyrite precursor bear in the black shales and replaced by the Cu (Cu-Fe) sulfides during the hydrothermal metals remobilization throughout the tectonic inversion.

In our hypothesis, it was assumed one uplifting event occurred at Late Cretaceous–Early Paleocene (fig. 2.14 lower) that allows the development of bedding-parallel fractures compatibles with the bedding-parallel Cu(Cu-Fe) sulfides dominant veins in the Kupferschiefer. However, several works simulating the tectonic evolution of Poland and Germany consider a basin inversion and erosion at Late Jurassic–Early Cretaceous time [Kotarba et al., 2006, Kossow and Krawczyk, 2002] (fig. 2.14 middle). This last event may allows the development of bedding-parallel veins following the same mechanism explained for the Late Cretaceous–Early Paleocene case proposed here. In that sense, the Late Jurassic ages obtained for the Kupferschiefer in Poland and Germany (e.g. reported by Symons et al. [2011] and by Michalik [1997]) may manifest an hydro-fracturing event produced during the Jurassic/Cretaceous basin inversion related to the Kupferschiefer mineralization.

2.7 Conclusions

The geological history of north-central Europe from the Upper Permian to the Late Cretaceous was carved by the formation of sedimentary basins created during extensional regime episodes. But during the Late Cretaceous-Early Paleocene time, a tectonic inversion event took place stopping the deposition and later starting erosion. Under these conditions, the erosion of the sediments induced a decrease in the normal regional stress σ_n, while the trapped fluid below

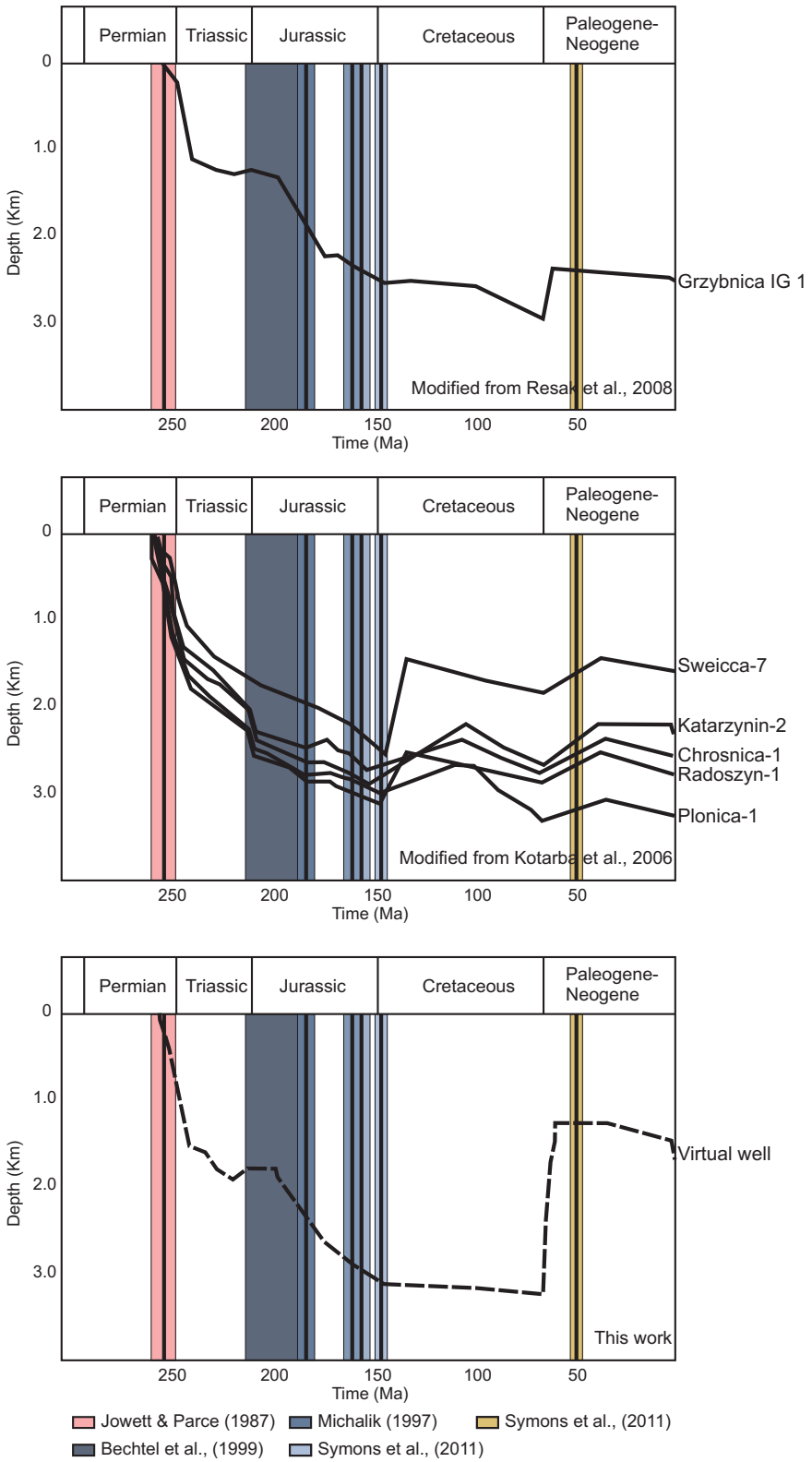

FIGURE 2.14 – 1D basin evolution simulations estimated on different locations in Poland. **Upper**: Basin evolution with a mayor single uplifting and erosion event at Late Cretaceous–Early Paleocene. **Middle**: Basin evolution with two mayors basin inversion events at Jurassic/Cretaceous and Cretaceous/Paleocene limits. **Lower**: Basin evolution simulation estimated in this work on the study area.

the impermeable Zechstein evaporites could not be re-equilibrated and are maintained in a high pressure state. Assuming a constant value for the tensile strength of layers, the decreasing normal regional stress by the erosion of the upper horizons induces the hydro-fracturing of the mineralized current layers. The leached metals from Upper Carboniferous and Rotliegend volcanics [Oszczepalski, 1999] are maintained isolated by the Zechstein evaporites, and can be transported, (re)circulated, and (re)precipitated only where the porous and fractures in rock are available.

The hydraulic-fractured interface basement/cover (Rotliegend-Weissliegend and base of Zechstein Kupferschiefer) may allow a last mineralization stage, from the interaction between the mineralizing fluids and the inner geochemical properties of the ore-series to form the current distribution Kupferschiefer Cu-deposit. This suggested model is in agreement with the alternative mineralization paleomagnetic age of 53 ± 3 Ma proposed by Symons et al. [2011] in the Sangerhausen Kupferschiefer of Germany. This study, shows that the 3D and 4D restoration techniques can be used as an exploration tool for sediment-hosted deposits, and provide useful structural attributes (in this case the hydro-fracturing) that may help to better understand the current distribution of metals in the ore-deposit. In this way, it is possible to define exploration targets from the link between the Cu content and the hydro-fracturing index such as in the present case study.

Chapitre 3

Curvature Attribute from Surface-Restoration as Predictor Variable in Kupferschiefer Copper Potentials: An Example from the Fore-Sudetic Region

Sommaire

3.1 Introduction **42**
3.2 General geology **43**
3.2.1 Geologic settings of the FSM 43
3.2.2 Mineralization 44
3.3 Modeling the Fore-Sudetic Monocline **44**
3.3.1 Modeling Outlines 44
3.3.2 Outcome FSM 3D Model 45
3.4 Detecting Fault Activity from Restoration **45**
3.4.1 Restoration Goals 45
3.4.2 Surface Restoration 45
3.4.3 Iterative Restoration 47
3.4.4 Internal Deformation and Fault Activity 49
3.4.5 Continuous-Surface Representation 49
3.4.6 Restored Models 49
3.4.7 Restoration Outputs 51
3.5 Curvature and Cu Assessments **53**
3.5.1 Potentials Assessments and Predictors Variables 53
3.5.2 Cu Potentials and Selected Predictors 53
3.5.3 LR Models by Predictor 54
3.5.4 Predictive Model and Conditional Independence 54
3.6 Perspectives **54**
3.7 Discussion **58**
3.8 Conclusions **58**

A paper corresponding to this chapter was published in *Natural Resources Research* [Mejía-Herrera et al., 2014b].

Abstract

This work explains a procedure to predict Cu potentials in the ore-Kupferschiefer using structural surface-restoration and logistic regression (LR) analysis. The predictor variables in the assessments are established from the restored horizon that contains the ore-series. Applying flexural-slip to unfold/unfault the 3D model of the Fore-Sudetic Monocline, we obtained the curvature attribute for each restored time. We found that the curvature represents one of the main structural features related to the Cu mineralization. The maximum curvature corresponds to high internal deformation in the restored layers, evidencing faulting and damaged areas in the 3D model. Thus, the curvature may highlight the fault systems that drove the fluid circulation from the basement and host the early mineralization stages. In the Cu potential modeling, the curvature, the distance to the Fore-Sudetic Block and the depth of restored Zechstein at Cretaceous time correspond to predictor variables and proven Cu-potential areas are targets. Then, we applied LR analysis, available in the free software ***R***, establishing the separating function between mineralized and non-mineralized locations. The LR models show a positive correspondence between the predicted probabilities of Cu-potentials and the curvature estimated in the surface that represents the mineralized layer. Nevertheless, the predicted probabilities are particularly higher using the curvatures obtained from Late Paleozoic and Late Triassic restoration steps.

3.1 Introduction

Fault systems in the basement have played a major role during the genesis of the Poland Kupferschiefer deposit (fig. 3.1). First, these structures have driven the fluid migration from brines present in deeper parts of bedrock [Jowett, 1986, Blundell et al., 2003, Muchez et al., 2005, Wedepohl and Rentzsch, 2006, Hitzman et al., 2010]. Second, relative high permeability and porosity, required for the circulation and accumulation of metals during the different stages of mineralization, occurred near to basement fault systems [Forster and Smith, 1989, Rentzsch et al., 1997, Wagner et al., 2010]. Rentzsch and Franzke [1997] have shown several examples about the close relationship between major tectonic structures and Kupferschiefer ores in central Germany. To identify the fault systems that are related to Kupferschiefer-ore locations is an important issue in present day exploration campaigns. However, to recognize these ore-controlling structures sometimes requires huge cost surveys. A first exploration challenge is that the buried basement faults are not easily detected, or subject to uncertainty inherent to data interpretation [Lecour et al., 2001, Bond et al., 2007]. A second challenge is due to deformation (folding and faulting developed during the structural evolution), which can blur the links between a given mineralized location and its corresponding basement fault system. Indeed, the fault activity may vary trough time and space, with possibly strong impact on rock permeability and mineralized fluid circulation. Even in cases where the fault systems are identified, it is necessary to establish their role and timing of activity to understand their role for a given mineralized locality. To overcome this, we propose to use the curvature values obtained from a sequential surface-restoration process for inferring the existence and activity of basement-faults related to Cu mineralization. Curvature, as geometric attribute measurable in the horizons of a surface-structural model, can reveal the internal deformation in those horizons due a faulting event [Mallet, 2002, Moretti et al., 2007]. Curvature, computed after several sequential restoration steps, can be translated as the signal of basement faults presence and also indicates their activity over the geologic record. Estimating the correlation between curvature and mineralized locations, it is possible to deduce the fault-fractures linked to Kupferschiefer-ores. Finally, we evaluated the usefulness of curvatures as predictor variable

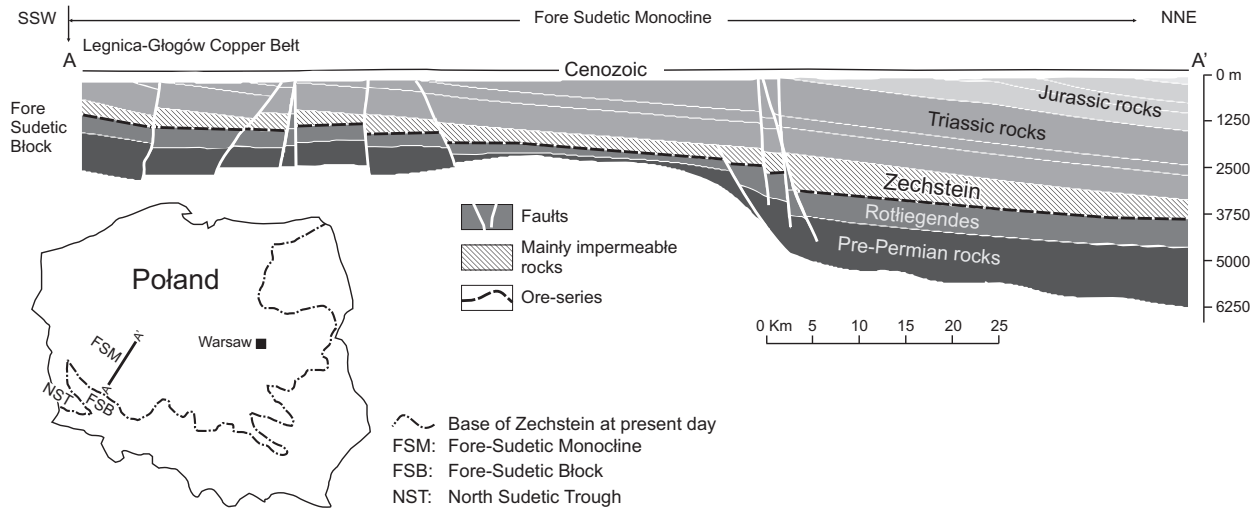

FIGURE 3.1 – Simplified geological cross section across the Fore-Sudetic Monocline. The image is based on the 3D modeling of the study area created in this work, taking into account the geological information and interpretation of Oszczepalski and Speczik [2011], Mazur et al. [2010], Pawlak et al. [2008], Krzywiec [2006], Dadlez et al. [2000], Wodzicki and Piestrzyński [1994].

in the Fore-Sudetic Monocline (FSM), SW of Poland, with the application of a multivariate data-driven predictive method. Particularly, we chose the logistic regression (LR) analysis to obtain a predictive model as a combination of the curvatures acquired in the restoration steps. The results show that in locations with high curvature values the predicted probability to host a Cu mineralization increases considerably. We suggest that this methodology provides useful evidential variables for the Cu potentials assessments in the FSM region.

3.2 General geology

The Kupferschiefer is a metal-bearing black shale, broadly spread across central Europe (from Ireland to Belarus), with very well-known high Cu-grade locations in southwest Poland and central Germany [Rentzsch and Franzke, 1997, Oszczepalski and Speczik, 2011]. The Kupferschiefer-ore exploitation in the Legnica-Głogów Copper Belt Area (LGCB), located within the FSM, is one of most important sources of copper and silver in the world [KGHM Polska Miedź S.A., 2012]. This layer was formed at the end of the Permian, overlaying volcanic and clastic terrestrial sequences (Rotliegendes and Wessliegendes) of Saxonian age [Oszczepalski, 1999], and overlain by the sedimentary products (mainly evaporites) of the eustatic variations during the Guadalupian to Lopingian (Zechstein Formation) [Lefebvre, 1989].

3.2.1 Geologic settings of the FSM

The Kupferschiefer Formation overlies a group of Early Permian sub-basins covering Paleozoic rocks affected by Caledonian and Variscan tectonics [Karnkowski, 1999]. The post-Permian sediments correspond to continental successions and shallow marine sediments of Triassic age followed by a Jurassic succession of shallow marine sediments. Basin analysis shows subsidence rates in the Late Permian-Early Triassic superiors to 80 m/m.y. (Central Basin) [Karnkowski,

1999, Resak et al., 2008]. This rate decreased substantially in Late Triassic and is maintained through to the Jurassic [Karnkowski, 1999]. At the end of the Jurassic, the top Rotliegend surface in the Lower Silesian basin was at a depth of up to 4 km [Blundell et al., 2003]. At the Jurassic–Cretaceous boundary, the Lower Silesian basin was inverted and uplifted, creating the Fore-Sudetic block, bounded by NW-SE trending faults extending from the basement to the post-Permian successions[Blundell et al., 2003]. The Cretaceous sediments, present in the eastern part of the Fore-Sudetic Monocline, comprise mainly to sandstones, conglomerates and marls. These rocks unconformably cover the older strata [Pieczonka et al., 2008]. Northern-Europe was affected by a Late Cretaceous–Early Paleocene tectonic inversion, probably linked to an early Alpine orogeny phase. This event produced the most intensive tectonic movements in the Fore-Sudetic Monocline [Pieczonka et al., 2008], provoking the erosion of hundreds to thousands meters of sediments [Mazur et al., 2005, Scheck-Wenderoth and Lamarche, 2005, Resak et al., 2008, Narkiewicz et al., 2010]. In the Lubin region, the uplift is estimated to more than 1,000 m [Stephenson et al., 2003], eroding the rocks from Triassic to Cretaceous. The pre-Cenozoic rocks were tilted 3° to 6° to the northeast, probably during the Alpine orogeny. The post-Variscan cover of Permian–Cenozoic formations is subdivided into the Kimmerian stage (Permian, Triassic, Jurassic), Laramide stage (Cretaceous), and post-Laramide stage (Tertiary, Quaternary) [Oszczepalski, 1999].

3.2.2 Mineralization

Three main mineralized sulfide levels both as grains and veinlets can be identified within the shales: a lower dolomite level, an intermediate bituminous black shale level and an upper dolomite black shale level. The main minerals found in the polymetallic Kupferschiefer ore in the Fore-Sudetic area are Cu(Cu-Ag) sulfides accompanied by other mineral species such as arsenides, sulphosalts, thiosulfates, arsenates and precious metals [Oszczepalski, 1999, Piestrzyński et al., 2002]. At least three stages are involved in the ore-Kupferschiefer formation [Vaughan et al., 1989, Wodzicki and Piestrzyński, 1994, Speczik, 1995, Wagner et al., 2010], which represent broadly the main post-Permian tectono-magmatic events in central Europe [Schmidt Mumm and Wolfgramm, 2004]. The first mineralization stage is associated with diagenesis during a Triassic to Early Jurassic rifting event [Ziegler, 1982, Bechtel et al., 1999]. A second stage is related to the Late Jurassic extensional tectonic event that formed the nearby North German Basin, reactivating Variscan basement faults and extending them upwards through the overlying strata [Symons et al., 2011]. Finally, basin inversion and uplifting occurred in northern Europe in the Late Cretaceous-Early Paleocene. This event led to erosion of several hundred meters of the Triassic to Cretaceous sedimentary formations [Resak et al., 2008]. This last erosion event likely provoked the increase of fluid/lithostatic pressure ratio, and the hydraulic fracturing allowing the circulation of mineralizing fluids, the remobilization of elements and the replacement and enrichment of Cu-sulfides [Mejía-Herrera and Royer, 2012].

3.3 Modeling the Fore-Sudetic Monocline

3.3.1 Modeling Outlines

The surface-based modeling of the FSM is established on cartographic and interpreted subsurface data, which were integrated in a *SKUA®-2011* framework, resulting in a consistent model that honors the input data. The management of data and the main model-building tasks were realized as suggested by Caumon et al. [2009] and PARADIGM [2012]. The topographic

information was obtained from the SRTM 90 m digital elevation data freely provided by the International Centre for Tropical Agriculture [Jarvis et al., 2008]. The subsurface data were introduced picking the lithological contacts and faults from regional cartographic information [Dadlez et al., 2000, Pawlak et al., 2008, Oszczepalski and Speczik, 2011]. Interpreted cross-section from wells and seismic surveys [Wodzicki and Piestrzyński, 1994, Krzywiec, 2006, Mazur et al., 2010] were used to establish thicknesses and shapes of the main rock units (fig. 3.2).

3.3.2 Outcome FSM 3D Model

The resulting model covers a surface of over 31000 km^2 extending from the Fore-Sudetic Block to Świebodzin at north and Kluczbork at east. The vertical extension is down to 6.3 Km *mbsl* in the deepest part. The grid resolution used in the implicit modeling was about 2 km per 0.5 km horizontally and vertically respectively. 17 horizons from Cenozoic to the top of Precambrian rocks were created, corresponding to five main depositional periods: Upper Permian to Triassic, Triassic, Jurassic, Cretaceous and Oligocene to present day. The geometry of the FSM consists of gently northeast-dipping strata except for the sub-horizontal Cenozoic units. In general, the final model is similar to an inclined layer cake horizontally eroded in the upper part, lightly folded in the central region with a northeast strike fold axis (fig. 3.3). Finally, we extracted the surfaces that represent the top of the five main sedimentary units corresponding to: pre-Rotliegend, Rotliegend, Zechstein, Triassic, Jurassic, erosion Cretaceous-Paleocene and post-Oligocene. The top of the Cretaceous (today eroded) was extrapolated in agreement with the shape and morphology of the preserved units.

3.4 Detecting Fault Activity from Restoration

3.4.1 Restoration Goals

Restoration aims at reconstructing the original geometry from the current structural geometry. For example, in deformed sedimentary rocks restoration is used to find the original depositional state at a given time. The first attempts to restore a starting geometry were conducted more than 100 years ago by Chamberlin [1910] using an areal preservation criterion in cross-section analysis. Later, his concepts were extended in a volume constant criterion in foreland compressive belts by Dahlstrom [1969]. In the last decade, restoration methods integrating the mechanical properties of rocks have been proposed [De Santi et al., 2002, Maerten and Maerten, 2006, Moretti et al., 2006, Moretti, 2008, Guzofski et al., 2009, Durand-Riard et al., 2013]. Although it is proved that accounting for the rock mechanic parameters in the restoration offers greater precision and provides better accuracy for describing strain and stress fields [Durand-Riard et al., 2010, Vidal-Royo et al., 2012, Durand-Riard et al., 2013], 3D conformable mesh generation represents a significant challenge at large scale. Mesh generation is often time-consuming and requires a very large number of elements to honor fine-scale structural features, especially in complex faulted contexts [Moretti, 2008, Caumon, 2010, Durand-Riard et al., 2010, Botella et al., 2013]. Therefore in this work, we use simple geometric analysis to restore the layers to their original depositional states applying surface restoration (also called 2.5D restoration). In the next sections, we will explain the basis and methods of 2.5D structural restoration, focusing its scope in our purpose for detecting faults presence and estimating their activity.

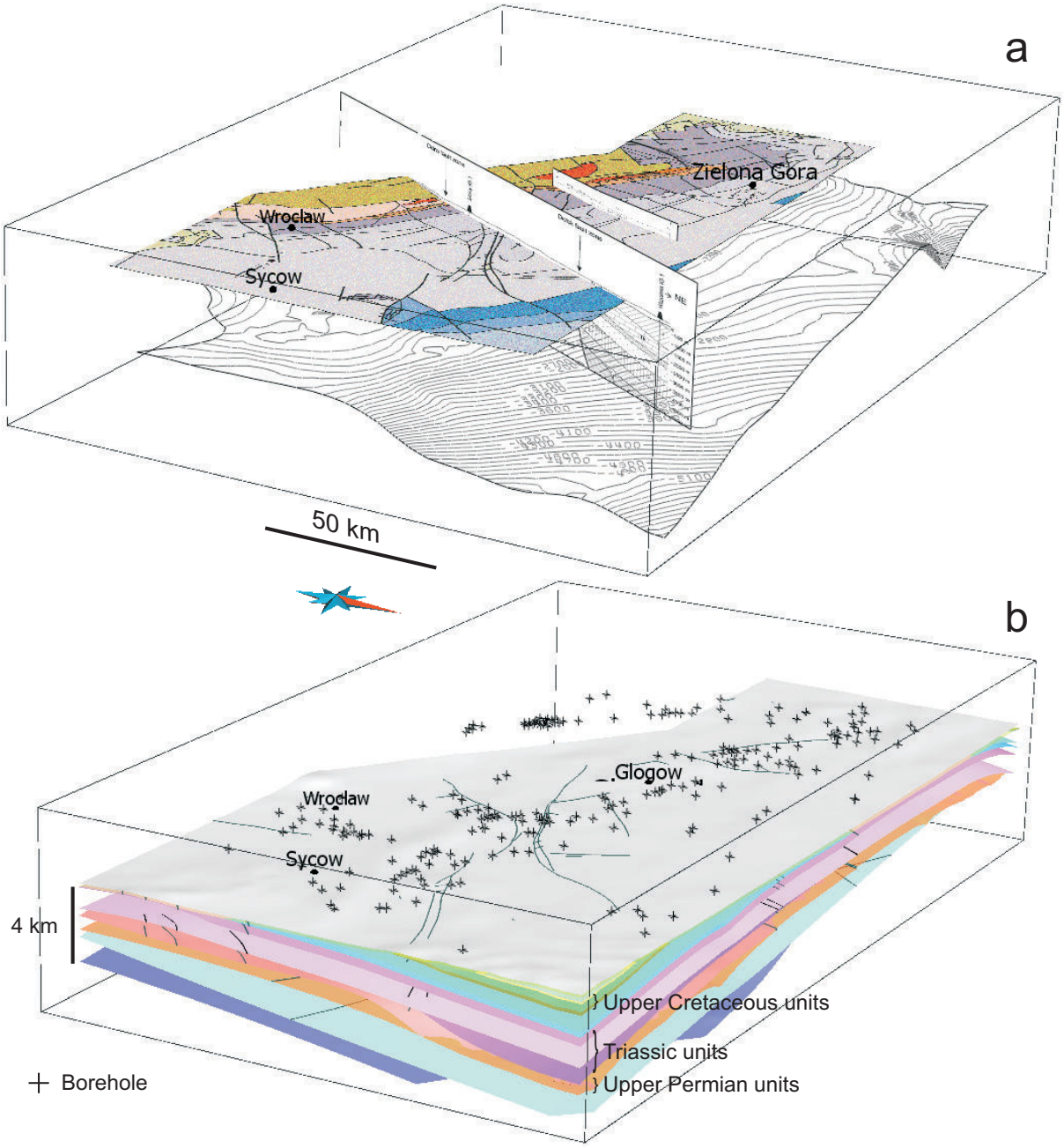

FIGURE 3.2 – Fore-Sudetic Monocline 3D model built using the *structure and stratigraphy SKUA®-2011* workflow. **a**: The input data comprise cross-sections, a regional geological map of the study area and the interpolated Kupferschiefer depth. The contacts and unit limits are introduced by picking both the map and the cross-sections (see section 3.3.1). **b**: The meshed domain necessary for the implicit modeling has a resolution of 2,000 m and 500 m horizontal and vertical respectively. The sedimentary units overlaying the pre-Triassic rocks are considered as conformable in the *structure and stratigraphy* workflow, except for the Post-Cretaceous units deposited upon the eroded Upper Cretaceous units. The Upper Permian units are considered deposited in baselap mode. The crosses represent the bore-hole locations from Oszczepalski et al. [1997].

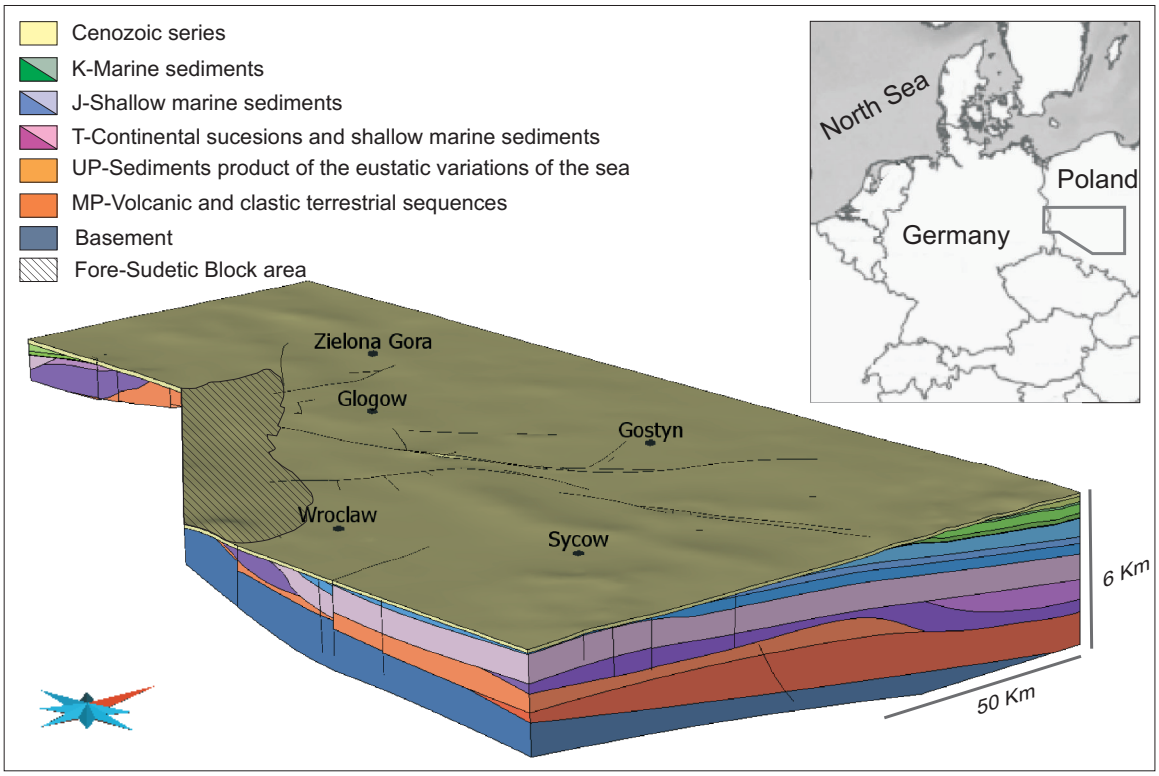

FIGURE 3.3 – Location of the study area and resulting model of the FSM.

3.4.2 Surface Restoration

The aim of 2.5D restoration is to remove fault slip and unfold the deformed surfaces. The unfaulting aims at matching the horizon cutoff lines on either sides of fault parts that compound a given surface. The simplest unfaulting procedure consists in a rigid-body displacement, generally acomplished by domino-block and circular-fault methods [Rouby, 1994, Groshong, 2006]. The unfolding intends to flatten a surface, considering that the continuous part of the surface can return to its original geometry following one of these methods:

Simple-shear: slip on closely spaced parallel planes [Verrall, 1981].
Flexural slip: slip parallel to bedding [Dahlstrom, 1969].

Because these concepts were initially defined in cross-sections, their applications to map restorations of faulted, and possibly non-developable surfaces, call for specific algorithms, among which are *triangle adjustment* [Gratier and Guillier, 1993], *extrapolation of parallel cross-sections* [Moretti et al., 2007] and *parameterization* [Mallet, 2002, Moretti, 2008]. In this work we applied *flexural slip*, which is achieved by *parameterization*, preserving the global area of folded and restored surfaces.

3.4.3 Iterative Restoration

In sequential-surface restoration, the horizons are restored iteratively from top to bottom. When a horizon is restored, the deformation is propagated to the underlying horizons [Mallet, 2002]. This implies that two parallel horizons are flattened at once when restoring the upper horizon only. If this is not the case, it probably means that a deformation event (or several) occurred before the deposition of the layer represented by the upper surface (fig. 3.4a). After

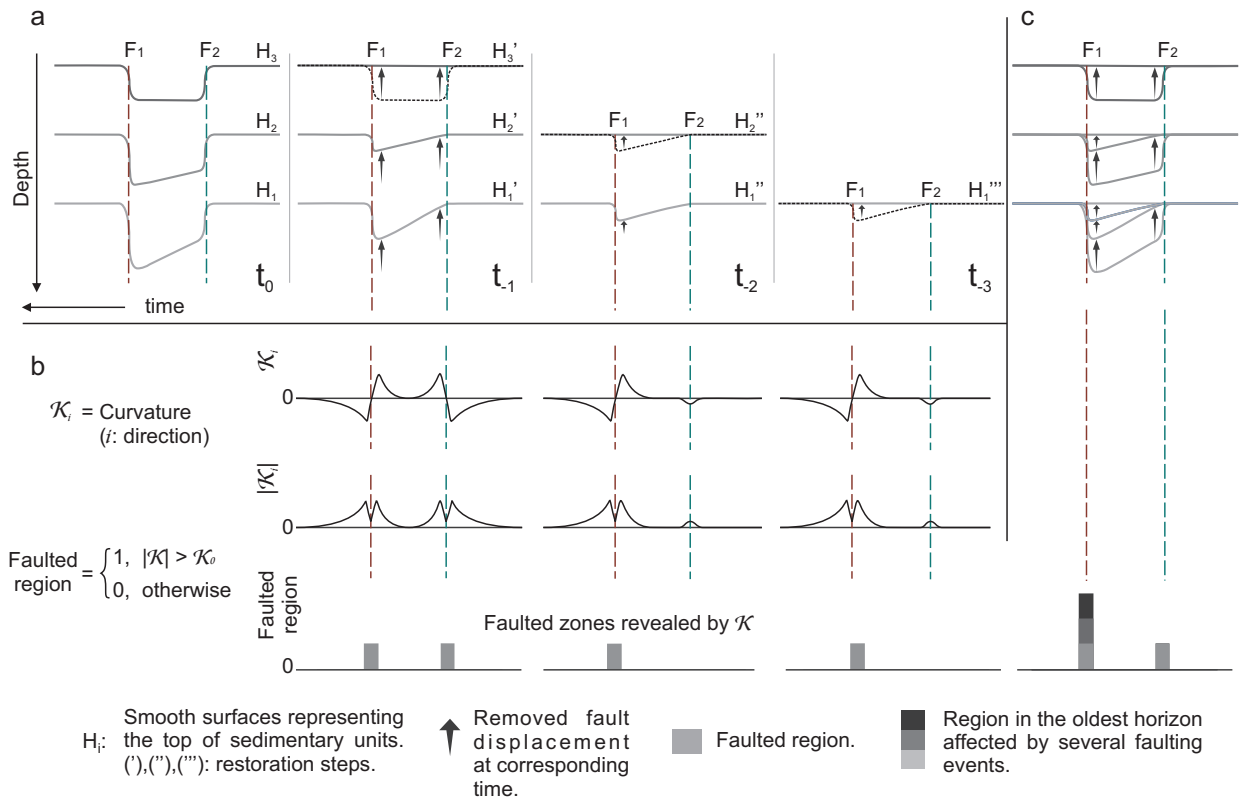

FIGURE 3.4 – Schematic surface-restoration workflow. **a**: The flattening of the upper surface removes the deformation caused by fault activity at the corresponding time. This flattening is propagated on the underlying surfaces. **b**: The curvature, obtained at each restoration step, is higher in the folded neighborhood than in the rest of the surface. **c**: For the overall restoration process, the regions affected by several faulting events are highlighted by high curvature values. In this example, the fault F_1 has been active for a longer period than the fault F_2.

removing the upper restored reference surface and decompacting the entire stack of sediments using an isostatic approach [Sclater and Christie, 1980], which is called back-stripping, sequential, deterministic, surface restoration is applied to simulate iteratively from youngest to the oldest sediment layer (fig. 3.5a). Although the iterative surface restoration cannot describe the detailed structural evolution of a study area, it is a useful method in the reconstruction of ancient structural stages [Moretti et al., 2007, Titeux, 2009].

3.4.4 Internal Deformation and Fault Activity

Although the main restoration aim is to get the original geometry at a given time, other outputs can be obtained during the unfolding and unfaulting. Three common outputs correspond to strain, dilation and curvature which account for the surface variations between deformed and restored geometry. The strain corresponds to the deformation tensor at each point of the reference surface before and after restoration. In 2.5D restoration, the strain considers only geometric deformation and does not generally reflect mechanical layering. The dilatation is the trace of the strain tensor and corresponds to the local area variation between the restored and the current geometry. Finally, curvature is a second order tensor defined on the surface. It is a static geometric measure corresponding to the inverse of the radius of all tangent circles orthogonal to the surface. If reveres, the direction in which the radius is

smaller corresponds to the maximum curvature, which relates to folding/faulting (fig. 3.4b). Assuming surfaces have the correct geometry, the curvature reveals high deformation zones in the horizons [Lisle, 1994, Roberts, 2001]. For each restoration step, the curvature analysis on a selected horizon highlights the most deformed regions at the corresponding geologic time. Other attributes from geometric analysis (e.g., curvature gradient using 3D seismic data [Gao, 2013]) can express high deformed areas related to faulting.

3.4.5 Continuous-Surface Representation

In our case study, the horizons have been represented as smoothed-continuous surfaces for two reasons:

Fault uncertainty: In the absence of direct fault observations, it could be hazardous to cut horizons with inferred faults. The aim of this work is to correlate mineralization process with fault activity. If we introduce an inferred fault that does not corresponds to the geologic record then the results will be biased. Wrong modeled faults can be the product of a bad interpretation, missing data or presence of noise in the raw data [Cherpeau et al., 2010]. Instead, it is possible to represent the horizons as smoothed continuous surfaces and then using geometric attributes to detect fault activity (see previous section) (fig. 3.4c).

Forced-extensional folds: Normal extensional faulting in the basement may develop folding in the sedimentary cover [Finch et al., 2004]. This is especially observed when a salt layer above the basement introduces a mechanical decoupling between the basement and the overlying rocks [Withjack et al., 1990, Withjack and Callaway, 2000]. This is the case in the Fore-Sudetic region, where the thick evaporite-rich Zechstein Formation is deposited directly above the basement (see fig. 3.1 and Sec. 3.3). In the FSM, the present day known faults in the cover may correspond to active basement faults. In early to medium stages of the structural evolution of the region, the faulting in the basement could develop forced extensional folding rather than faulting in the above layers. Examples of salt-related folding due to Zechstein presence have been documented in several locations of Europe [Krzywiec, 2006, Kane et al., 2010, Duffy et al., 2013].

For these reasons, we adress the problem of detection of fault zones in the basement and their time activity by studying the internal deformation in the cover horizons represented as continuous surfaces (fig. 3.5b).

3.4.6 Restored Models

The restoration of the FSM is achieved as a multi-sequential surface flattening. Taking as reference the horizon at the top of the stack, an unfolding procedure is applied on the hanging wall of this horizon, thus obtaining the field of restoration vectors for this horizon. Then, the deformation on the stack is achieved applying the field of restoration vectors on the bottom horizons. Finally, the top layer is removed and the unfolding process starts again [Mallet, 2002]. We chose the flexural slip method KINE3D-2®, available in *SKUA*, looking for preserving thickness and the global area of the layers. After each restoration step, we decompacted the sedimentary units applying the methodology suggested by Sclater and Christie [1980]. A total of six restoration routines were realized using the KINE3D-2® workflow. During the restoration, some surface inconsistencies (e.g. unrealistic folding, wrong thickness variations, underlying horizons crossing upper horizons) are adjusted manually. In practice, the structural restoration is an iterative process which imposes eventually the reconstruction of the initial surface model attempting to correct these inconsistencies. It was achieved by modifying the

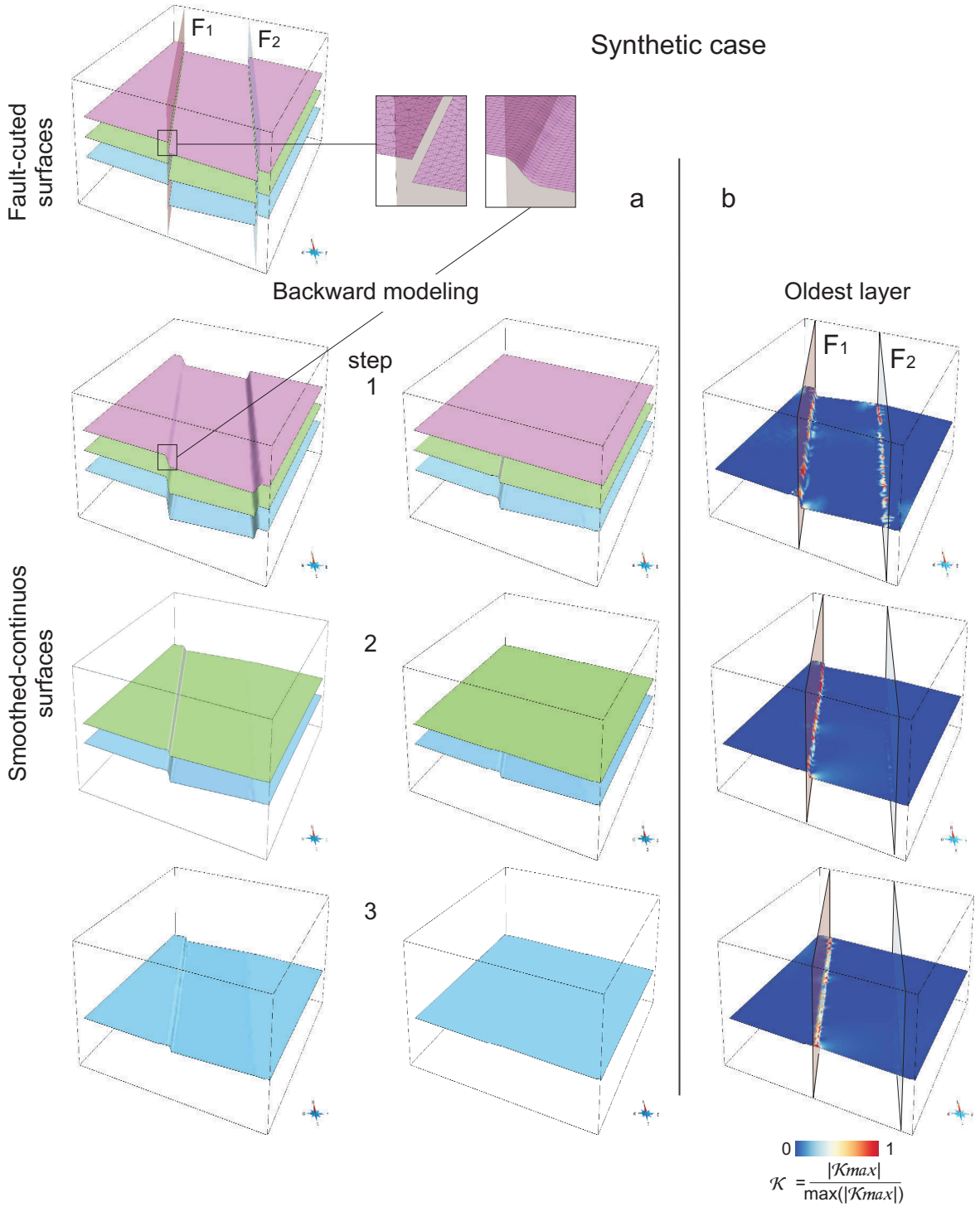

FIGURE 3.5 – Synthetic case of structural restoration. **a**: The faulted horizons are represented by smoothed-continuous-triangulated surfaces. After flattening, the upper restored horizon is removed and the restoration process starts again. **b**: The high $Kmax$ values, stored in the nodes of the oldest layer, reveal the fault activity. The fault F_1 starts its activity before the deposition of the middle layer, contrary to fault F_2 whose activity is evidenced only after the deposition of the middle layer.

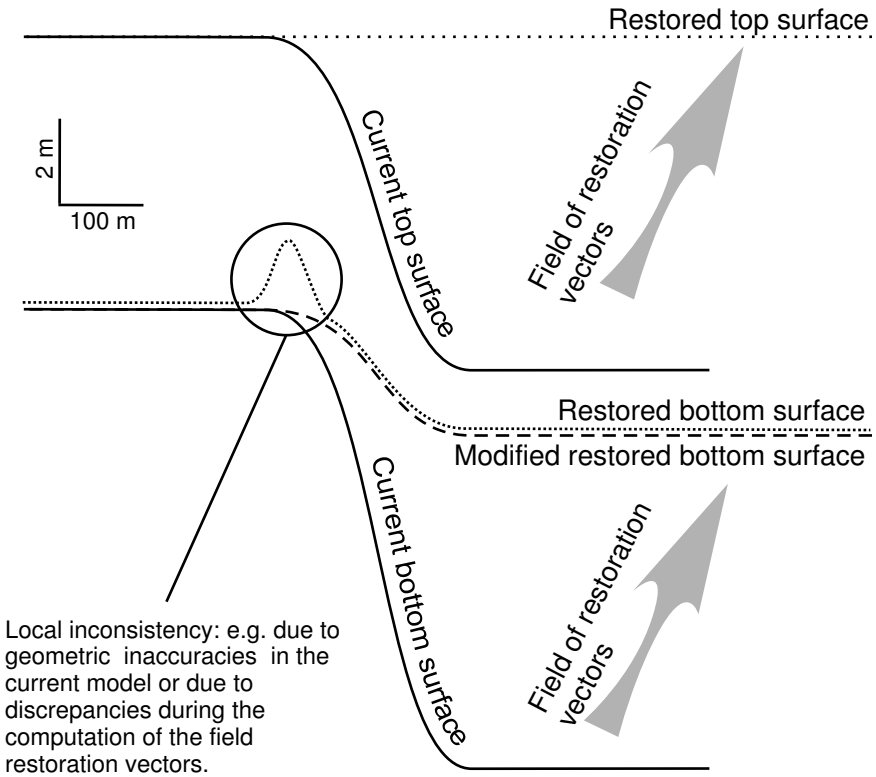

FIGURE 3.6 – Cartoon showing some discrepancies that may arise in the unflattened surfaces for a given restoration step. These discrepancies are corrected before starting a new restoration routine on the remaining horizons.

initial surface shapes honoring the input data. These corrections are performed before making any new restoration operation (fig. 3.6).

3.4.7 Restoration Outputs

For each of the five restoration outputs simulating the main depositional phases (Cenozoic, Cretaceous, Jurassic, Triassic and Upper Permian), we obtained the restoration vectors, the strain tensor, the dilatation and the curvature. We defined the variable K as the ratio of: the maximum curvature found in the mineralized horizon ($K_{max} = max(K_i, K_j)$, i, j orthogonal main directions) as positive values ($|K_{max}|$), and the maximun value of $|K_{max}|$ over the surfaces. The more deformed areas are then highlighted as function of the K magnitude between **0** and **1** (fig. 3.7).

3.5 Curvature and Cu Assessments

3.5.1 Potentials Assessments and Predictors Variables

In mineral potential modeling, the analytical or empirical relationships between descriptive features and a mineral target express the possibility to predict a given mineral concentration in a location as function of descriptive features (see for example Bonham-Carter et al. [1989], Agterberg et al. [1993], de Quadros et al. [2006], Cheng [2008], Zuo and Carranza [2011],

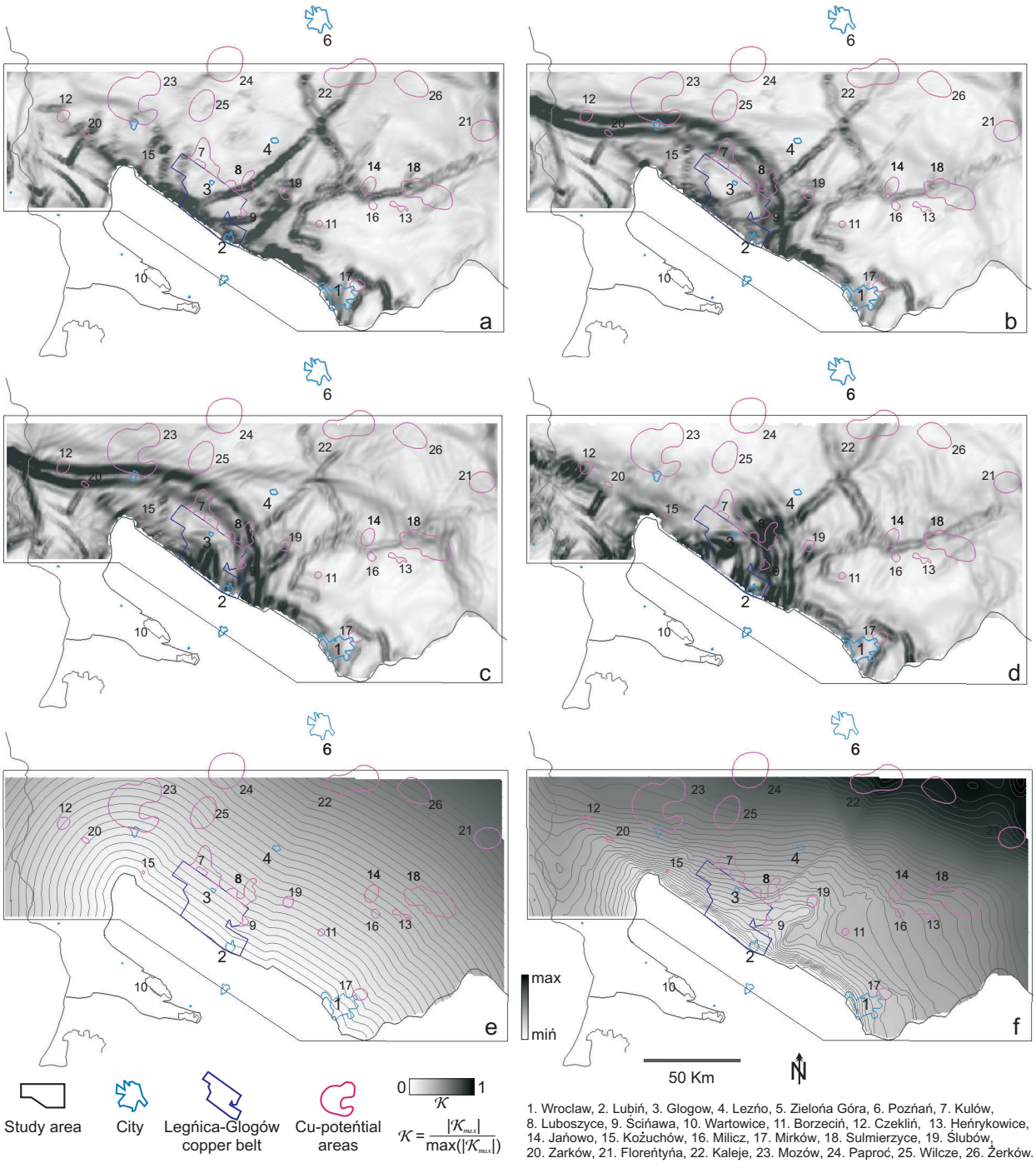

FIGURE 3.7 – Maximum curvature corresponding to each restoration step from Cretaceous to Upper Permian. **a**: Cretaceous, **b**: Jurassic, **c**: Triassic and **d**: Upper Permian. **e**: Horizontal distance to Fore-Sudetic Block. **f**: Depth of the Zechstein base at Late Cretaceous. Some locations related to mining activities are highlighted. Cu-potential areas from Oszczepalski and Speczik [2011] are the result of several exploration programs accounting for more than 370 archival boreholes outside of the LGCB district.

Schaeben [2012]). Let evidences denote the set of observed features that are directly related to the mineralization process (e.g., the mineral alterations in rocks during a hydrothermal event, or the sorting of heavy-minerals grains during a depositional process). And let geo-variables denote the set of features that control the system during the mineralization (e.g. pressure, temperature, pH, Eh). Then, in principle, it is possible to build a potential model for a given mineralization integrating (as predictor variables) evidences and geo-variables in terms of multivariate statistical analysis [Agterberg et al., 1993, Kerrich, 1993, de Araújo and Macedo, 2002]. Several mathematical methods are available to accomplish this, logistic regression (LR) being one of the most employed. Compared to other popular methods (e.g. weight-of-evidence), LR has the advantage of deal properly with respect to conditional independence assumptions and works both continuous and discrete variables [Schaeben, 2013, 2014]. Specifically, the LR determines a relationship between the linear combination of evidential predictor variables and the logit-transformed conditional mean using the logit transform as link function (eq. 3.1) [McCullagh and Nelder, 1989]:

$$\begin{gathered} log(Odds) = \beta_0 + \beta_l x_1 + \beta_2 x_2 +, ..., +\beta_m x_m \\ x_{1m} : \{predictors\} \\ \beta_{0m} : \{coefficients\} \end{gathered} \tag{3.1}$$

Thus, using the curvature as a predictor variable in LR analysis, it is possible to test the relevance of this restoration output in Cu-potentials predictive models.

3.5.2 Cu Potentials and Selected Predictors

We digitized the Cu-potential areas reported by Oszczepalski and Speczik [2011] in Lower Silesia, including the Legnica-Głogów Copper Belt district. These areas are based mainly in Cu-Ag grades observed in several exploration programs (e.g. *Metallogenic Atlas of the Zechstein Copper-bearing Series in Poland*) accounting for more than 370 archival boreholes outside of the LGCB district [Oszczepalski et al., 1997, Speczik et al., 2007]. Subsequently, we created a binary attribute corresponding to **1** for the highest potentials and **0** for the rest. According to the above ideas, we generated LR predictive models using the logits of these higher Cu- potentials. The K, estimated in the mineralized horizon after each restoration step, is added in the predictive models. The curvature of the Top of Cenozoic restoration was not taken into account because it is posterior to the mineralization. Thereby, four predictor variables $K_{l=0}$:4 (l: restoration step from Cretaceous to Upper Permian) have been integrated in the LR models. Looking to obtain more accurate predictions, we added two other variables in the analysis: the horizontal distance from the Fore-Sudetic Block (HFB) and the depth of Zechstein base at Late Cretaceous (ZBK), both as continuous predictor variables. These two attributes were selected among other continuous variables (e.g. distance to current faults, layer thickness, restored depths) due to their good correlation coefficients (0.430 and 0.339 respectively) with the Cu distribution showed by Oszczepalski et al. [1997]. The LR models for Cu-potentials taking individually each selected predictor is shown in Tables 3.1 and 3.2 and fig. 3.8.

3.5.3 LR Models by Predictor

The LR models for the curvature show that the high curvature values, obtained at each restored time, increase the *log Odds* of having a Cu-potential locality (versus not having a Cu-potential locality). These positive coefficients obtained by the K models indicate a

TABLE 3.1 – LR model by restoration step curvature.

Curvature at restoration step	Model parameters	Estimate	Std. Error	z value	Pr(>|z|)
Cretaceous	Intercept	-2.1238	0.0126	-168.51	0.0000
K_1	coefficient	1.8593	0.1397	13.31	0.0000
Jurassic	Intercept	-2.1284	0.0125	-170.37	0.0000
K_2	coefficient	2.3498	0.1630	14.42	0.0000
Triassic	Intercept	-2.2602	0.0131	-172.59	0.0000
K_3	coefficient	3.6023	0.1147	31.40	0.0000
Upper Permian	Intercept	-2.3008	0.0132	-174.76	0.0000
K_4	coefficient	4.4837	0.1196	37.48	0.0000

The z-values with the associated p-values correspond to Wald z-statistic. The resulting p-values indicate that the null-hypothesis can be rejected, and therefore each predictor individually is statistically significant in the predictive model for Cu-potentials (for more details about the significance test of predictors see Hosmer Jr and Lemeshow [2004]).

TABLE 3.2 – LR model by complementary predictors.

Complementary predictors	Model parameters	Estimate	Std. Error	z value	Pr(>|z|)
HBF	Intercept	-1.5656	0.0188	-83.17	0.0000
	coefficient	-0.0092	0.0003	-27.44	0.0000
ZBK	Intercept	-1.4691	0.0508	-28.90	0.0000
	coefficient	-0.1360	0.0122	-11.19	0.0000

positive link between the deformation in the horizons, highlighted by the curvature, and the Cu-potentials zones defined by Oszczepalski and Speczik [2011]. Another tendency is observed in relation to the restoration steps, where the coefficient obtained for K increases by restored time. This trend is readily observable in fig. 3.8 where the predicted probabilities increase by geologic-time-restoration step. On the contrary, the negative coefficients for the distance *HFB* and the depth *ZBK* show that the *log Odds* to have a Cu-potential location (versus non Cu-potential) decrease where these variables increase.

3.5.4 Predictive Model and Conditional Independence

Attempting to build a general predictive model of Cu-potentials with the above predictors, we integrated all predictors in a single LR model. Because $K_{(1,2,3,4)}$, *HFB* and *ZBK* appear to be mutually dependent conditionally to Cu-potentials (fig. 3.9), the interaction terms for them are integrated as predictors trying to yield the true conditional probability [Schaeben, 2014, 2013, Schaeben and Schmidt, 2013]. Table 3.3 corresponds to the LR predictive model integrating all predictors and significant interaction terms. The resulting LR general model was applied in the study region, thus obtaining the predicted probability map for Cu-potential locations (fig. 3.10.)

3.6 Perspectives

The high curvature values obtained during all the restoration steps match locally with known mineralized zones. The most important correlations correspond to the present day exploitation area of LGCB, and also in the adjacent Cu-potential locations of Luboszyce, Ścinawa and Ślubów. Other Cu-potential areas that seem related to high curvature for all restoration steps are: Mirków, Sułmierzyce, Czeklin and Kożuchów. The areas of Janowo, Kaleje and Florentyna are related to the high curvatures found in the of Upper Permian (Top Zechstein) and Cretaceous restored steps. In the Milicz area, good potential may exist in the northern part (fig. 3.7).

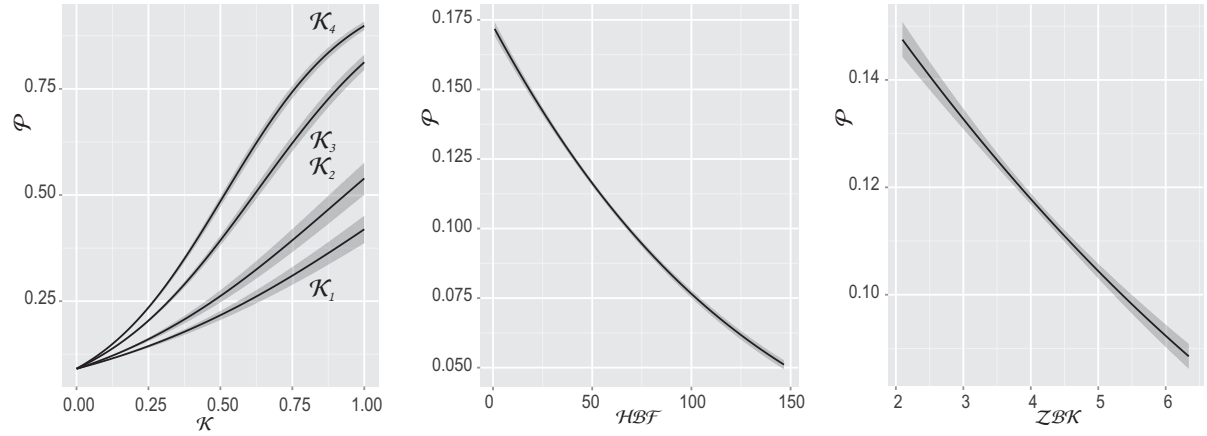

FIGURE 3.8 – Predicted probabilities from the LR models by predictor. Each image corresponds to the predicted probability of having a Cu-potential location according to the predictor individually (*HFB* and *ZBK* in km)

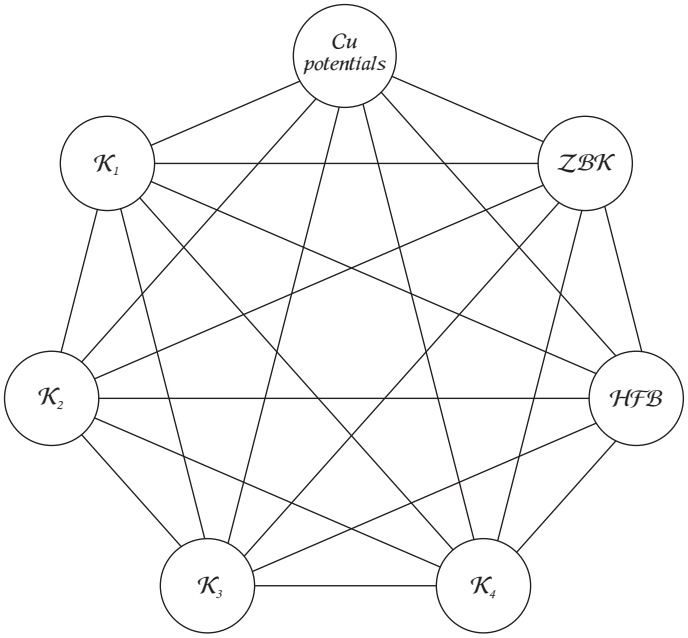

FIGURE 3.9 – *Graph* of the conditional independence test for K_l (l=1: Cretaceous, 2: Jurassic, 3: Triassic, 4: Upper Permian), *HFB* and *ZBK* given Cu-potentials. Each arc represents the lack of the conditional independence for the predictors in the corresponding nodes. For the test we used the *bnlearn-R* package (for more details about the conditional independence test see Scutari [2010])

TABLE 3.3 – LR model coefficients with significant interaction terms.

	Estimate	Std. Error	z value	Pr(>|z|)
(Intercept)	-9.6360	0.2061	-46.74	0.0000
K_1	57.9567	2.6291	22.04	0.0000
K_2	-154.8190	6.9061	-22.42	0.0000
K_3	101.7225	4.2253	24.07	0.0000
K_4	60.7357	2.2193	27.37	0.0000
HFB	-0.1236	0.0030	-40.89	0.0000
ZBK	2.6126	0.0560	46.62	0.0000
HFB*ZBK	0.0100	0.0005	20.36	0.0000
K_1*K_2	38.3345	6.0877	6.30	0.0000
K_1*K_3	-35.0253	5.4303	-6.45	0.0000
K_1*K_4	-31.4186	2.7922	-11.25	0.0000
K_1*HFB	0.4292	0.0262	16.36	0.0000
K_1*ZBK	-19.2036	0.8572	-22.40	0.0000
K_2*K_3	-16.2740	3.0681	-5.30	0.0000
K_2*K_4	27.5323	6.4375	4.28	0.0000
K_2*HFB	-0.8229	0.0576	-14.29	0.0000
K_2*ZBK	44.2964	2.0726	21.37	0.0000
K_3*K_4	-38.5078	4.1089	-9.37	0.0000
K_3*HFB	0.5444	0.0389	14.01	0.0000
K_3*ZBK	-28.3073	1.3762	-20.57	0.0000
K_4*HFB	0.5212	0.0246	21.22	0.0000
K_4*ZBK	-18.9501	0.7905	-23.97	0.0000

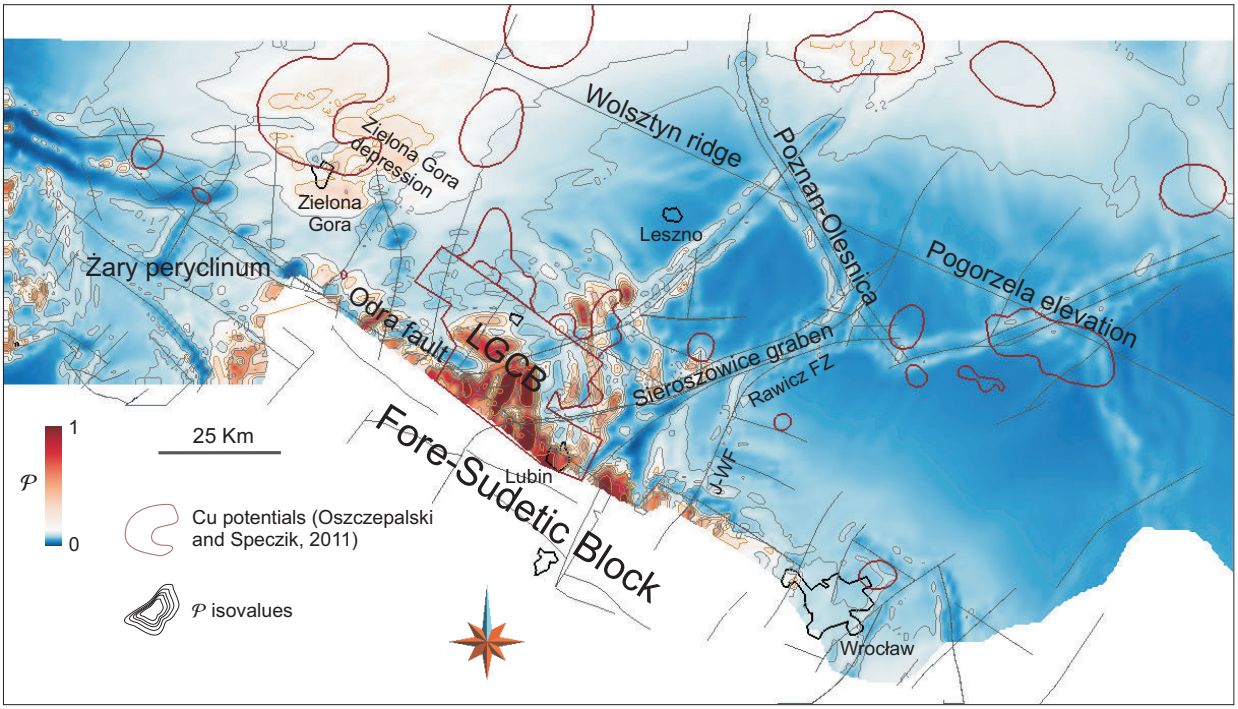

FIGURE 3.10 – Predicted probabilities of Cu-potentials (P) in the FSM. Some main structures and Cu potential locations are highlighted. The match between high P and the Cu-potential areas are close to main regional structures as the Pogorzela elevation, the Sieroszowice graben and the Odra fault system among others.

TABLE 3.4 – Restoration steps, geodynamic setting and high curvature in Cu-potential areas.

Restoration step	Estimated age (Ma)	Tectonic process	Geodynamic setting	Cu-potential area*
Upper Permian–Early Triassic	256±6 Paleomagnetism Jowett et al. [1987] (Study area)	Ending tectono-magmatic pulses. Rapid subsidence.	Ending Variscan orogeny. Opening Tethys sea.	Luboszyce, Scinawa, Czeklin, Kożuchów, Kaleje, LGCB.
Late Triassic–Early Jurassic	190 to 216 K-Ar illite Bechtel et al. [1999] (Study area)	Subsidence, extensional tectonics.	Rifting phase.	Luboszyce, Czeklin, Slubów, Zarków, Mozów, Wiłcze, LGCB.
Late Jurassic–Early Cretaceous	163.7±3.8, 158.8±3.6 K-Ar illite Michalik [1997] (Fore-Sudetic Monocline)	Increasing subsidence rates, extensional tectonics. Late Jurassic uplift.	Arctic–North Atlantic rifting. Late Jurassic basin inversion.	Luboszyce, Scinawa Czeklin, Zarków, Mozów, LGCB.
Late Cretaceous–Early Paleocene	53.3±3 Paleomagnetism Symons et al. [2011] (Sangerhausen, Germany)	Uplift.	Alpine-related basin inversion.	Janowo, Kożuchów Milicz, Sułmierzyce, Slubów Zarków, Kaleje Mozów, LGCB.

* According to Oszczepalski and Speczik [2011]

For the Triassic restoration step, the distribution of high curvature values shows strong differences in relation to the Permian restoration step. Outside of LGCB, the high curvature values are found in the regions of Żary Pericline and Zielona Gora depression. The Cu-potentials areas of Kulów, Wilcze and Zarków appear linked to the increase in curvature values for this restoration step (fig. 3.7c). On the contrary, Triassic and Jurassic restoration steps show a similar feature in the obtained curvature, except for the LGCB and Sułmierzyce areas. (fig. 3.7 b, c). The Cretaceous restoration step gives high curvature values on the central part of the study area and close to the border with the Fore-Sudetic Block. The Paproć and Borzęcin areas present similar curvature values and distribution as in the Jurassic step.

In relation with deformation stages, mineralization and Cu-enrichment times, the Odra Fault system may have played a significant role during the Late Permian and Cretaceous at locations such as the LGCB, the north part of the Żary Pericline, and in the Wrocław proximity (fig. 3.7 d and fig. 3.10). On the contrary, fault systems associated to the Pogorzela elevation seem to have controlled the Cu mineralization during the Triassic. The Cu-potentials on the Zielona Góra depression suggest a link to active structures during the Triassic and Jurassic and less strongly during the Cretaceous (fig. 3.7d, c and b). Finally, the Cretaceous restoration step indicates a relationship between the fault systems of Sieroszowice graben with proximal potential areas for this period (fig. 3.7a and fig. 3.10).

Several attempts have been made to determine the age of the Kupferschiefer mineralization (e.g. Jowett et al. [1987], Michalik [1997], Bechtel et al. [1999], Symons et al. [2011]). The wide range of different ages obtained in those and similar works (from Late Permian to Early Paleocene) have been explained in terms of multi-stage mineralization process [Speczik, 1995]. The curvature obtained at each time-restoration step reveals a strong spatial correlation between the high curvature values and Cu-potentials. This association between high curvature and Cu-mineralization/enrichment could help in the understanding about timing and structural mechanisms involved in the ore formation. Table 3.4 presents synthetically the geodynamic setting, the dominant tectonic process that occurred in the region and the Cu-potential areas having high curvature values for the corresponding restoration step. The method exposed in this work may improve metallogenic models for this kind of ore-deposit, relating the geodynamic evolution, fluid pathways, and mineralized areas.

3.7 Discussion

In this work we decided to represent the horizons overlying the Zechstein Formation as continuous surfaces, assuming that the different tectonic events that occurred before the Alpine

orogeny have caused folding rather than faulting in these horizons. The resulting surface geometry depends on the interpretive points used as input data for the 3D modeling, on the way interpolation is done between these points and on the mesh resolution used to represent the surface. All three elements are potential sources of uncertainty and inaccuracy in the final structural geometry, which could possibly affect the potential mapping results. More precisely, we used discrete smooth interpolation (DSI) [Mallet, 2002] for creating these continuous triangulated surfaces. In DSI, the nodes of the triangular mesh are placed so as to minimize data misfit and roughness (Laplacian). Given the data spacing and the chosen surface resolution, we consider that the interpolation error due smoothing is minimal. The error due to the limited surface mesh resolution is probably more significant in high-curvature areas. Consequently, the detection of fault activity using curvature analysis may be under-estimated due to the limited surface mesh resolution. In the final potential map, this means that basement faults having a slight displacement may remain undetected due to negligible curvature in the overlying horizons. This effect could easily be mitigated by refining the mesh in the neighborhood of the faults [Caumon et al., 2009].

In this study, we nonetheless chose a constant resolution to avoid overfitting effects. Indeed, we believe the main source of uncertainty in the results stems from the depth maps and interpreted seismic sections used for the structural modeling. The geometry of these "data" and of the associated the fault locations is well constrained close to boreholes but is obviously more uncertain in sparsely drilled areas. Structural uncertainty assessment methods [Wellmann et al., 2010, Cherpeau et al., 2010] could be used to address these sources of uncertainty. In the present study, we consider that bias due to possible interpretation errors may be present in areas with low borehole density, especially in the north-eastern and south-eastern parts of the study area (fig. 3.2b).

The map of predicted probabilities for Cu-potential areas using the curvature values with the interaction terms (fig. 3.10) shows several regions with medium to high potentials. The predictive model applied to obtain this map only considers geometric parameters relating fault systems that may have played a role with the Kupferschiefer formation. However, the Kupferschiefer ore creation has involved other factors such as the passage of metalliferous solutions [Oszczepalski, 1999], the amount of organic matter present in the Kupferschiefer Formation [Bechtel et al., 2001a, Gouin, 2008] and the presence of meteoric recharge systems [Brown, 2011], among others. In this sense, a predictive model accounting only for structural parameters is necessarily incomplete. This last may explain the divergences existing in some areas having high curvature values but without a known Cu-potential area. Future work could, therefore, consider these other sources of information as additional predictor variables (if they can be extrapolated with limited uncertainties) or as a means to locally test the predictability of the proposed potential model.

3.8 Conclusions

The curvature from the FSM restoration is related geographically to the Cu-potential areas established in previous works. This relation probably expresses the impact of fault systems active during the mineralization process. Upward migration of thermal fluids along deep faults and damaged areas in the rocks mass could directly influence the Cu-sulfides formation. The Cu distribution patterns in the FSM were caused by the variation of the stress regime during the tectonic evolution from Late Permian to Late Cretaceous. The Odra fault system has controlled the mineralization at Late Permian times, but during the Triassic and Jurassic other fault-systems ruled the mineralization, especially the faults related to the Pogorzela

elevation, the Sieroszowice graben and the Zielona Góra depression.

The utility of curvature as predictor variable is evidenced from the LR analysis, completing the set of structural parameters also obtained from the restoration modeling. We believe that the above ideas and methods can be applied in similar cases where the fault system are sealed by an impermeable cap and the occurrence of hot brines expulsion events from the basement.

Acknowledgments

This work has been performed in the frame of the Gocad research project. We thank the industry and academic members of the Gocad Research Consortium [1] for supporting this research. We also thank Paradigm for the Gocad software. We appreciated the collaboration of Clementine Fourrier (Université de Lorraine). We also thank Piotr Krzemiński (Mozów Copper SP z o.o.) for his comments and remarks which helped improving this paper. Finally, our special thanks go to Laurent Ailleres (Monash University) and Tobias Bauer (Luleå University of Technology) for very helpful observations and discussions. Part of the above research received funding from the European Union's Seventh Framework Program under grant agreement n°228559 (ProMine Project), and was performed in the framework of Investissements d'avenir **Labex** RESSOURCES21 (ANR-10-LABX-21).

1. http://www.gocad.org/w4/index.php/consortium/members

Chapitre 4

Using strain parameters from 3D restoration to estimate distant off-fault gold potentials, Mount Pleasant Area, Western Australia

Sommaire

4.1 Introduction . . . 62
4.2 Evolution of Rocks Properties . . . 62
4.3 Mount Pleasant Gold System . . . 64
4.3.1 Geological Settings . . . 64
4.3.2 Mineralization . . . 65
4.4 3D Mechanical Restoration . . . 65
4.4.1 Mount Pleasant Region Modeling . . . 65
4.4.2 3D Geomechanical Restoration . . . 65
4.5 Gold Occurrences and Distant Off-fault Damage . . . 69
4.6 Discussion . . . 69

A preliminary version of this research has been presented as a conference paper at the 34^{th} Gocad Meeting [Mejía-Herrera et al., 2014a].

Abstract

A broad variety of gold-deposits are related to fault systems developed during a deformation event. Such discontinuities control the metals transport and allow the relatively high permeability necessary for the metals accumulation during the ore-deposits formation. However, some gold deposits formed during the same deformation event occur at locations far from the main faults. In those cases, the fracture systems are related with the rock heterogeneity that partially controls the damage development on the rock mass. We used geomechanical restoration to simulate the strain developed during a shortening episode occurred in the Mount Pleasant region, Western Australia, and show how the rock heterogeneity allows damage in locations far from the fault systems. The distant off-fault damage areas are located preferentially in lithological contacts and also follow the deformation trend of the region. We show that off-fault zones with high density gold occurrences correlate spatially on locations with locally-high-gradient first deformational parameter, obtained from the restoration strain field.

This contribution may provide the explanation for the presence of gold accumulations away from main fault systems. The method could be used for inferring favorable areas in exploration surveys.

4.1 Introduction

Gold deposits within the Yilgarn Craton are related mainly with faulting, fracturing and damage areas occurred during the latest stages of an Archean orogenic event that affected the entire craton [Witt and Vanderhor, 1998]. In these gold-deposits exist several elements favorable to the formation of major gold deposits, such as diverse Au sources, facilities in fluid transport and effective Au deposition mechanisms [Phillips et al., 1996]. Nevertheless, the structural feature is one of the main factors that control the gold distribution in Yilgarn Block [Phillips et al., 1996, Witt and Vanderhor, 1998, Groves et al., 2000]. Recent works have tried to establish predictive models of gold deposits in the Mount Pleasant area, within the Yilgarn Craton (fig. 4.1), exploiting the well-known structural setting of the gold deposits. From the analysis of deformation, stress and damage in the host rocks, predictive maps pointing potential areas have been proposed [Micklethwaite and Cox, 2004, Sheldon and Micklethwaite, 2007, Zhang et al., 2012, Moir et al., 2013] . Those works, most of them performing a 2D approach, have successfully emphasized the relationship between deformation, rock properties and Au occurrences. The change of the strain type results in the variation of the rock properties, which favors the development of damage or healing in the mass rock [Lyakhovsky et al., 1997a,b]. In this contribution, we propose to use 3D geomechanical restoration to obtain the strain values for inferring the deformational parameters (ξ and ζ) that express the strain types. During a shortening episode related to the Archean orogenic event, the stress reverses from compression to tension (or vice-versa depending of the location), affecting the rock properties and generating damage zones. The presumed distant off-fault damaged areas obtained by this approach are compared with locations having strong Au occurrences on the fracture-hosted deposits system in the Mount Pleasant area.

4.2 Evolution of Rocks Properties

We based our investigation on the continuum damage model proposed by Lyakhovsky et al. [1997a,b]. This approach is applicable to rock masses with a large number of cracks that allow quantitative description through properties of the crack distribution rather than those of the individual cracks [Finzi et al., 2011]. The damage rheology model states that the strength degradation due to crack formation and opening can be simulated as function of the rock properties and the deformation type. To account for the evolution of the rock properties, the deformational parameters ξ and β are introduced and make the elastic moduli a function of the strain type as follows:

$$\begin{aligned} \lambda^e &= \lambda - \gamma\frac{\beta}{\xi} \\ \mu^e &= \mu - \gamma\beta^2 - \gamma\beta\xi \end{aligned} \tag{4.1}$$

Where λ and μ are the Lamé parameters of linear Hookean elasticity, $\xi = I_1/\sqrt{I_2}$ is the first deformational parameter ($I_1 = \mathscr{E}_{11}+\mathscr{E}_{22}+\mathscr{E}_{33}$ and $I_2 = \mathscr{E}_{11}^2+\mathscr{E}_{22}^2+\mathscr{E}_{33}^2$, $\mathscr{E}_{ii}$ being the eigenvalues of the elastic strain tensor), γ is a third elastic modulus that describes the strain energy of a damaged material, and β is maximum value of the three roots of:

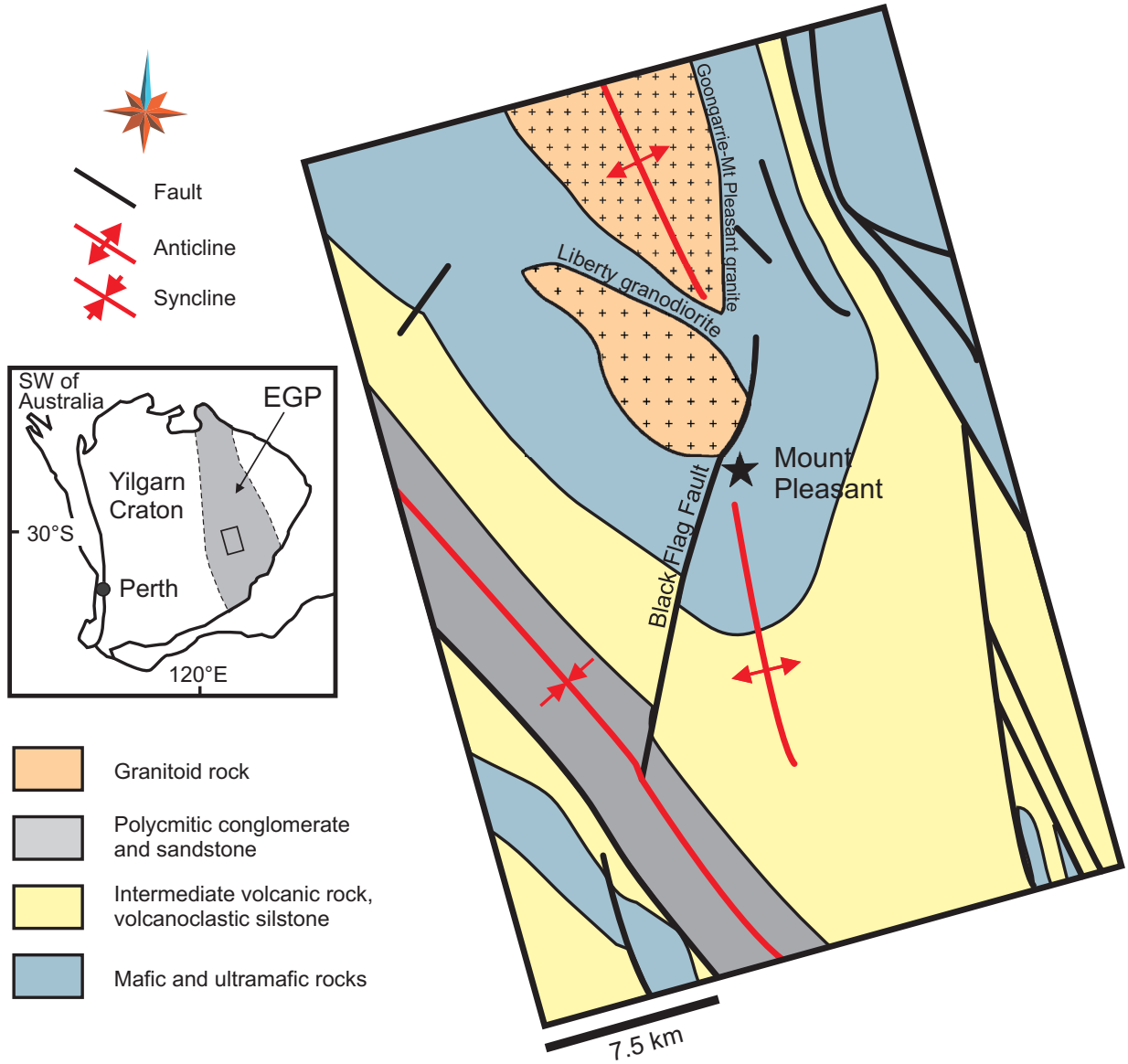

FIGURE 4.1 – Simplified geologic map of the Mount Pleasant area. The study area is located in the Kalgoorlie Terrane, Eastern Goldfields province (EGP). Modified from Wyche [1993] and Mickleth-waite and Cox [2004].

$$x^3 - \frac{1}{2}x(1 - \frac{1}{3}\xi^2) - (\frac{1}{6}\xi - \frac{5}{54}\xi^3 + \zeta) = 0 \tag{4.2}$$

Where $\zeta = I_3/(I_2\sqrt{I_2})$ is the second deformational parameter ($I_3 = \mathscr{E}_{11}\mathscr{E}_{22}\mathscr{E}_{33}$) [Lyakhovsky et al., 1997b]. The expression of the effective elastic moduli $(\lambda, \mu)^e$ in the equation 4.1, shows that degradation of the rock properties resulting by damage can be estimated from the analysis of the deformation type using the strain tensor and assuming initial values for the elastic moduli.

4.3 Mount Pleasant Gold System

4.3.1 Geological Settings

The Mount pleasant area is located 30 km at NW of Kalgoorlie, Western Australia, within the Archean Yilgarn Craton. The gold deposits in the Yilgarn Craton are considered as a late-orogenic (aprox. 2.63 Ga), structurally controlled, single class, but showing a wide variety of host rocks, structural styles and alteration characteristics [Witt and Vanderhor, 1998, Groves et al., 2000]. The geology in the Mount Pleasant area consists of a variable succession of mafic-ultramafic volcanic rocks, felsic volcano-sedimentary materials, felsic-intermediate porphyry type intrusions and differentiated mafic-ultramafic intrusions. These Archean rocks were deformed during a regional ENE-WSW shortening, and as a result it generates a succession of NNW trending anticlines-synclines, overthrust and shear zones [Wyche, 1993, Phillips et al., 1996, Groves et al., 2000].

4.3.2 Mineralization

The gold mineralization system in the Kalgoorlie greenstone terrain is the product of several hydrothermal events at different times relative to the regional structural sequence, but they show similarities in conditions of formation and mineralization style. The ore is hosted mainly in mafic volcanic and intrusive rocks. The mineralization temperatures at Mount Pleasant location are in the range of 250–350° being constrained by alteration assemblages, fluid inclusion and isotopic constraints [Cassidy and Bennett, 1993, Micklethwaite and Cox, 2006]. Three distinct and successive stages of hydrothermal activity and late quartz-carbonate veining resulted in multiple veining and/or brecciation. This brittle-fractures hosting the mineralization are linked to short, small displacement faults and shear zones [Gebre-Mariam et al., 1993], as well as in the weathering profile derived from underlying veins [Moir et al., 2013].

4.4 3D Mechanical Restoration

To perform the 3D restoration accounting for the rock properties, a solid-model was created from geologic maps and interpreted structural cross-sections. The backward model was obtained flattening a shortening-representative reference surface selected from the lithology sequence. The modeling and restoration process are explained in the next sections.

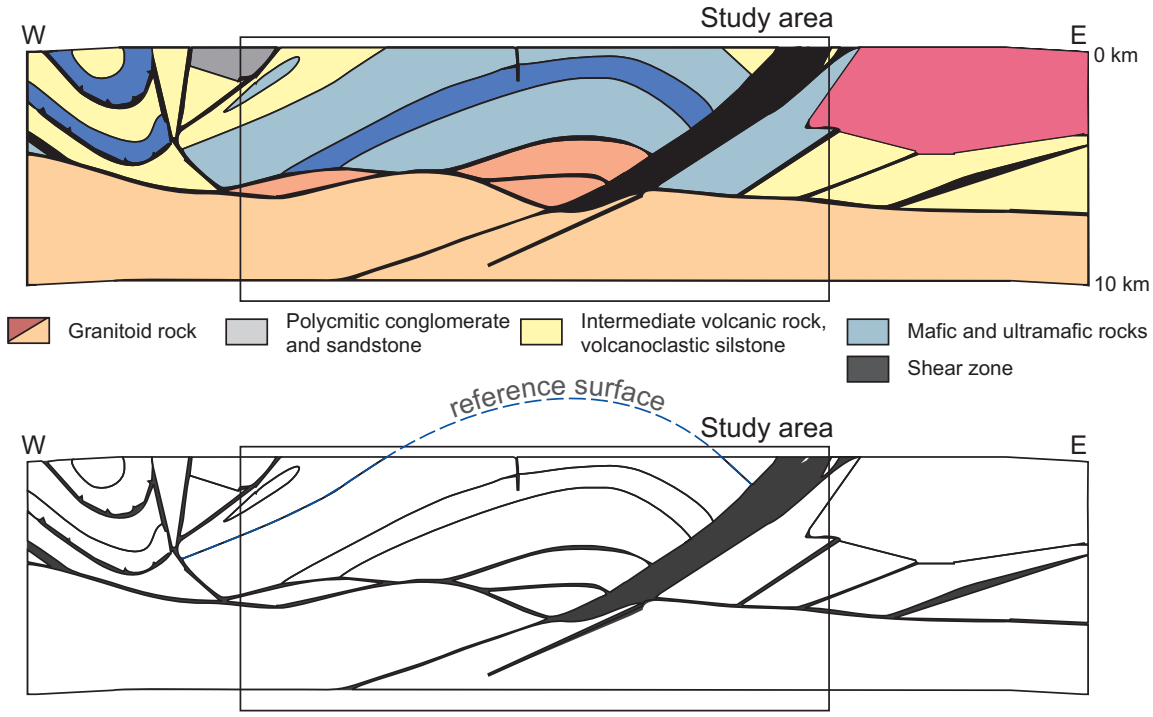

FIGURE 4.2 – Cross-section of the study area showing the structural configuration of the main rock units. **a**: These Archean rocks were deformed during a regional shortening, resulting a succession of anticlines, synclines, over-thrust and shear zones. **b**: We defined the top of the mafic-ultramafic succession surface as boundary condition for the restoration, because is the most complete horizon in the study area and its shape represents the shortening at mineralization time.

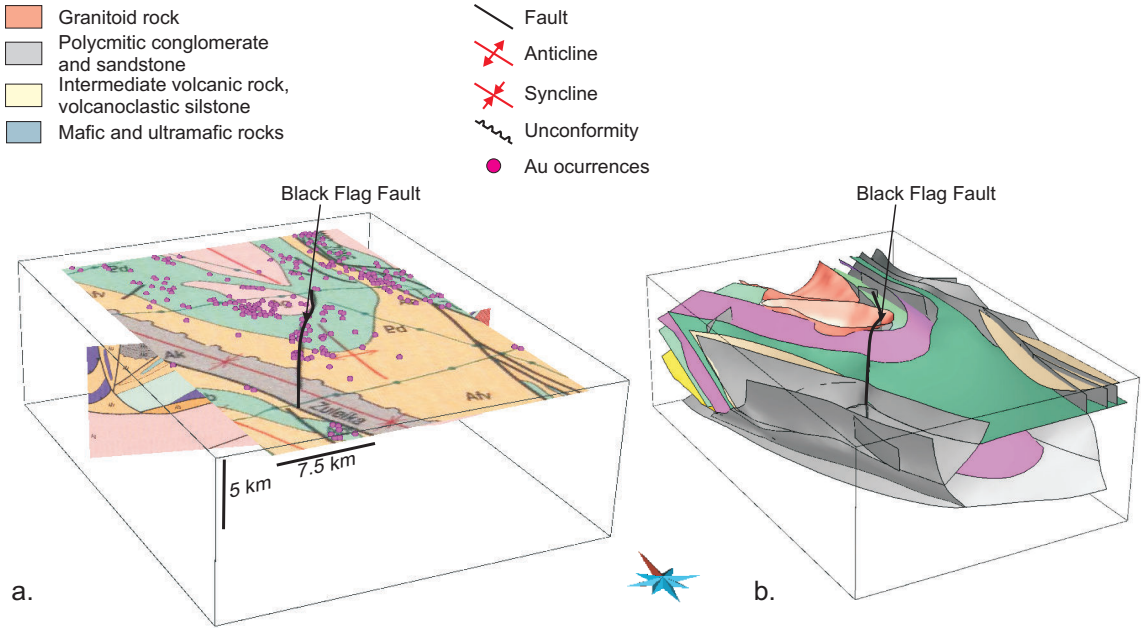

FIGURE 4.3 – 3D model of the Mount Pleasant area. **a**: The input data comprise a regional geological map of the study area and interpreted cross-sections (mainly from Wyche [1993]). The contacts and unit limits were introduced by picking both the map and the cross-sections. The meshed domain has a resolution of 360 m. **b**: The volcano-sedimentary units overlaying the basement were considered deposited in onlap mode in the structure and stratigraphy workflow. Gold occurrences after EGL [2014].

4.4.1 Mount Pleasant Region Modeling

The surface-based model of the study area is established on cartographic and interpreted subsurface data [Swager and Griffin, 1990, Wyche, 1993], which were integrated in a *SKUA®-2011* framework, resulting in a consistent model that honors the input data. The management of data and the main model-building tasks were realized building and initial surface-based structural model as is suggested by Caumon et al. [2009]. After that, this model was improved using an implicit approach PARADIGM [2012] (fig. 4.3). Complementary geological information, interpreted cross-sections and 3D models of the Yilgarn region were obtained from the Y4 pmd*CRC project [Henson, 2006, Blewett et al., 2010] and provided by Richard Blewett of **Geoscience Australia**.

4.4.2 3D Geomechanical Restoration

We applied a finite element method [Zienkiewicz, 1977] to compute the volume restoration in a 600 m tetrahedral-mesh-resolution solid fig. 4.4. We used the values reported by Moir et al. [2013] for the mechanical properties of rocks (fig. 4.5). The 3D structural restoration of the region was performed in RestorationLab [Durand-Riard et al., 2010], flattening the surface that represents the top of mafic-ultramafic rocks (see fig. 4.2b and the green surface in fig. 4.6). We fixed a pin-point and a datum level for this surface or reference, and we assumed a flexural slip deformation style for the shortening event. We assumed an elastic deformation mechanism acting during the shortening episode, because at the moment it is not possible to integrate the plastic-viscous component of the deformation in the RestorarionLab plug-in. For this reason, it is necessary to consider our results as an approximation of the real deformation

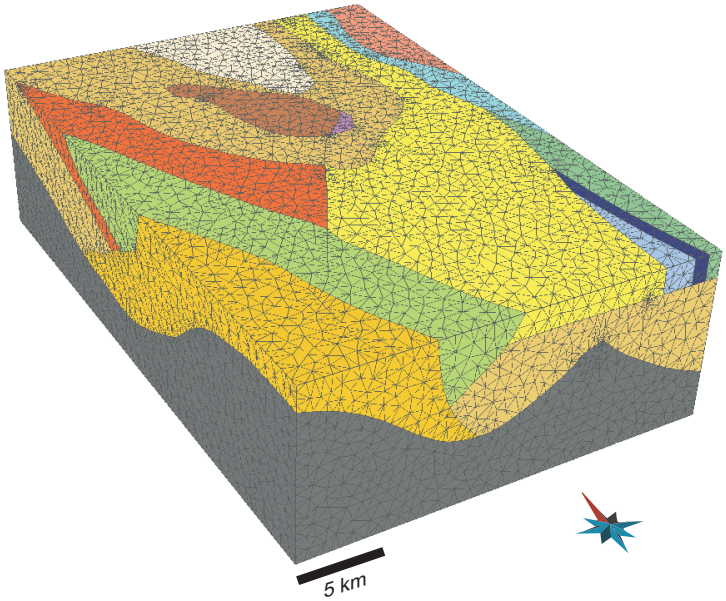

FIGURE 4.4 – 3D solid model used for the geomechanical restoration. Tetrahedral-mesh resolution about 600 m. Each colored region corresponds at each independent volume into the solid model.

mechanism. The fig. 4.7 shows the strain values obtained from the restoration.

4.5 Gold Occurrences and Distant Off-fault Damage

The eigenvalues from the restoration strain field were used to estimate the deformational parameters ξ and ζ. β is achieved in the restored solid solving the equation 4.2 with the *Scipy* **Python** package [Jones et al., 2001] in *GoPy* [Antoine and Caumon, 2008]. We plot the distance to main faults ($\mathscr{X}_f$), the forward dilatation ($\mathscr{D}$), β and the spatial gradient of ξ in the shortening direction (x) (fig. 4.8). These plots highlight structural and mechanical attributes that are related to gold distribution in the Mount Pleasant area. We focused on the gold occurrences at the margin W of the Liberty granodiorite, considering those as typical cases of distant off-fault mineralization.

The distance to fault ($\mathscr{X}_f$) attribute shows the strong association of gold distribution in the Mount Pleasant region with the main faults systems, indicating that the mineralization developed on the Liberty granodiorite depends on other factors that only proximity to those primary discontinuities (fig. 4.8 a). The medium to high dilatation ($\mathscr{D}$) in the Liberty granodiorite could represent a relatively high-level fracturing development on this igneous body that in the surrender rocks, but do not discriminate the concentration of gold occurrences at the W margin of the granodiorite (fig. 4.8 b). The β values seem related to high-density gold occurrences at the W margin of the granodiorite, as well as, the spatial gradient of ξ.

We defined a new domain inside Mount Pleasant study area (fig. 4.9a), centered in the Liberty granodiorite to test the level of correspondence between the structural and strain variables with off-fault gold occurrences, using logistic regression analysis (LR) [Hosmer Jr and Lemeshow, 2004] in R (eq. 4.3). In such a way, we evaluated probabilistically those variables ($\mathscr{X}_f$, β, $\mathscr{D}$, $d\xi/dx$) as predictors [Schaeben, 2014] for high-density gold occurrences not related spatially with the fault systems (fig. 4.9b).

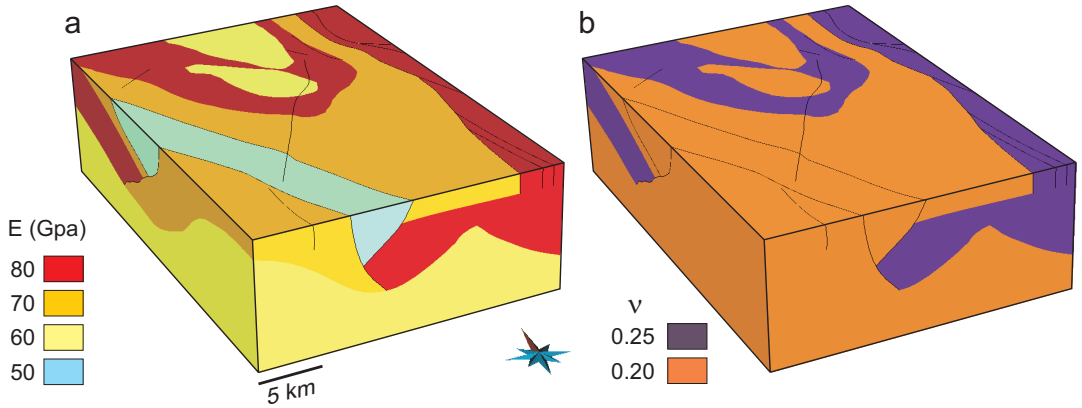

FIGURE 4.5 – Rock properties used for the geomechanical restoration. The different classes for the rock properties correspond roughly to the lithological units. **a**: Young's Modulus E (MPa): mafics and shear zones (red), volcanics (orange), granitoids and greenstone (yellow) and sandstone (blue). **b**: Poisson's ratio ν (after Moir et al. [2013]).

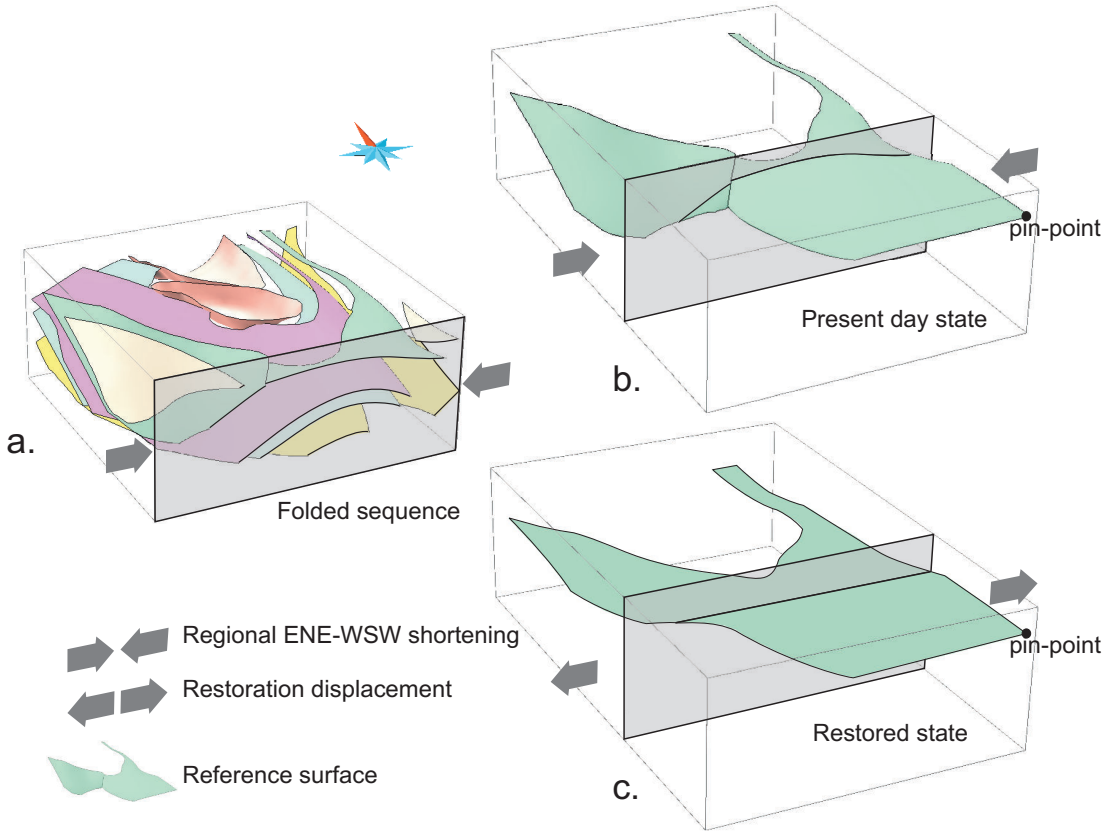

FIGURE 4.6 – 3D surface-based model of the Mount Pleasant area. **a**: Perspective cross-section showing the structural setting of the upper rocks units forming the Mount Pleasant Anticline. **b**: Reference surface folded in present day. **c**: After-restoration reference surface.

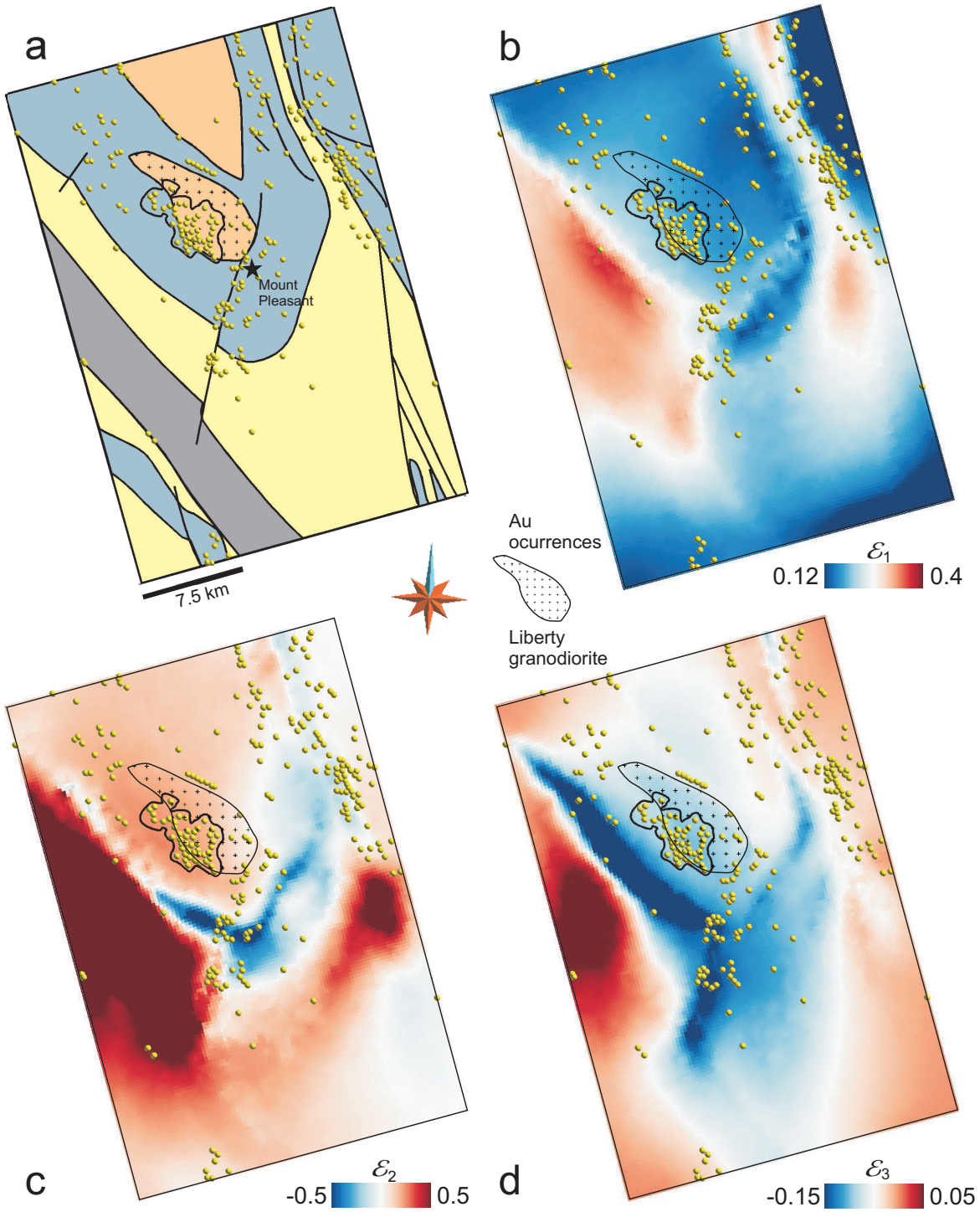

FIGURE 4.7 – Top view of the study area showing the strain eigenvalues from restoration. ($\mathcal{E}_i$, i=orthogonal directions). The plots show the association between the lithology (expressing different mechanical behavior) and the strain values. The Liberty granodiorite and the near gold occurrences are highlighted.

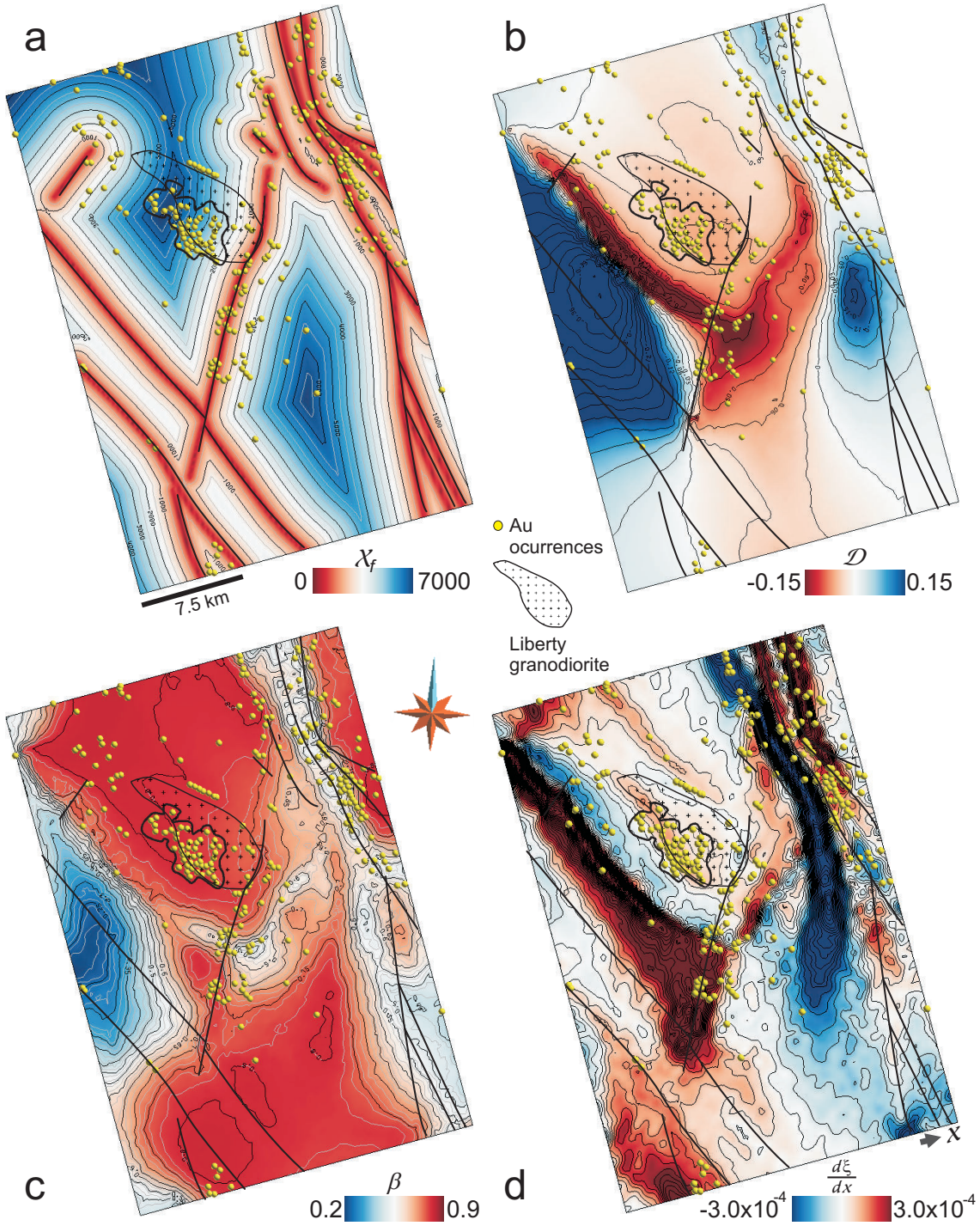

FIGURE 4.8 – Structural attributes related to ore-forming process. **a**: X_f is distance to main faults. **b**: β corresponds to deformational parameter from the **max(roots)** of equation 4.2. **c**: D is the obtained forward dilatation property from restoration. **d**: $d\xi/dx$ is the gradient of ξ in the shortening direction **x**.

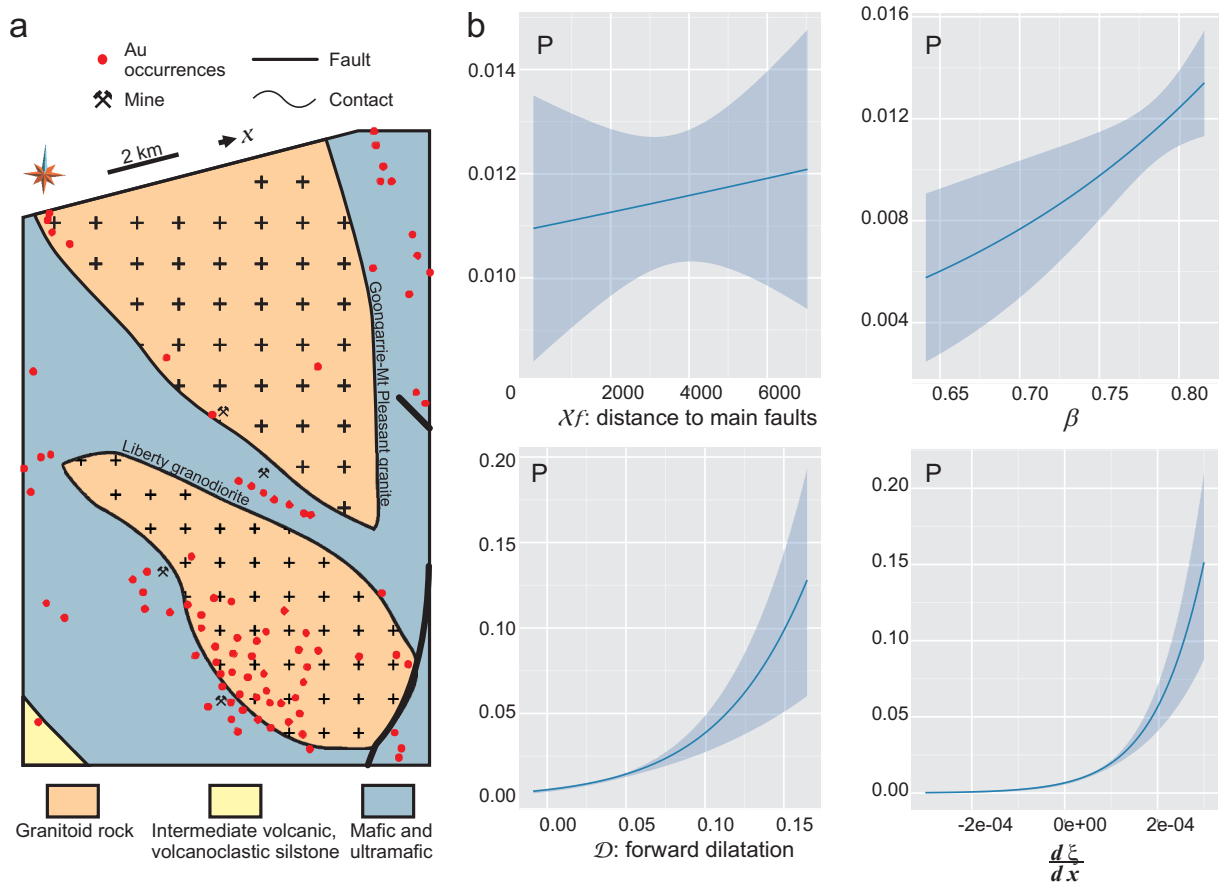

FIGURE 4.9 – Predicted probabilities using LR analysis for gold occurrences in the Liberty granodiorite area. **a**: Domain chosen to evaluate the strain parameters and the structural attributes for gold occurrences. **b**: Predicted probability, and their estimated errors, for gold occurrences by each one of the attributes with presumption that are linked with the gold distribution.

$$\begin{gathered} log(Odds) = \beta_0 + \beta_l x_1 + \beta_2 x_2 +, ..., +\beta_m x_m \\ x_{1m} : \{predictors\} \\ \beta_{0m} : \{coefficients\} \end{gathered} \tag{4.3}$$

The predicted probabilities plotted for the attributes show that, in probabilistic terms, the dilatation and $d\xi/dx$ seem to be associated to the gold distribution (fig. 4.9b). However, although the dilatation can be a predictor for off-fault gold locations (fig. 4.10a), this attribute does not discriminate the gold occurrences between the two borders of the Liberty granodiorite. On the contrary, the gold accumulation in the western border of the intrusion correlates with $d\xi/du$ (fig. 4.10b), and from the statistical point of view this gradient is a better predictor having the lowest error of the fourth evaluated attributes (fig. 4.9b).

4.6 Discussion

Assuming that damage is positively correlated with permeability, it is possible to consider that high-permeability pathways over off-fault locations are related with high damage zones. For those cases, the strain parameters ξ and β express the degradation of the mechanical properties due to a deformation event (equation 4.1) and, hence, the damage of the rock mass.

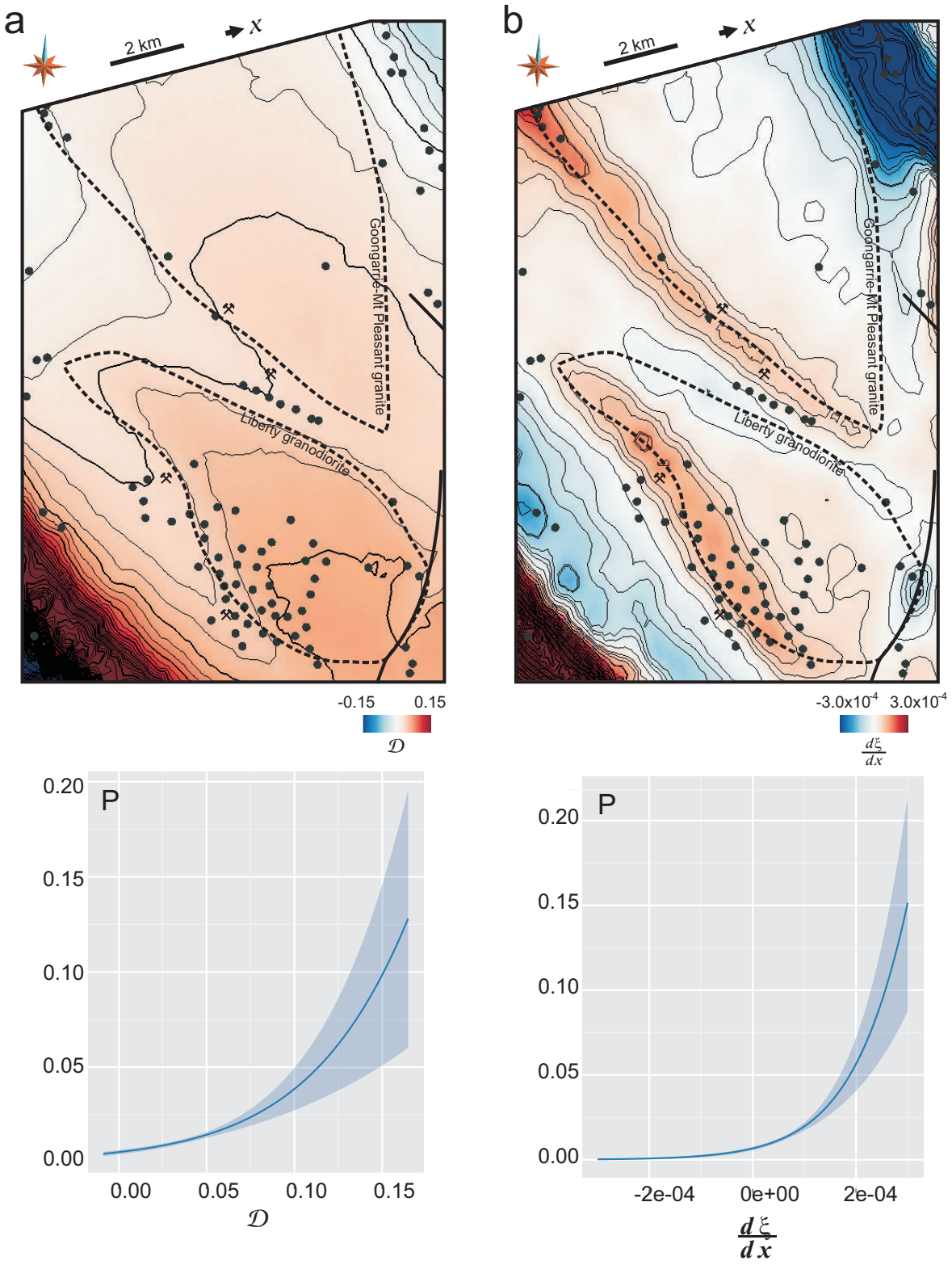

FIGURE 4.10 – Comparison of the forward dilatation and the gradient of ξ as predictors for off-fault gold distribution. **a**: $\mathscr{D}$ can be a predictor but this attribute does not discriminate the high-density gold occurrences between the two borders of the Liberty intrusion. **b**: The high-density gold occurrences in the western border of the intrusion correlates spatially with the gradient of ξ and is a better predictor than $\mathscr{D}$, having also a lower error in the predicted probability model.

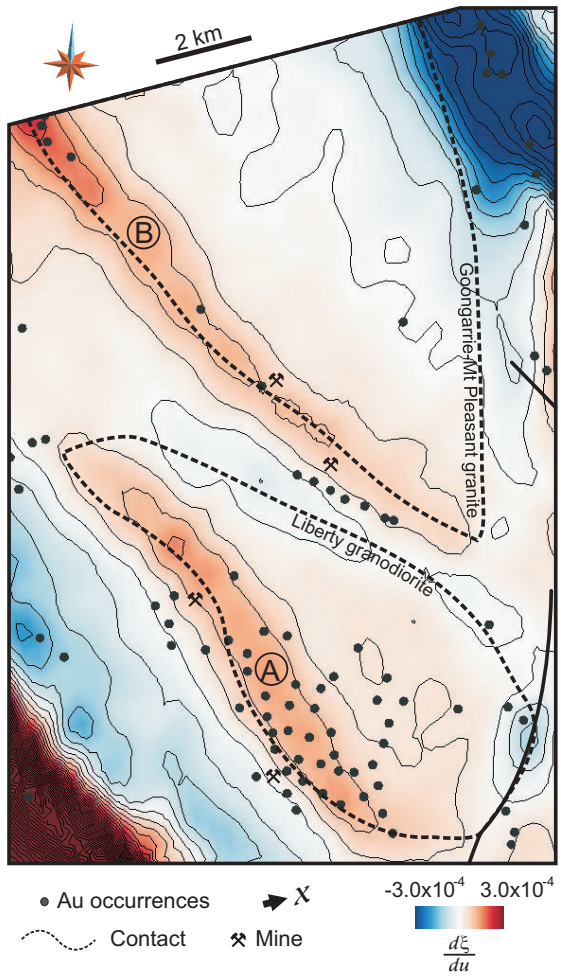

FIGURE 4.11 – Relation between gold occurrences locations and the gradient of ξ in the shortening direction $\boldsymbol{x}$. The range of values at W of the Liberty granodiorite margin (A) is similar that the range of values at W of the Goongarrie-Mt Pleasant granite (B).

In the Mount Pleasant area, the mineralization near to the Liberty Granodiorite boundary is an example of distant off-fault mineralization. Moir et al. [2013] explained those gold concentrations are controlled by the fracture system associated with the mechanical heterogeneity. In a similar case, Ojala et al. [1993] discussed about the relationship between high-grade gold distribution and the irregular contact of the Granny Smith Granodiorite (NE of Easter Goldfields Province), considering the mechanical heterogeneity and the geometry of the contact as main factors that control the ore-deposit.

The strain parameter β has high to extremely-high values at the W boundary of the Liberty granodiorite (fig. 4.8 c), matching roughly with the high presence of gold. A comparison of $d\xi/dx$ with the mapped gold occurrences shows a high level of correspondence between this derived attribute and the high-density gold locations on the W border of the Liberty granodiorite (fig. 4.8 d). The $d\xi/dx$ range of values found at the W of the Liberty granodiorite boundary is also present in the W margin of the Goongarrie-Mt Pleasant granite (fig. 4.11). The gold distribution in both igneous bodies could be the result of the same process It is possible that the deformation type controls the rock damage that leads the gold-bearing fluids flux and the fracturing that hosts the mineralization.

Conclusions

The 3D restoration provides both structural and mechanical behavior of the study area, simulating the deformation caused during the shortening episode which is involved in the mineralization process. The obtained results, appointing for a more developed damage area in the western border of the Liberty granodiorite, are consistent with distant off-fault gold systems in the Mount Pleasant region. The methodology here explained leads relate material heterogeneity, the geometrical configuration of the rocks units and a deformation event with a damage process. In this way, it is possible to use the derived strain parameters to infer the more brittle-fractured areas that may host the mineralization and control the off-fault gold distribution. The strain field obtained from a 3D restoration, simulating a deformation event linked to an ore-forming process, could be applied to find high permeability fractured zones for hydrothermal systems. In such a way, the presented methodology provide a tool to define potential mineralized areas for hydrothermal systems with similar features.

Acknowledgments

This work has been performed in the frame of the Gocad research project. We thank the industry and academic members of the Gocad Research Consortium [1] for supporting this research. We also thank Paradigm for the Gocad software. Finally, our special thanks go to Richard Blewett and Terry Brennan (*Geoscience Australia*) for supporting scientific and 3D information.

1. http://www.gocad.org/w4/index.php/consortium/members

Conclusion générale

Des études de cas où la modélisation et la restauration structurale ont été utilisées pour définir des modèles conceptuels ou mathématiques capables d'expliquer une minéralisation donnée, ont été présentées tout au long de ce mémoire. C'est ainsi qu'il a été possible de démontrer l'utilité de la modélisation 3D et 4D, non seulement dans la compréhension des concepts géologiques et physiques impliqués dans la formation des gisements, mais aussi dans la définition des zones potentielles pour orienter la prospection. L'ensemble de ces méthodes et stratégies sont mises en œuvre pour optimiser les probabilités d'identifier de nouvelles zones minéralisées. Les techniques de modélisation spatio-temporelle assistée ont été utilisées pour mieux comprendre l'évolution des structures géologiques au cours du temps pendant la formation d'un gisement, et ainsi d'établir un modèle prédictif efficace. Les principales contributions de cette thèse sont :

La restauration surfacique pour reconstituer l'état structural antérieur, afin de déterminer les conditions de fracturation hydraulique pour une période géologique donnée.

L'utilisation de la restauration surfacique dans le district minier de la Ceinture de Cuivre de Legnica-Głogów (sud-ouest de la Pologne) est décrite dans le deuxième chapitre de ce mémoire. L'état structural antérieur aux évènements d'exhumation fin Crétacé a été restauré pour les horizons minéralisés à partir des valeurs publiées de maturité de la matière organique dans la région et de la température maximale d'enfouissement calculée à partir des valeurs de réflectance de la vitrinite. A partir des profondeurs restaurées du système minéralisé, les pressions fluides dans la masse rocheuse ont été recalculées en prenant en compte l'isolement hydraulique par les formations imperméables du Zechstein du système minéralisé. La fracturation hydraulique, due à la variation des contraintes lors de l'exhumation, est évoquée pour expliquer la remobilisation et l'enrichissement de certains métaux (notamment du cuivre). L'index de fracturation défini en tenant compte des propriétés rhéologiques des roches et de la pression fluide, montre une corrélation avec les zones minéralisées en cuivre. Cet exemple montre la possibilité d'intégrer des concepts divers comme la teneur en matière organique, l'exhumation des terrains, et la fracturation hydraulique pour expliquer les processus de minéralisation tardive.

Utilisation de la courbure des surfaces en tant qu'attribut pour déterminer l'activité des failles liées aux minéralisations cuprifères dans les Sudètes (Sud-ouest de la Pologne).

Les attributs géométriques obtenus lors d'une restauration structurale surfacique peuvent indiquer la présence et l'activité des failles. La courbure des horizons géologiques a été utilisée comme attribut structural pour évaluer l'activité des failles dans les Sudètes (sud-est de la Pologne). Les fortes valeurs de courbures calculées sur les horizons stratigraphiques sont fortement liées géographiquement aux zones avec un fort potentiel cuprifère reporté dans les travaux antérieurs. Cette relation entre courbure et activité des failles exprime probablement

le rôle des systèmes des failles actives pendant les processus de minéralisation. La migration des fluides hydrothermaux verticalement vers la surface, le long des failles du socle et dans les zones endommagées à proximité, pourrait directement influencer la formation des sulfures de cuivre et des autres métaux. Les modèles probabilistes utilisés pour estimer les zones à fort potentiel cuprifère obtenus à partir de variables prédictives telles que la courbure, ont montré que la distribution des minéralisations cuprifères dans le Sudètes polonais semble dépendre de la variation du régime des contraintes au cours de l'histoire tectonique de la fin du Permien et au Crétacé supérieur.

Estimation des paramètres de déformation pour identifier les zones d'endommagements hors des zones faillées favorables aux minéralisations aurifères dans le district minier de Mount Pleasant, Australie

En supposant que l'endommagement est positivement corrélé à la perméabilité des roches lors d'une déformation régionale, il est possible d'identifier ces zones hors failles à forte perméabilité en cartographiant les forts endommagements calculés à partir d'une restauration volumique. Ainsi, les paramètres de déformation expriment la dégradation des propriétés mécaniques et, par conséquence, l'endommagement de la masse rocheuse. La restauration mécanique a été appliquée pour quantifier le comportement structural et mécanique des zones étudiées, en simulant la déformation provoquée lors d'un épisode de raccourcissement impliqué lors de la minéralisation. Les résultats obtenus sont conformes à l'endommagement calculé hors des systèmes de failles, mais aussi aux distributions aurifères de la région de Mount Pleasant, Australie. Les paramètres de déformation font le lien entre les hétérogénéités des roches et leur configuration géométrique avec le processus d'endommagement et, donc, au développement des fractures qui contrôlent la distribution de l'or. L'utilisation du champ de déformation, obtenu lors de la restauration volumique, a permis de définir des domaines aurifères en fonction des paramètres d'endommagement et des facturations associées au processus de minéralisation.

Bibliographie

F. Agterberg and G. Bonham-Carter. Logistic regression and weights of evidence modeling in mineral exploration. In *Proceedings of the 28th International Symposium on Applications of Computer in the Mineral Industry (APCOM), Golden, Colorado*, p. 483–490, 1999.

F. Agterberg, G. Bonham-Carter, Q. Cheng, and D. Wright. Weights of evidence modeling and weighted logistic regression for mineral potential mapping. In *Computers in geology–25 years of progress*, p. 13–32, 1993.

P. Allen and J. Allen. Chapter subsidence and thermal history. In *Basin Analysis : Principles and Applications*, p. 349–401, 2005.

P. An, W. Moon, and G. Bonham-Carter. On knowledge-based approach of integrating remote sensing, geophysical and geological information. In *Geoscience and Remote Sensing Symposium, 1992. IGARSS'92. International*, p. 34–38, 1992.

C. Antoine and G. Caumon. Rapid algorithm prototyping in gocad using python plugin. In *Proceedings of 28th Gocad Meeting, Nancy*, 2008.

M. Apel. From 3D geomodelling systems towards 3D geoscience information systems : Data model, query functionality, and data management. *Computers & Geosciences*, 32(2) : 222–229, 2006. ISSN 0098-3004. doi : 10.1016/j.cageo.2005.06.016.

M. E. Barley and D. I. Groves. Supercontinent cycles and the distribution of metal deposits through time. *Geology*, 20(4) : 291–294, 1992. doi : 10.1130/0091-7613(1992)020<0291:SCATDO>2.3.CO;2.

A. Bechtel, W. C. Elliott, J. M. Wampler, and S. Oszczepalski. Clay mineralogy, crystallinity, and K-Ar ages of illites within the Polish Zechstein Basin ; implications for the age of Kupferschiefer mineralization. *Economic Geology*, 94(2) : 261–272, 1999.

A. Bechtel, R. Gratzer, W. Püttmann, and S. Oszczepalski. Variable alteration of organic matter in relation to metal zoning at the Rote Fäule front (Lubin-Sieroszowice mining district, SW Poland). *Organic Geochemistry*, 32(3) : 377–395, 2001a. ISSN 0146-6380.

A. Bechtel, Y. Sun, W. Püttmann, S. Hoernes, and J. Hoefs. Isotopic evidence for multi-stage base metal enrichment in the Kupferschiefer from the Sangerhausen Basin, Germany. *Chemical Geology*, 176(1-4) : 31–49, 2001b.

G. Bertrand, L. Guillou-Frottier, and C. Loiselet. Distribution of porphyry copper deposits along the western Tethyan and Andean subduction zones : Insights from a paleotectonic approach. *Ore Geology Reviews*, 60(0) : 174–190, 2014. ISSN 0169-1368. doi : 10.1016/j.oregeorev.2013.12.015.

R. Blewett, P. Henson, I. Roy, D. Champion, and K. Cassidy. Scale-integrated architecture of a world-class gold mineral system : The Archaean eastern Yilgarn Craton, Western Australia. *Precambrian Research*, 183(2) : 230–250, 2010. ISSN 0301-9268. doi : 10.1016/j.precamres.2010.06.004.

D. J. Blundell, P. H. Karnkowski, D. H. M. Alderton, S. Oszczepalski, and H. Kucha. Copper mineralization of the Polish Kupferschiefer : a proposed basement fault-fracture system of fluid flow. *Economic Geology*, 98(7) : 1487–1495, 2003.

C. Bond, A. Gibbs, Z. Shipton, and S. Jones. What do you think this is ? "Conceptual uncertainty" in geoscience interpretation. *GSA today*, 17(11) : 4–10, 2007.

G. Bonham-Carter, F. Agterberg, and D. Wright. Weights of evidence modeling : a new approach to mapping mineral potential. In *Statistical Applications in the Earth Sciences. Eds. F.P. Agterberg and G.F. Bonham-Carter*, number 9 in Paper 89, p. 171–183. Geological Survey of Canada, 1989.

A. Botella, B. Lévy, and G. Caumon. Indirect hex-dominant mesh generation using a matching tetrahedra method. In *33rd Gocad Meeting Proceedings*, 2013.

A. C. Brown. Adding geochemical rigor to the general basin-scale genetic model for sediment-hosted stratiform copper mineralization. In *11th SGA Biennial Meeting. Antofagasta, Chile*, 11th SGA Biennial Meeting. Antofagasta, Chile, 2011.

E. J. M. Carranza. Improved wildcat modelling of mineral prospectivity. *Resource geology*, 60(2) : 129–149, 2010.

K. Cassidy and J. Bennett. Gold mineralisation at the Lady Bountiful mine, Western Australia : An example of a granitoid-hosted Archaean lode gold deposit. *Mineralium Deposita*, 28(6) : 388–408, 1993. ISSN 0026-4598. doi : 10.1007/BF02431598.

G. Caumon. Towards stochastic time-varying geological modeling. *Mathematical Geosciences*, 42 (5) : 555–569, 2010.

G. Caumon, P. Collon-Drouaillet, C. Le-Carlier-de Veslud, S. Viseur, and J. Sausse. Surface-based 3D modeling of geological structures. *Mathematical Geosciences*, 41(8) : 927–945, 2009. doi : 10.1007/s11004-009-9244-2.

R. T. Chamberlin. The Appalachian folds of central Pennsylvania. *The Journal of Geology*, 18(3) : 228–251, 1910.

Q. Cheng. Non-linear theory and power-law models for information integration and mineral resources quantitative assessments. In *Progress in Geomathematics*, p. 195–225. Springer, 2008.

Q. Cheng and F. Agterberg. Fuzzy weights of evidence method and its application in mineral potential mapping. *Natural Resources Research*, 8(1) : 27–35, 1999.

N. Cherpeau, G. Caumon, and B. Lévy. Stochastic simulations of fault networks in 3D structural modeling. *Comptes Rendus Geoscience*, 342(9) : 687–694, 2010. ISSN 1631-0713.

J.-P. Chiles and P. Delfiner. *Geostatistics : modeling spatial uncertainty*, vol. 497. John Wiley & Sons, 2009. ISBN 0470317833.

J. W. Cosgrove. Hydraulic fracturing during the formation and deformation of a basin : A factor in the dewatering of low-permeability sediments. *AAPG Bulletin*, 85(4) : 737 –748, 2001.

J. R. Craig, D. J. Vaughan, and R. D. Hagni. *Ore microscopy and ore petrography*, vol. 406. Wiley New York, 1981.

M. Cuney. Felsic magmatism and uranium deposits. *Bulletin de la Societe Geologique de France*, 185(2) : 75–92, 2014.

R. Dadlez, W. Jóźwiak, and S. Młynarski. Subsidence and inversion in the western part of Polish Basin-data from seismic velocities. *Geological Quarterly*, 41(2) : 197–208, 1997.

R. Dadlez, S. Marek, and J. Pokorski. Geological map of Poland without Cainozoic deposits. *Państwowy Instytut Geologiczny, Warszawa*, 2000.

C. Dahlstrom. Balanced cross sections. *Canadian Journal of Earth Sciences*, 6(4) : 743–757, 1969.

C. C. de Araújo and A. B. Macedo. Multicriteria geologic data analysis for mineral favorability mapping : application to a metal sulphide mineralized area, Ribeira Valley Metallogenic Province, Brazil. *Natural Resources Research*, 11(1) : 29–43, 2002.

T. de Quadros, J. Koppe, A. Strieder, and J. Costa. Mineral-potential mapping : A comparison of weights-of-evidence and fuzzy methods. *Natural Resources Research*, 15(1) : 49–65, 2006.

M. De Santi, J. Campos, and L. Martha. A finite element approach for geological section reconstruction. In *22th Gocad Meeting Proceedings*, 2002.

O. B. Duffy, R. L. Gawthorpe, M. Docherty, and S. H. Brocklehurst. Mobile evaporite controls on the structural style and evolution of rift basins : Danish Central Graben, North Sea. *Basin Research*, 25(3) : 310–330, 2013.

P. Durand-Riard. *Gestion de la Complexité Géologique en Restauration Géomécanique 3D.* PhD thesis, Institut National Polytechnique de Lorraine, 2010.

P. Durand-Riard, G. Caumon, and P. Muron. Balanced restoration of geological volumes with relaxed meshing constraints. *Computers & Geosciences*, 36(4) : 441–452, 2010. ISSN 0098-3004. doi : 10.1016/j.cageo.2009.07.007.

P. Durand-Riard, L. Salles, M. Ford, G. Caumon, and J. Pellerin. Understanding the evolution of synsedimentary faults : coupling decompaction and 3D sequential restoration. *Marine and Petroleum Geology*, 28(8) : 1530–1539, 2011.

P. Durand-Riard, C. A. Guzofski, G. Caumon, and M.-O. Titeux. Handling natural complexity in 3D geomechanical restoration, with application to the recent evolution of the outer fold-and-thrust belt, deepwater Niger Delta. *AAPG Bulletin*, 97(1) : 87–102, 2013.

EGL. Excelsior Gold Limited : Mineral exploration in north of Kalgoorlie, Western Australia, 2014.

E. Finch, S. Hardy, and R. Gawthorpe. Discrete-element modelling of extensional fault-propagation folding above rigid basement fault blocks. *Basin Research*, 16(4) : 467–488, 2004. ISSN 1365-2117.

Y. Finzi, E. H. Hearn, V. Lyakhovsky, and L. Gross. Fault-zone healing effectiveness and the structural evolution of strike-slip fault systems. *Geophysical Journal International*, 186(3) : 963–970, 2011.

C. Forster and L. Smith. The influence of groundwater flow on thermal regimes in mountainous terrain : A model study. *Journal of Geophysical Research : Solid Earth (1978–2012)*, 94(B7) : 9439–9451, 1989.

M. Frantz. *Geomechanics to solve geological structure issues : forward, inverse and restoration modeling.* PhD thesis, Montpellier 2, Montpellier, France, 2010.

D. Gao. Integrating 3D seismic curvature and curvature gradient attributes for fracture characterization : Methodologies and interpretational implications. *Geophysics*, 78(2) : O21–O31, 2013.

M. Gebre-Mariam, D. Groves, N. McNaughton, E. Mikucki, and J. Vearncombe. Archaean Au–Ag mineralisation at Racetrack, near Kalgoorlie, Western Australia : a high crustal-level expression of the Archaean composite lode-gold system. *Mineralium Deposita*, 28(6) : 375–387, 1993. ISSN 0026-4598. doi : 10.1007/BF02431597.

R. J. Goldfarb, D. Bradley, and D. L. Leach. Secular variation in economic geology. *Economic Geology*, 105(3) : 459–465, 2010. doi : 10.2113/gsecongeo.105.3.459.

J. Gouin. *Mode de genése et valorisation des minerais de type black shales : cas du Kupferschiefer (Pologne) et des schistes noirs de Talvivaara (Finlande).* Ph.D. thesis report., Université d'Orléans, Orléans, 2008.

J.-P. Gratier and B. Guillier. Compatibility constraints on folded and faulted strata and calculation of total displacement using computational restoration (UNFOLD program). *Journal of structural geology*, 15(3) : 391–402, 1993.

R. Groshong. *3-D Structural Geology. A Practical Guide to Quantitative Surface and Subsurface Map Interpretation, 2nd ed.* Springer-Verlag, Berlin Heidelberg, 2006.

L. Gross, L. Bourgouin, A. J. Hale, and H.-B. Muhlhaus. Interface modeling in incompressible media using level sets in escript. *Physics of the Earth and Planetary Interiors*, 163 : 23–34, 2007a.

L. Gross, B. Cumming, K. Steube, and D. Weatherley. A python module for PDE-Based numerical modelling. *PARA*, 4699 : 270–279, 2007b.

L. Gross, C. Altinay, A. Amirbekyan, J. Fenwick, P. Hornby, T. Poulet, H. Sheldon, and K. Steube. Solving transport problems for the exploration of mineral deposits and geothermal reservoirs. In *4th International Conference on High Performance Scientific Computing Simulation, Modeling and Optimization of Complex Processes*, 2009.

L. Gross, C. Altinay, A. Amirbekyan, J. Fenwick, L. M. Olsen-Kettle, K. Steube, L. Graham, and H. B. Muhlhaus. esys-escript user's guide : Solving partial differential equations with escript and finley. *Release-3.2. The University of Queensland, Australia*, 2010.

D. I. Groves and F. P. Bierlein. Geodynamic settings of mineral deposit systems. *Journal of the Geological Society*, 164(1) : 19–30, 2007. doi : 10.1144/0016-76492006-065.

D. I. Groves, R. J. Goldfarb, C. M. Knox-Robinson, J. Ojala, S. Gardoll, G. Y. Yun, and P. Holyland. Late-kinematic timing of orogenic gold deposits and significance for computer-based exploration techniques with emphasis on the Yilgarn Block, western Australia. *Ore Geology Reviews*, 17(1–2) : 1–38, 2000. ISSN 0169-1368. doi : 10.1016/S0169-1368(00)00002-0.

D. I. Groves, K. C. Condie, R. J. Goldfarb, J. M. Hronsky, and R. M. Vielreicher. 100th anniversary special paper : Secular changes in global tectonic processes and their influence on the temporal distribution of gold-bearing mineral deposits. *Economic Geology*, 100(2) : 203–224, 2005. doi : 10.2113/gsecongeo.100.2.203.

U. Grubenmann. *Die kristallinen Schiefer*, vol. 2. Gebrüder Borntraeger, 1910.

J. M. Guilbert and C. F. Park Jr. *The geology of ore deposits.* Waveland Press, 2007.

C. Guzofski, J. Mueller, J. Shaw, P. Muron, D. Medwedeff, F. Bilotti, and C. Rivero. Insights into the mechanisms of fault-related folding provided by volumetric structural restorations using spatially varying mechanical constraints. *AAPG Bulletin*, 93 : 479–502, 2009.

A. Hallam, L. Gross, C. Altinay, A. Amirbekyan, J. Fenwick, and L. Gao. The escript cookbook : Release-3.2 (r3422). 2010.

P. Henson. Chapter 2 : an integrated geological and geophysical 3D map for the EYC. *3D Geological Models of the Eastern Yilgarn Craton—Y2 Final Report pmd* CRC. Geoscience Australia Record*, 4(2006) : 32–85, 2006.

M. Hillier, E. Schetselaar, E. de Kemp, and G. Perron. Three-dimensional modelling of geological surfaces using generalized interpolation with radial basis functions. *Mathematical Geosciences*, 46 (8) : 931–953, 2014. ISSN 1874-8961. doi : 10.1007/s11004-014-9540-3.

M. W. Hitzman, D. Selley, and S. Bull. Formation of sedimentary rock-hosted stratiform copper deposits through Earth history. *Economic Geology*, 105(3) : 627–639, 2010.

B. E. Hobbs, Y. Zhang, A. Ord, and C. Zhao. Application of coupled deformation, fluid flow, thermal and chemical modelling to predictive mineral exploration. *Journal of Geochemical Exploration*, 69-70(0) : 505 – 509, 2000.

D. W. Hosmer Jr and S. Lemeshow. *Applied logistic regression*. John Wiley & Sons, London, 2004.

S. E. Ingebritsen and M. S. Appold. The physical hydrogeology of ore deposits. *Economic Geology*, 107(4) : 559 –584, 2012.

A. Jarvis, H. Reuter, A. Nelson, and E. Guevara. Hole-filled SRTM for the globe version 4. *Available from the CGIAR-SXI SRTM 90m database*, 2008.

M. Jébrak and E. Marcoux. *Géologie des ressources minérales*. Ressources naturalles et Faune. Gouvernement du Québec, Québec, 2008. ISBN 9782551237371.

M. Jessell. Three-dimensional geological modelling of potential-field data. *3D reconstruction, modelling & visualization of geological materials*, 27(4) : 455–465, 2001. ISSN 0098-3004. doi : 10.1016/S0098-3004(00)00142-4.

E. Jones, T. Oliphant, P. Peterson, and others. *SciPy : Open source scientific tools for Python*. 2001. [Online ; accessed 2014-08-07].

JORC. *Australasian code for reporting of exploration results, mineral resources and ore reserves*. 2012 edition, 2012.

E. Jowett. Role of organics and methane in sulfide ore formation, exemplified by Kupferschiefer Cu-Ag deposits, Poland. *Chemical Geology*, 99(1-3) : 51–63, 1992.

E. C. Jowett. Genesis of Kupferschiefer Cu-Ag deposits by convective flow of Rotliegendes brines during Triassic rifting. *Economic Geology*, 81(8) : 1823–1837, 1986.

E. C. Jowett, G. W. Pearce, and A. Rydzewski. A Mid-Triassic paleomagnetic age of the Kupferschiefer mineralization in Poland, based on a revised apparent polar wander path for Europe and Russia. *Journal of Geophysical Research*, 92(B1) : 581–598, 1987.

K. E. Kane, C. A.-L. Jackson, and E. Larsen. Normal fault growth and fault-related folding in a salt-influenced rift basin : South Viking Graben, offshore Norway. *Journal of Structural Geology*, 32(4) : 490–506, 2010.

P. H. Karnkowski. Origin and evolution of the Polish Rotliegend Basin. *Polish Geological Institute Special Papers*, 3 : 1–93, 1999.

R. Kerrich. Perspectives on genetic models for lode gold deposits. *Mineralium Deposita*, 28(6) : 362–365, 1993.

KGHM Polska Miedź S.A. ANNUAL REPORT 2006. Technical report, Poland, 2007.

KGHM Polska Miedź S.A. Report on the mining assets of KGHM Polska Miedź S.A. located within the Legnica-Głogów Copper Belt Area. Report prepared by an internal team of KGHM Polska Miedź S.A. 50, KGHM Polska Miedź S.A., Poland, 2012.

L. C. Kinsey. *Topology of surfaces*. Springer, Berlin, 1993. ISBN 0387941029.

D. Kossow and C. M. Krawczyk. Structure and quantification of processes controlling the evolution of the inverted NE-German basin. *Marine and Petroleum Geology*, 19(5) : 601 – 618, 2002.

M. Kotarba, T. Peryt, P. Kosakowski, and D. Więcław. Organic geochemistry, depositional history and hydrocarbon generation modelling of the Upper Permian Kupferschiefer and Zechstein Limestone strata in south–west Poland. *Marine and Petroleum Geology*, 23(3) : 371–386, 2006. ISSN 0264-8172. doi : 10.1016/j.marpetgeo.2005.10.003.

P. Krzywiec. Triassic−Jurassic evolution of the Pomeranian segment of the Mid-Polish Trough : Basement tectonics and subsidence patterns. *Geological Quarterly*, 50(1) : 139–150, 2006.

J. Lamarche and M. Scheck-Wenderoth. 3D structural model of the Polish Basin. *Integration of Geophysical and Geological Data and Numerical Models in Basins*, 397(1–2) : 73–91, 2005. ISSN 0040-1951. doi : 10.1016/j.tecto.2004.10.013.

L. Launay. *Traité de métallogénie : gîtes minéraux et métallifères*, vol. 1. Ch. Béranger, 1913.

M. Lecour, R. Cognot, I. Duvinage, P. Thore, and J.-C. Dulac. Modelling of stochastic faults and fault networks in a structural uncertainty study. *Petroleum Geoscience*, 7(S) : S31–S42, 2001.

J. Lefebvre. Les gisements stratiformes en roche sédimentaire d'Europe centrale (Kupferschiefer) et de la Ceinture Cuprifère du Zaïre et de Zambie. *Annales de la Societé Géologique de Belgique*, 112(1) : 121–135, 1989.

A. M. Lemon and N. L. Jones. Building solid models from boreholes and user-defined cross-sections. *Computers & Geosciences*, 29(5) : 547–555, 2003. ISSN 0098-3004. doi : 10.1016/S0098-3004(03)00051-7.

P. Les and T. Wayne. The NURBS book. *Springer Verlag, Berlin*, Monographs in visual communications, 1997.

H. Lewis and G. D. Couples. Carboniferous basin evolution of Central Ireland-simulation of structural controls on mineralization. *Geological Society, London, Special Publications*, 155(1) : 277–302, 1999.

W. Lindgren. Metallogenetic epochs. *Economic Geology*, 4(5) : 409–420, 1909. doi : 10.2113/gsecongeo.4.5.409.

W. Lindgren. A suggestion for the terminology of certain mineral deposits. *Economic geology*, 17 (4) : 292–294, 1922.

W. Lindgren. Mineral deposits , 930 p. *New York and London, McGraw-HillBook Co*, 1933.

R. Lisle. Detection of zones of abnormal strains in structures using Gaussian curvature analysis. *AAPG Bulletin*, 78(12) : 1811–1819, 1994.

L.-M. Liu, G.-Y. Yang, S.-L. Peng, and C. Zhao. Numerical modeling of coupled geodynamical processes and its role in facilitating predictive ore discovery : An example from tongling, china. *Resource Geology*, 55(1) : 21–31, 2005. ISSN 1751-3928. doi : 10.1111/j.1751-3928.2005.tb00225.x.

V. Lyakhovsky, Y. Ben-Zion, and A. Agnon. Distributed damage, faulting, and friction. *Journal of Geophysical Research*, 102(B12) : 27635–27, 1997a.

V. Lyakhovsky, Z. Reches, R. Weinberger, and T. E. Scott. Non-linear elastic behaviour of damaged rocks. *Geophysical Journal International*, 130(1) : 157–166, 1997b. doi : 10.1111/j.1365-246X.1997.tb00995.x.

L. Maerten and F. Maerten. Chronologic modeling of faulted and fractured reservoirs using geomechanically based restoration : Technique and industry applications. *AAPG Bulletin*, 90(8) : 1201–1226, 2006.

J.-L. Mallet. *Geomodeling.* Oxford University Press, Oxford, 2002.

J. Massot. *Implémentation de méthodes de restauration équilibrée 3D.* PhD thesis, Institut National Polytechnique de Lorraine, INPL, Nancy, France, 2002.

S. Mazur, M. Scheck-Wenderoth, and P. Krzywiec. Different modes of the Late Cretaceous−Early Tertiary inversion in the North German and Polish basins. *International Journal of Earth Sciences*, 94(5) : 782–798, 2005.

S. Mazur, P. Aleksandrowski, K. Turniak, L. Krzemiński, K. Mastalerz, A. Górecka-Nowak, L. Kurowski, P. Krzywiec, A. Żelaźniewicz, and M. Fanning. Uplift and late orogenic deformation of the Central European Variscan belt as revealed by sediment provenance and structural record in the Carboniferous foreland basin of western Poland. *International Journal of Earth Sciences*, 99 (1) : 47–64, 2010.

P. McCullagh and J. A. Nelder. Generalized linear models (monographs on statistics and applied probability 37). *Chapman Hall, London*, 1989.

K. McQueen. Ore deposit types and their primary expressions. *Regolith Expression of Australian Ore Systems*, 2005.

P. Mejía-Herrera and J.-J. Royer. Explicit surface restoration-decompaction procedure to estimate the hydraulic fracturing : Case of the Kupferschiefer in the Lubin Region, Poland. In *Proceedings of the 32nd gOcad Meeting*, p. 19, 2012.

P. Mejía-Herrera, M. Kakurina, and J.-J. Royer. Using strain parameters from 3D restoration to estimate distant off-fault gold potentials, Mount Pleasant Area, Western Australia. In *Proceedings of the 34th Gocad Meeting*, p. 10, 2014a.

P. Mejía-Herrera, J.-J. Royer, G. Caumon, and A. Cheilletz. Curvature Attribute from Surface-Restoration as Predictor Variable in Kupferschiefer Copper Potentials. *Natural Resources Research*, p. 1–16, 2014b. ISSN 1520-7439. doi : 10.1007/s11053-014-9247-7.

C. Meyer. Ore deposits as guides to geologic history of the Earth. *Annual Review of Earth and Planetary Sciences*, 16 : 147, 1988.

M. Michalik. Chlorine containing illites, copper chlorides and other chloride bearing minerals in the Fore-Sudetic copper deposit (Poland). *Mineral deposits, research and exploration–Rotterdam Balkema*, p. 543–546, 1997.

S. Micklethwaite and S. F. Cox. Fault-segment rupture, aftershock-zone fluid flow, and mineralization. *Geology*, 32(9) : 813–816, 2004. doi : 10.1130/G20559.1.

S. Micklethwaite and S. F. Cox. Progressive fault triggering and fluid flow in aftershock domains : Examples from mineralized Archaean fault systems. *Earth and Planetary Science Letters*, 250 (1–2) : 318–330, 2006. ISSN 0012-821X. doi : 10.1016/j.epsl.2006.07.050.

A. R. Miller, C. D. Densmore, E. T. Degens, J. C. Hathaway, F. T. Manheim, P. F. McFarlin, R. Pocklington, and A. Jokela. Hot brines and recent iron deposits in deeps of the Red Sea. *Geochimica et Cosmochimica Acta*, 30(3) : 341–359, 1966.

H. Moir, R. Lunn, S. Micklethwaite, and Z. Shipton. Distant off-fault damage and gold mineralization : The impact of rock heterogeneity. *Tectonophysics*, 608 : 461–467, 2013.

I. Moretti. Working in complex areas : New restoration workflow based on quality control, 2D and 3D restorations. *Marine and Petroleum Geology*, 25(3) : 205–218, 2008.

I. Moretti, F. Lepage, and M. Guiton. KINE3D : a new 3D restoration method based on a mixed approach linking geometry and geomechanics. *Oil & Gas Science and Technology – Revue d'IFP Energies nouvelles*, 61(2) : 277–289, 2006.

I. Moretti, V. Delos, J. Letouzey, A. Otero, and J. C. Calvo. The use of surface restoration in foothills exploration : Theory and application to the sub-Andean zone of Bolivia. In *Thrust Belts and Foreland Basins*, Frontiers in Earth Sciences, p. 149–162. Springer Berlin Heidelberg, 2007.

P. Muchez, W. Heijlen, D. Banks, D. Blundell, M. Boni, and F. Grandia. 7 : Extensional tectonics and the timing and formation of basin-hosted deposits in Europe. *Special Issue on Geodynamics and Ore Deposit Evolution in Europe*, 27(1–4) : 241–267, 2005. ISSN 0169-1368. doi : 10.1016/j.oregeorev.2005.07.013.

P. Muron. *Méthodes numériques 3-D de restauration des structures géologiques faillées*. PhD thesis, Institut National Polytechnique de Lorraine, 2005.

M. Narkiewicz, M. Resak, R. Littke, and L. Marynowski. New constraints on the Middle Palaeozoic to Cenozoic burial and thermal history of the Holy Cross mts. Central Poland : results from numerical modelling. *Geologica Acta*, 8(2) : 189–205, 2010.

V. Ojala, J. Ridley, D. Groves, and G. Hall. The Granny Smith gold deposit : the role of heterogeneous stress distribution at an irregular granitoid contact in a greenschist facies terrane. *Mineralium Deposita*, 28(6) : 409–419, 1993. ISSN 0026-4598. doi : 10.1007/BF02431599.

J. Ortiz and X. Emery. Geostatistical estimation of mineral resources with soft geological boundaries : a comparative study. *JOURNAL-SOUTH AFRICAN INSTITUTE OF MINING AND METALLURGY*, 106(8) : 577, 2006. ISSN 0038-223X.

J. M. Ortiz and C. V. Deutsch. Indicator simulation accounting for multiple-point statistics. *Mathematical Geology*, 36(5) : 545–565, 2004.

S. Oszczepalski. Origin of the Kupferschiefer polymetallic mineralization in Poland. *Mineralium Deposita*, 34(5) : 599–613, 1999.

S. Oszczepalski and S. Speczik. Prospectivity analysis of the polish Kupferschiefer - new insight. In *Proceedings of the 11th SGA Biennial Meeting*, 2011.

S. Oszczepalski, A. Rydzewski, and I. Geologiczny. *Metallogenic atlas of Zechstein copper-bearing series in Poland*. Wydawnictwo Kartograficzne Polskiej Agencji Ekologicznej, 1997.

PARADIGM. *Training guide : modeling reservoir architecture. SKUA - Paradigm*. PARADIGM, 2012.

W. Pawlak, J. Aniol-Kwiatkowska, J. Pawlak, E. Nowak-Ferdhus, P. Migoń, A. Malicka, A. Marciniak, W. Żak, U. Wrocławski, and P. A. Nauk. *Atlas Śląska dolnego i opolskiego*. Uniwersytet Wrocławski. Pracownia Atlasu Dolnego Śląska, 2008.

G. N. Phillips, D. I. Groves, and R. Kerrich. Factors in the formation of the giant Kalgoorlie gold deposit. *Ore Geology Reviews*, 10(3-6) : 295–317, 1996. doi : 10.1016/0169-1368(95)00028-3.

J. Pieczonka, A. Piestrzyński, J. Mucha, A. Głuszek, M. Kotarba, and D. Więcław. The red-bed-type precious metal deposit in the Sieroszowice-Polkowice copper mining district, SW Poland. *Annales Societatis Geologorum Poloniae*, 78 : 151–280, 2008.

A. Piestrzyński, J. Pieczonka, and A. Głuszek. Redbed-type gold mineralisation, Kupferschiefer, south-west Poland. *Mineralium Deposita*, 37(5) : 512–528, 2002.

A. Piestrzyński and Z. Sawlowicz. Exploration for Au and PGE in the Polish Zechstein copper deposits (Kupferschiefer). *Journal of Geochemical Exploration*, 66(1-2) : 17–25, 1999.

A. Piestrzyński and A. Wodzicki. Origin of the gold deposit in the Polkowice-West Mine, Lubin-Sieroszowice mining district, Poland. *Mineralium Deposita*, 35(1) : 37–47, 2000.

W. Pytel. Rock mass—mine workings interaction model for Polish copper mine conditions. *International Journal of Rock Mechanics and Mining Sciences*, 40(4) : 497–526, 2003.

T. Rawling, P. Schaubs, L. Dugdale, C. Wilson, and F. Murphy. Application of 3D models and numerical simulations as a predictive exploration tool in western Victoria. *Australian Journal of Earth Sciences*, 53(5) : 825–839, 2006.

J. Rentzsch and H. Franzke. Regional tectonic control of the Kupferschiefer mineralization in Central Europe. *Zeitschrift für Geologische Wissenschaften*, 25 : 141–150, 1997.

J. Rentzsch, H. Franzke, and G. Friedrich. Die laterale Verbreitung der Erzmineralassoziationen im deutschen Kupferschiefer. *Zeitschrift für Geologische Wissenschaften*, 25 : 121–140, 1997.

M. Resak, M. Narkiewicz, and R. Littke. New basin modelling results from the Polish part of the Central European Basin system : implications for the late Cretaceous−Early Paleogene structural inversion. *International Journal of Earth Sciences*, 97(5) : 955–972, 2008.

J. P. Richards. Tectono-Magmatic Precursors for Porphyry Cu-(Mo-Au) Deposit Formation. *Economic Geology*, 98(8) : 1515–1533, 2003. doi : 10.2113/gsecongeo.98.8.1515.

A. Roberts. Curvature attributes and their application to 3D interpreted horizons. *First break*, 19 (2) : 85–100, 2001.

D. Rouby. *Restauration en carte des domaines faillés en extension. Mééthode et applications.* PhD thesis, Universit Rennes 1, 1994.

F. J. Sawkins. Sulfide ore deposits in relation to plate tectonics. *The Journal of Geology*, p. 377–397, 1972.

F. J. Sawkins. *Metal deposits in relation to plate tectonics*, vol. 17. Springer-Verlag Berlin, 1984.

H. Schaeben. Comparison of mathematical methods of potential modeling. *Mathematical Geosciences*, 44(1) : 101–129, 2012.

H. Schaeben. Bits of mathematics of potential modelling. In *Mineral deposits research for a high–tech world. 12th Biennial SGA Meeting*, vol. 2, p. 489–491, 2013.

H. Schaeben. Potential modeling : conditional independence matters. *GEM - International Journal on Geomathematics*, 5(1) : 99–116, 2014. ISSN 1869-2672.

H. Schaeben and S. Schmidt. Theoretical and practical comparison of weights-of-evidence and logistic regression models based on the notion of Markov random fields. In *33rd Gocad Meeting Proceedings*, 2013.

M. Scheck-Wenderoth and J. Lamarche. Crustal memory and basin evolution in the Central European Basin system : new insights from a 3D structural model. *Tectonophysics*, 397(1-2) : 143–165, 2005.

A. Schmidt Mumm and M. Wolfgramm. Fluid systems and mineralization in the north German and Polish basins. *Geofluids*, 4(4) : 315–328, 2004.

J. G. Sclater and P. A. F. Christie. Continental stretching : an explanation of the Post-Mid-Cretaceous subsidence of the Central North Sea basin. *Journal of Geophysical Research.*, 85 (B7) : 3711–3739, 1980.

M. Scutari. Learning Bayesian networks with the bnlearn R package. *Journal of Statistical Software*, 35(i03), 2010.

H. A. Sheldon and S. Micklethwaite. Damage and permeability around faults : Implications for mineralization. *Geology*, 35(10) : 903–906, 2007.

R. H. Sibson. Brittle-failure controls on maximum sustainable overpressure in different tectonic regimes. *AAPG Bulletin*, 87(6) : 901 –908, 2003.

R. H. Sibson. Controls on maximum fluid overpressure defining conditions for mesozonal mineralisation. *Journal of Structural Geology*, 26 : 1127–1136, 2004.

R. H. Sillitoe. A plate tectonic model for the origin of porphyry copper deposits. *Economic Geology*, 67(2) : 184–197, 1972. doi : 10.2113/gsecongeo.67.2.184.

D. A. Singer and R. Kouda. Application of a feedforward neural network in the search for Kuroko deposits in the Hokuroku district, Japan. *Mathematical Geology*, 28(8) : 1017–1023, 1996.

S. Speczik. The Kupferschiefer mineralization of Central Europe : New aspects and major areas of future research. *Ore Geology Reviews*, 9(5) : 411–426, 1995.

S. Speczik, S. Oszczepalski, M. Karwasiecka, and G. Nowak. Kupferschiefer – a hunt for new reserves. In *Digging deeper. 9th Biennial SGA Meeting. Irish Association for Economic Geology, Dublin*, p. 237–240, 2007.

K. Sprague and E. de Kemp. Interpretive tools for 3-d structural geological modelling part II : Surface design from sparse spatial data. *GeoInformatica*, 9(1) : 5–32, 2005. ISSN 1384-6175. doi : 10.1007/s10707-004-5620-8.

H. J. Stein, R. J. Markey, J. W. Morgan, J. L. Hannah, and A. Scherstén. The remarkable Re–Os chronometer in molybdenite : how and why it works. *Terra Nova*, 13(6) : 479–486, 2001. ISSN 1365-3121. doi : 10.1046/j.1365-3121.2001.00395.x.

R. A. Stephenson, M. Narkiewicz, R. Dadlez, J.-D. van Wees, and P. Andriessen. Tectonic subsidence modelling of the Polish basin in the light of new data on crustal structure and magnitude of inversion. *Sedimentary Geology*, 156(1-4) : 59–70, 2003.

C. Swager and T. Griffin. Geology of the Archaean Kalgoorlie Terrane, Northern and Southern Sheets, 1 :250 000., 1990.

D. Symons, K. Kawasaki, S. Walther, and G. Borg. Paleomagnetism of the Cu−Zn−Pb−bearing Kupferschiefer black shale (Upper Permian) at Sangerhausen, Germany. *Mineralium Deposita*, 46 (2) : 137–152, 2011.

M.-O. Titeux. *Restauration et incertitudes structurales : changement d'échelles des propriétés mécaniques et gestion de la tectonique salifière*. PhD thesis, Institut National Polytechnique de Lorraine, 2009.

D. J. Vaughan, M. A. Sweeney, G. Friedrich, R. Diedel, and C. Haranczyk. The Kupferschiefer ; an overview with an appraisal of the different types of mineralization. *Economic Geology*, 84(5) : 1003 –1027, 1989.

P. Verrall. *Structural interpretation with application to North Sea problems. Course note no. 3.* Joint Association for Petroleum Exploration courses (UK), 1981.

O. Vidal-Royo, N. Cardozo, J. A. Muñoz, S. Hardy, and L. Maerten. Multiple mechanisms driving detachment folding as deduced from 3D reconstruction and geomechanical restoration : the Pico del Águila anticline (External Sierras, southern Pyrenees). *Basin Research*, 24(3) : 295–313, 2012.

T. Wagner, M. Okrusch, S. Weyer, J. Lorenz, Y. Lahaye, H. Taubald, and R. Schmitt. The role of the Kupferschiefer in the formation of hydrothermal base metal mineralization in the Spessart ore district, Germany : insight from detailed sulfur isotope studies. *Mineralium Deposita*, 45(3) : 217–239, 2010.

G. Wang, S. Zhang, C. Yan, Y. Song, Y. Sun, D. Li, and F. Xu. Mineral potential targeting and resource assessment based on 3D geological modeling in Luanchuan region, China. *Computers & Geosciences*, 37(12) : 1976–1988, 2011. ISSN 0098-3004. doi : 10.1016/j.cageo.2011.05.007.

K. Wedepohl and J. Rentzsch. The composition of brines in the early diagenetic mineralization of the Permian Kupferschiefer in Germany. *Contributions to Mineralogy and Petrology*, 152(3) : 323–333, 2006.

J. F. Wellmann, F. G. Horowitz, E. Schill, and K. Regenauer-Lieb. Towards incorporating uncertainty of structural data in 3D geological inversion. *Tectonophysics*, 490(3–4) : 141–151, 2010.

M. O. Withjack and S. Callaway. Active normal faulting beneath a salt layer : an experimental study of deformation patterns in the cover sequence. *AAPG bulletin*, 84(5) : 627–651, 2000.

M. O. Withjack, J. Olson, and E. Peterson. Experimental models of extensional forced folds (1). *AAPG Bulletin*, 74(7) : 1038–1054, 1990.

W. Witt and F. Vanderhor. Diversity within a unified model for Archaean gold mineralization in the Yilgarn Craton of Western Australia : An overview of the late-orogenic, structurally-controlled gold deposits. *Ore Geology Reviews*, 13(1–5) : 29–64, 1998. ISSN 0169-1368. doi : 10.1016/S0169-1368(97)00013-9.

A. Wodzicki and A. Piestrzyński. An ore genetic model for the Lubin-Sieroszowice mining district, Poland. *Mineralium Deposita*, 29(1) : 30–43, 1994.

S. Wyche. Kalgoorlie Western Australia Map : 1 :250 000, Geological Series Sheet SH51-9, 1993.

Y. Zhang, A. Karrech, P. M. Schaubs, K. Regenauer-Lieb, T. Poulet, and J. S. Cleverley. Modelling of deformation around magmatic intrusions with application to gold-related structures in the Yilgarn Craton, Western Australia. *Tectonophysics*, 526-529(0) : 133–146, 2012. doi : 10.1016/j.tecto.2011.08.013.

P. Ziegler. *Geological atlas of Western and Central Europe*. Number vol. 1. Shell International Petroleum Maatschappij B.V., 1982.

O. C. Zienkiewicz. *The finite element method*. London ; New York : McGraw-Hill, expanded and reviewed edition, 1977. ISBN 0070840725.

R. Zuo and E. J. M. Carranza. Support vector machine : A tool for mapping mineral prospectivity. *Computers & Geosciences*, 37(12) : 1967–1975, 2011.

Table des figures

1 Quelques éléments géométriques de base utilisés dans la modélisation 3D 2
2 Six différents types de représentations appliquées dans la modélisation 3D 4
3 Application de la restauration structurale d'un modèle surfacique dans un cas hypothétique 6

1.1 Quelques relations spatiales et temporelles dans les gisements hydrothermaux 13
1.2 Relation temporelle de quelques gisements à l'échelle globale 14
1.3 Principales échelles dans la modélisation des gisements et des phénomènes géologiques liés à leur formation 15
1.4 Exemples simplistes des différentes approches dans la modélisation de gisements . . 17
1.5 Exemple schématique des différentes approches dans la modélisation spatio-temporelle de gisements 19

2.1 Presente day distribution of the Zechstein Formation in Europe 23
2.2 Location and 3D model of the Legnica-Głogów Copper Belt district 23
2.3 Schematic representation of the Kupferschiefer mineralization 24
2.4 Stratigraphic column of LGCB district based on exploration drill-holes 25
2.5 Input data and resulting 3D model of the Legnica-Głogów Copper Belt district . . . 27
2.6 Simple-shear restoration method 28
2.7 Graphic illustrating an example of the steps involved in the decompaction-restoring algorithm for a syndepositional folding scenario without faulting 29
2.8 3D models from the restoration of the LGCB region showing the restored top of the Rotliegend Formation with the compaction effects 31
2.9 1D basin evolution and some datations of the Kupferschiefer mineralization in Germany and Poland 32
2.10 Burial history from PetroMod 1D analysis in a virtual well located in the LGCB model 34
2.11 Fluid pressure and hydraulic fracturing development under different tectonic regime conditions 35
2.12 Stratigraphical grid representing the LGCB 3D model at Late Cretaceous–Early Paleocene with HF estimations 36
2.13 Relationship between the Cu content and the hydro-fracturing index (HF) 37
2.14 1D basin evolution simulations estimated on different locations in Poland 38

3.1 Simplified geological cross section across the Fore-Sudetic Monocline 43
3.2 Fore-Sudetic Monocline 3D model built using the *structure and stratigraphy SKUA®-2011* workflow 46
3.3 Location of the study area and resulting model of the FSM 47
3.4 Schematic surface-restoration workflow 48
3.5 Synthetic case of structural restoration 50
3.6 Cartoon showing some discrepancies that may arise in the unflattened surfaces for a given restoration step 51

3.7 Maximum curvature corresponding to each restoration step from Cretaceous to Upper Permian . . . 52
3.8 Predicted probabilities from the LR models by predictor . . . 55
3.9 *Graph* of the conditional independence test for K_l (l=1: Cretaceous, 2: Jurassic, 3: Triassic, 4: Upper Permian), *HFB* and *ZBK* given Cu-potentials . . . 55
3.10 Predicted probabilities of Cu-potentials (P) in the FSM . . . 56

4.1 Simplified geologic map of the Mount Pleasant area . . . 63
4.2 Cross-section of the study area showing the structural configuration of the main rock units . . . 64
4.3 3D model of the Mount Pleasant area . . . 66
4.4 3D solid model used for the geomechanical restoration . . . 66
4.5 Rock properties used for the geomechanical restoration . . . 67
4.6 3D surface-based model of the Mount Pleasant area . . . 67
4.7 Top view of the study area showing the strain eigenvalues from restoration . . . 68
4.8 Structural attributes related to ore-forming process . . . 70
4.9 Predicted probabilities using LR analysis for gold occurrences in the Liberty granodiorite area . . . 71
4.10 Comparison of the forward dilatation and the gradient of ξ as predictors for off-fault gold distribution . . . 72
4.11 Relation between gold occurrences locations and the gradient of ξ in the shortening direction $\boldsymbol{x}$ . . . 73

12 Flowchart showing the main steps for applying *escript* in Gocad models . . . 101
13 Simulation of stationary Darcy's law flux on a Gocad model representing a sector of the Furfooz region, Belgium . . . 103
14 Models with different structural complexity . . . 108
15 a: Training data and b: re-created geology . . . 108
16 SVM predictions estimating accuracy and error for the models . . . 109
17 Scheme integrating the concepts used in this work . . . 113
18 Restoring workflow in a synthetic case . . . 114
19 Main sedimentary units in the FSM . . . 116
20 (a) Decompaction parameters applied during restoration. (b) Rotliegend Formation in the FSM corresponding at restored times . . . 116
21 High positive dilatation values achieved from the FSM restoring . . . 117
22 Extracted layers from the 3D model of the FSM showing Cu distribution, Cu potentials and dilatation from 2D-restoration . . . 118
23 Probabilities of Cu potentials from LR analysis applying different cut-off and mineralized zones in the predictive modeling . . . 119
24 Positive dilatations as categorical variable (PDC) in the FSM . . . 120
25 Schematic image representing the the SVM function . . . 126
26 Main *Cu Zn, Pb* occurrences in Central Europe . . . 126

27 Comparing results using SVM and LR for Cu-potentials 128

Liste des tableaux

2.1 Rock properties used for the modeled horizons of the LGCB area 30
2.2 Input data used for the 1D simulation in PetroMod 33

3.1 LR model by restoration step curvature 54
3.2 LR model by complementary predictors 54
3.3 LR model coefficients with significant interaction terms 56
3.4 Restoration steps, geodynamic setting and high curvature in Cu-potential areas . . . 57

Annexes

A.0. Algorithmes et procédures

Decompaction

The core of the **decompaction_Surf(GObj)** GoPy procedure here described applies the eq. 2.1 used in the chapter 2. It comprises:

– A main program which calls the **decompaction_Surf(GObj)** function with the appropriate parameters such as the depth porosity factor (c)and the initial porosity (ϕ_0, ϕ_0), where $Surf$ is a list of surfaces (top surface) separating the different layers to be decompacted.

– The function **Decompacting_Surf(GObj)** reads the list of surfaces from top to bottom and performs the decompaction, i.e. computes the true layer depths solving eq. (2.1) using a recursive function $Optimum(z, z_{new}, z_1, z_{1new}, \phi_0, c)$.

– The recursive $Optimum$ function finds the zeros x of a function $f(x) = 0$

The user gives the list of the surfaces and launches the **decompaction_Surf(GObj)** GoPy plug-in. The procedure builds automatically a new set of corresponding decompacted surfaces following the decompaction procedure described by Allen and Allen [2005].

```
#---* DECOMPACTION SURFACES IN GOCAD *---

#From Scatter & Christie (1980) JGR,85,3711-3729
#The equation governing the upward movement of a stratigraphic horizon is
#used to decompact an horizon.

#Input parameters:
# z = initial layer depth
# znew = layer depth after decompaction
# porosity = surace porosity of sediments to decompact
# deep_porosity_factor = rock type dependent compressibility factor used
# to estimate increase in porosity during decompaction,
# c = 0.62E-3 m^{-1} e.g. for silt and sandstones

#Loading packages
import math
from scipy.optimize import fsolve

def Decompacting_One_Surf(surf):
# Input parameters:
# Surf = GObj surface name
# SurfUp = name of the Z of the upper horizont property attached to surf.
# SurfUp_dec = neame of the Z of the upper horizon after decompaction property attached to surf
# SurfPorosity  = name of the surface porosity property attached to surf
# SurfDPF = name of the deep_porosity_factor attached to surf
for i in GObj(surf):

        z = - i.Z
```

```
        z1 = - i.property(ZUp).get()
        z1new = - i.property(ZUp_dec).get()
        phi  = 0.000051  # ... i.property(SurfPorosity).get()
        dpf = 0.000000062 # ... i.property(SurfDPF).get()
        fc = phi/dpf
        def Optimize_SC_equation (p):

            znew = p
            return(znew - z1new + (fc)*(math.exp(-dpf*znew)-math.exp(-dpf*z1new) + \
            math.exp(-dpf*z1) - math.exp(-dpf*z)) -(z - z1))

        i.Z = - fsolve(Optimize_SC_equation, (100))

#---* Main * ----

surface = "target_surface"
surf = "target_surface_dec"
surfaceUp = "upper_target_surface"
surfaceUp_dec = "upper_target_surface_dec"
ZUp = "Zup"
ZUp_dec="Zup_dec"

#SurfPorosity = "SP" # This property is defined by the material on top: taget - 1
#SurfDPF = "DPF"     # This property is defined by the material on top: target - 1
#_____________________________________________________________________
gocad.run('gocad on GObj "%s" remove_property name "Zup";'%(surface))
gocad.run('gocad on GObj "%s" remove_property name "Zup_dec";'%(surface))
#_____________________________________________________________________
gocad.run('gocad on VerticalPropertyClient "%s" fill_vertically_from_property \
region "everywhere" new_property_name "Zup" from "%s" from_region "everywhere" \
property "Z" share_property_class "false";' %(surface,  surfaceUp))
gocad.run('gocad on AtomicGroup "%s" init_dsi_property property "Zup";' %(surface))
gocad.run('gocad on AtomicGroup "%s" run_dsi_property property "Zup" region "everywhere" \
nbiter 10 smooth "false" conjugate "false" fitting_factor 2;' %(surface))
gocad.run('gocad on VerticalPropertyClient "%s" fill_vertically_from_property \
region "everywhere" new_property_name "Zup_dec" from "%s" from_region "everywhere" \
property "Z" share_property_class "false";' %(surface,  surfaceUp_dec))
gocad.run('gocad on AtomicGroup "%s" init_dsi_property property "Zup_dec";' %(surface))
gocad.run('gocad on AtomicGroup "%s" run_dsi_property property "Zup_dec" region "everywhere"
nbiter 10 smooth "false" conjugate "false" fitting_factor 2;' %(surface))
gocad.run('gocad copy GObj "%s" name "%s" copy_properties "true" copy_regions "true" copy_style \
"true" copy_points "true" copy_constraints "false";' %(surface, surf))
#_____________________________________________________________________
Decompacting_One_Surf(surf)
```

Export data, logistic regression analysis (LR) and import results from Gocad to R assisted by GoPy

The core of the *logistic regression modeling* procedure here described applies the eqs. 3.1 and 4.3 used in the chapters 3 and 4.

In GoPy to write:

```
#---- *** WRITE *** ----
# Created by Christophe Antoine

# This script read given property values in a Voxet, write them down in a file.
# Function to write the given properties (in plist) on the given voxet in the given filename
# The .txt file will be placed in the same folder that your gocad project.
```

```
def write_data(voxet, filename, plist) :
    f=open(filename,"w")
    f.write('\t'.join(plist)+'\n')

    for i in GObj(voxet):
       value = tuple(str(i.property(j).get()) for j in plist)
       f.write('\t'.join(value)+'\n')
    f.close()


voxet ="name_voxet"
filename = "file_name_voxet.txt"

p1 = "p1" # continuous or discret variable
p2 = "p2" # continuous or discret variable
p3 = "p3" # continuous or discret variable
p4 = "binary_target" # binary variable: 0 and 1

plist = [p1, p2,  p3, p4]

write_data(voxet, filename, plist)
```

In R :

```
#---- *** LR ANALYSIS *** ----

# reading data from voxet
Q36 <- read.table("pathway"/file_name_voxet.txt",header=TRUE)

# creating a LR model
lrM <- glm(binary_targetd ~ p1 + p2 + p3 + p4, family=binomial("logit"),data=Q36)
summary(lrM)

# obtainig predicted probabilities using the LR model
log_pred <- predict(lrM, newdata = Q36, type = "response", se.fit=TRUE)

# writing the results in a txt file
write(t(log_pred),file='pred_study.txt',ncolumns=2, sep = "\$")
```

In GoPy to read:

```
#---- *** READ *** ----
# Created by Christophe Antoine

# Function to read the data from the file and put them back as properties in the Voxet
# ignore_col gives the number of columns to ignore in the file (i.e. input data)

def read_data(voxet,filename, plist, ignore_col=0):
    f = open(filename)
    minlen = ignore_col + len(plist)

    for i in GObj(voxet) :
        #reqd line
        x = f.readline().strip().split('\t')
        assert len(x)>= minlen, "Line too short"
        ci = ignore_col
        for j in plist :
            i.property(j).set(float(x[ci]))
            ci +=1
```

```
    f.close()

# creating property to store the predicted probability
voxet_name = "name_voxet"
gocad.run('gocad on GObj "%s" create_property  property_name d1 no_datavalue_specified 1 \
no_datavalue -99999 number_of_elements 1 property_kind "unknown" storage Memory;' %(voxet_name))

# creating proerty to store the error associated to the predicted probability
gocad.run('gocad on GObj "%s" create_property  property_name d2 no_datavalue_specified 1 \
no_datavalue -99999 number_of_elements 1 property_kind "unknown" storage Memory;' %(voxet_name))

plist = ('d1', 'd2')
nb_input_prop=len(plist)

# File used to communicate with R
filename = "pred_study.txt"

read_data(voxet_name, filename, plist)
```

A.1. Solving non-linear PDEs on Gocad models using *escript*

Presented at: 34^{th} Gocad Meeting. September 2014. Nancy School of Geology. Vanodoeuvre-Les-Nancy.

Pablo Mejía-Herrera[1,2], Côme Le Breton[2], Arnaud Botella[1,2,3]

1. GeoRessources (UMR 7359), Université de Lorraine, ENSG, CREGU, 2 rue du Doyen Marcel Roubault, Vandoeuvre-lès-Nancy, 54518, France
2. Université de Lorraine-ENSG, Vandoeuvre-lès-Nancy, 54518, France
3. INRIA Lorraine-LORIA, Project Alice, 615 rue de Jardin Botanique, Villers-lès-Nancy, 54600, France

abstract

This paper proposes a workflow to solve on Gocad 3D models mathematical systems, coupled, non-linear and time-dependent partial differential equations. Using *escript*, a *Python*-based environment for applying and then obtaining the PDEs solutions, a large variety of problems such as heat transfer, elastic deformation or wave propagation simulations can be solved directly in Gocad. Assisted by the GoPy plugin, the 3D model defines the space where the PDEs solver is computed. The finite-element-method mesh volume required for the simulations is provided by a *Tsolid*, where a python script reads the *Tsolid* ASCII file and then creates the 3D domain adapted to apply *escript*. The solution can be stored in the initial 3D model or exported for generic visualization platforms. The proposed workflow is demonstrated on a highly curved 3D model from the Furfooz region. There, we simulated a stationary darcy flux that evidences the utility and simplicity of the method.

Introduction

In Earth Sciences, as in other physical sciences, the modeling of geological phenomena become more and more complex. To be able to simulate those phenomena, progress have been made in two computational branches : the 3D modeling of geological objects and structures, and the capacity to solve physical problems. This second, has led the development of scientific libraries (in several programming languages), allowing the geoscientists to build mathematical models for both theoretical and applied cases.

Python is a high-level interface tool largely used by the community because of free distribution, open-source advantages and learning facilities [Swinnen, 2012]. A broad offer of numerical packages are available using the *Python* interface, *escript* being one of the most complete and user-friendly to solve complex mathematical models, particularly coupled, non-linear and time-dependent partial differential equations (PDEs) [Gross et al., 2010]. *escript* was developed by the Earth Systems Science

Computational Centre (ESSCC) to describe numerical models using computational components implemented in C and C++ for achieving high performance for time-intensive, numerical calculations [Gross et al., 2007b]. Although it is well known that implementing a high-level language brings the risk of loss of computing time, this is often offset by reducing development time, especially when the computational tasks are performed in C and C ++ and *Python* is used only as interface for executing calculations [Gross et al., 2007a].

The aim of the present contribution is to show the advantages of solving PDEs on 3D structural models created in Gocad. Using the the GoPy plugin [Antoine and Caumon, 2008], it is possible to extract the tetrahedral mesh domain that represents the structural model and then run the *escript* package to solve PDEs. Coupling *escript* to Gocad allows to easily compute under the same platform simulations of physical phenomena on complex geological 3D configurations. The result data can either stored in the input discretized domain or exported in a format suitable for visualization.

Mesh for FEM Simulations

Finite element method (FEM) aims to solve numerically PDEs for either static or dynamic physical phenomena [Zienkiewicz, 1977]. It was popularized in the sixties and seventies with the development of specialized FEM softwares, and more recently by available open source FEM programs on a large variety of platforms [Zienkiewicz, 1977, Ingebritsen and Appold, 2012].

The principle of FEM is to estimate the PDE solution using the nodes of a discretized space, being the PDEs solution approximated by its values on the nodes. In a surface-based structural model, the surfaces represent geological interfaces such as horizons and faults [Caumon et al., 2009], and could be considered as the boundaries of physical or mechanical properties. In those cases, the domain is discretized usually using a mesh to fill the whole domain.

The *escript* environment provides the *esys.pycad* module, which offers a user-tool to build and manipulate simple geometries for the finite element simulation. Additionally, with the *esys.finley* module, it is possible to create a domain using primitive geometric objects and then generate a mesh (being *Gmsh* [Geuzaine and Remacle, 2009] the currently mesh generator coupled with *escript*).

Nevertheless, for complex geological geometries, such as realistic 3D structural models, it is necessary creating the FEM space with an efficient geomodeller and then to read the mesh file that contains the 3D model where the PDEs will be solved.

Running *escript* in Gocad

To perform *escript* on a Gocad structural model it is necessary to discretize it. We choose the *Tsolid* with linked 3D boundary representation model (a tetrahedral mesh with macro-topological information) for representing the discretized structural model. In the *Tsolid* the logical regions are defined according to the extension of their dimensions : **3** for regions composed by tetrahedrons, **2** for regions composed by tetrahedral faces, **1** for regions composed by the intersections of faces, and **0** defined by a tetrahedron node [Lepage, 2003].

From the *Tsolid* file format (*.so), is obtained the finite element mesh that defines the domain applying the *python* script **so2msh_VRTX_v0** [Le Breton, 2014]. This script reads the *Tsolid* file format (*.so) and then writes the *Gmsh* file format (*.msh) that allows to define the PDEs domain for *escript*.

To reduce errors in PDEs solutions, a remeshing method can be used to increase the quality of the tetrahedral mesh. We use the Tweedle plugin [Botella et al., 2014, Pellerin et al., 2014] to remesh

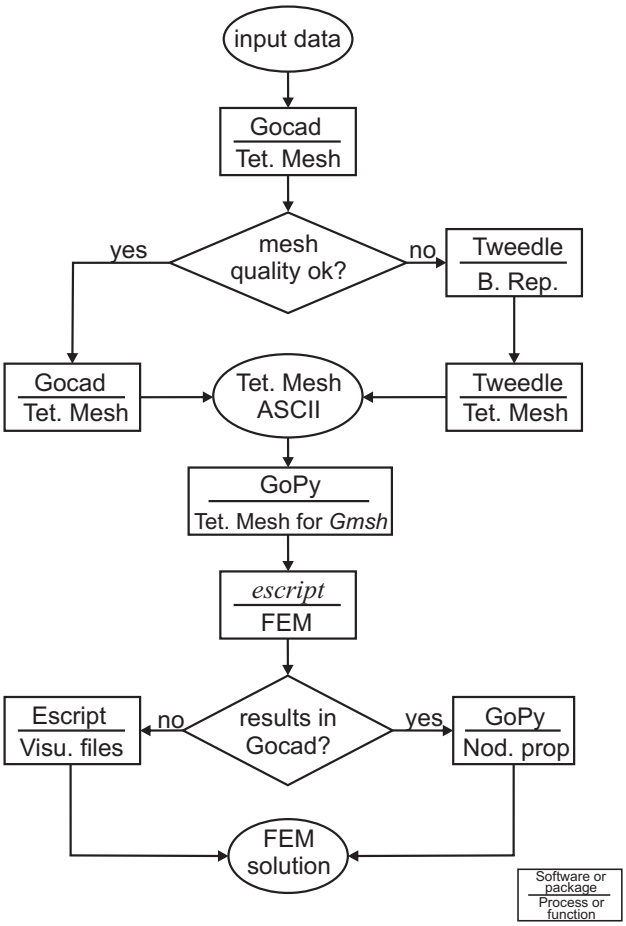

FIGURE 12 – Flowchart showing the main steps for applying *escript* in Gocad models.

the model before the conversion to *Gmsh* format using the Tweedle package. Finally, the result data can be stored in the *Tsolid* or can be saved as dataset in *VTK, SILO* or other generic formats. The Figure 12 presents the overall workflow for using *escript* in a Gocad structural model.

Study Case

For this section, we used the structural model from a terrain portion of the Furfooz karstic region in Belgium (Figure 13a) [Dewaide et al., 2013], for a stationary darcy flux case implementing FEM with *escript*. This model comprises 11 surfaces (2D regions including the boundaries), and 6 volumes (3D regions). The 2D regions **7** and **11**, as well as the 3D region **15**, are highlighted in the Figures 13a and 13b then they have specific attributes in the simulation .

We followed and applied the *escript* functions as described by Hallam et al. [2010] and Gross et al. [2010], and we encourage the reader to see those works for a better comprehension of *escript* and its scope. First, we create the domain of a PDE using the *Tsolid* (Figure 13b, c) file format using the *python* script :

```
#... setting domain
from esys.escript import *
from so2msh_VRTX_v0 import *
from esys.finley import ReadGmsh
solidmodel = PyGocadFile("file.so") # Tsolid file format
```

```
solidmodel.writeInMshFile("file.msh") # Gmsh file format
mydomain=ReadGmsh("file.msh",numDim=3) # 3=(int) number dimension.
```

The material properties, such as the permeability (K0) in this example, can be defined for each 3D and 2D logical regions of the *Tsolid* using the function **setTaggedValue** as follows :

```
#... setting properties
K0=Scalar(1e-5,Function(mydomain))
K0.setTaggedValue(15, 1e-2) # 15 = id. number of the logical region.
```

Where the value 10^{-5} is the permeability defined as scalar in the whole domain, except for the 3D region **15** which has a tagged permeability of 10^{-2}. For boundary conditions, it is possible to define them on the 3D and 2D logical regions using the function **MaskFromBoundaryTag**. The below script shows how to use this function to specify the solution in the 2D regions **7** and **11** of the model :

```
#... setting boundary conditions
from esys.escript.linearPDEs import LinearPDE
darcy=LinearPDE(mydomain)
from esys.escript.pdetools import MaskFromBoundaryTag
mask1 = MaskFromBoundaryTag(mydomain, 7)
mask2 = MaskFromBoundaryTag(mydomain,11)
r1 = 50. * mask1
r2 = 100. * mask2
darcy.setValue(q=mask1+mask2, r=r1+r2)
```

Where **LinearPDE** is the solver method applied for this example. The constraint of the darcy equation is in the form $u = r$ where $q > 0$, being u the variable we are solving for. The solution of the PDEs is set where q is positive, and the function **MaskFromBoundaryTag** assigns a positive value in those 2D regions. It means that the solution has the values 50 and 100 in the two surfaces **7** and **11** now defined as **mask1** and **mask2**.

Once the physical properties, solver method and boundary conditions were specified, we computed the darcy problem. It is possible to export the results as data in the *VTK* file format (Figure 13d, e and f) using the *esys.weipa* module :

```
#... getting results
darcy.setValue(A=K0*kronecker(Function(mydomain)), D=epsilon, Y=flow_source)
p=darcy.getSolution()
#.. calculate flux
del darcy
flux = - grad(p)
#... output ...
from esys.weipa import saveVTK
from esys.escript.pdetools import Projector
saveVTK(os.path.join('save_path',"data.%03d"), p=p, flux=proj(flux))
```

Where A, D and Y are the coefficients of the PDE expressed in the form :

$$-(A_{jl}u_{,l})_{,j} - (B_j u)_{,j} + C_l u_{,l} + Du = X_{j,j} + Y \tag{4}$$

Here $u_{,j}$ denotes the derivative of u with respect to the j^{th} direction (Einstein's summation notation assumed).

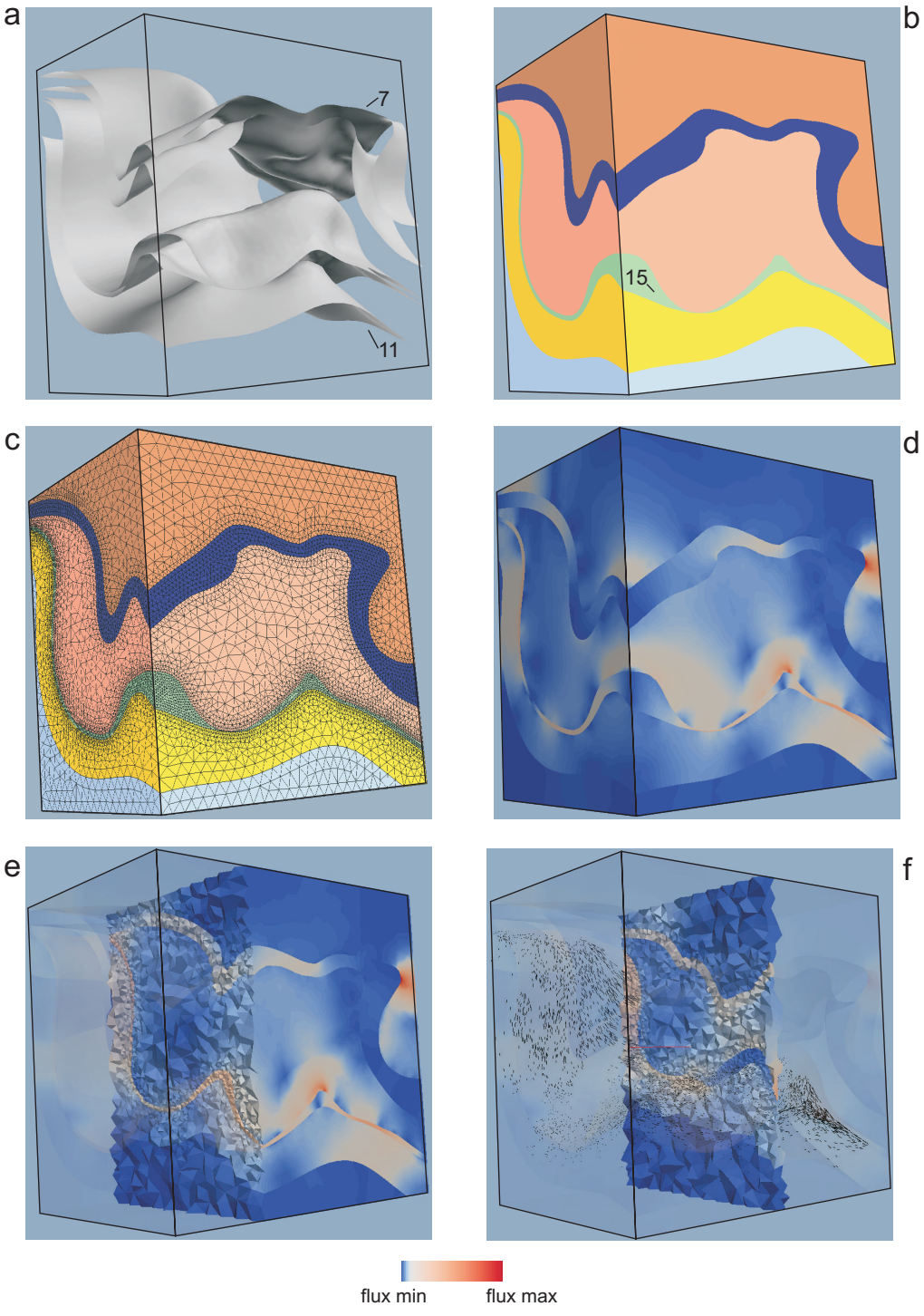

FIGURE 13 – Simulation of stationary Darcy's law flux on a Gocad model representing a sector of the Furfooz region, Belgium. Using the adaptive meshing technique introduced by Botella et al. [2014], the tetrahedral resolution was refined in the green and blue layers while the rest was adjusted to coarse resolution. (a) : surface-based model. (b) : boundary representation model. (c) : adaptive meshing the Tsolid. (d) to (f) : views of the flow simulation.

Conclusions

In this contribution, we show the convenience of using *escript* coupled to GOCAD via GoPy. The implementation of *escript* is quite simple and does not require rigorous programming knowledge to perform complex simulations. Modeling directly in Gocad the domain of PDEs, offers great advantages when it comes to simulate physical phenomena with mathematical models in complex structural frameworks.

Acknowledgments

This work has been performed in the frame of the Gocad research project. We thank the industry and academic members of the Gocad Research Consortium [2] for supporting this research. We also thank Paradigm for the Gocad software.

Bibliography

C. Antoine and G. Caumon. Rapid algorithm prototyping in gocad using python plugin. In *28th Gocad Meeting Proceedings*, pages 1–4, Nancy, France, June 2008. ASGA.

A. Botella, B. Levy, and G. Caumon. Constrained tetrahedra mesh generation : application to structural models and hex-dominant meshing. In *Proc. 34th Gocad Meeting*, Nancy, Sept. 2014. ASGA.

G. Caumon, P. Collon-Drouaillet, C. Le-Carlier-de Veslud, S. Viseur, and J. Sausse. Surface-based 3D modeling of geological structures. *Mathematical Geosciences*, 41(8) :927–945, Nov. 2009. 10.1007/s11004-009-9244-2. URL `http://dx.non_ido.org/10.1007/s11004-009-9244-2`.

L. Dewaide, J.-M. Baele, P. Collon-Drouaillet, G. Rochez, S. Vandycke, and V. Hallet. Dedolomitization process associated to karstification in the dolomitized Waulsortian mudmounds (Belgium). *Geologica Belgica*, 2013. ISSN 1374-8505.

C. Geuzaine and J.-F. Remacle. Gmsh : A 3-D finite element mesh generator with built-in pre- and post-processing facilities. *International Journal for Numerical Methods in Engineering*, 79(11) : 1309–1331, Sept. 2009. ISSN 1097-0207. 10.1002/nme.2579. URL `http://dx.doi.org/10.1002/nme.2579`.

L. Gross, L. Bourgouin, A. J. Hale, and H.-B. Muhlhaus. Interface modeling in incompressible media using level sets in escript. *Physics of the Earth and Planetary Interiors*, 163 :23–34, Aug. 2007a. doi :10.1016/j.pepi.2007.04.004. URL `http://www.sciencedirect.com/science/article/pii/S0031920107000647`.

L. Gross, B. Cumming, K. Steube, and D. Weatherley. A python module for PDE-based numerical modelling. In *Applied Parallel Computing. State of the Art in Scientific Computing*, pages 270–279. Springer, 2007b. ISBN 3540757546. URL `http://www.tp.umu.se/~nylen/PARA06/springer/46990270.pdf`.

L. Gross, C. Altinay, A. Amirbekyan, J. Fenwick, L. M. Olsen-Kettle, K. Steube, L. Graham, and H. B. Muhlhaus. esys-escript user's guide : Solving partial differential equations with Escript and Finley. *Release-3.2. The University of Queensland, Australia*, 2010. URL `http://espace.library.uq.edu.au/view/UQ:253350`.

2. http ://www.gocad.org/w4/index.php/consortium/members

A. Hallam, L. Gross, C. Altinay, A. Amirbekyan, J. Fenwick, and L. Gao. The escript cookbook : Release-3.2 (r3422). *Release-3.2. The University of Queensland, Australia*, 2010. URL `http://espace.library.uq.edu.au/view/UQ:289614`.

S. E. Ingebritsen and M. S. Appold. The physical hydrogeology of ore deposits. *Economic Geology*, 107(4) :559 –584, July 2012.

C. Le Breton. Applying *escript* on Gocad. 2nd year project report, Université de Lorraine-ENSG, Nancy, France, Apr. 2014.

F. Lepage. *Génération de maillages tridimensionnels pour la simulation des phénomènes physiques en géosciences*. PhD thesis, Institut National Polytechnique de Lorraine, 2003.

J. Pellerin, B. Lévy, G. Caumon, and A. Botella. Automatic surface remeshing of 3D structural models at specified resolution : A method based on Voronoi diagrams. *Computers & Geosciences*, 62(0) :103–116, Jan. 2014. ISSN 0098-3004. 10.1016/j.cageo.2013.09.008. URL `http://www.sciencedirect.com/science/article/pii/S0098300413002483`.

G. Swinnen. *Apprendre á programmer avec Python 3*. Editions Eyrolles, 2012.

O. C. Zienkiewicz. *The finite element method*. London ; New York : McGraw-Hill, expanded and reviwed edition, 1977. ISBN 0070840725.

A.2. Estimating structural complexity from statistical learning predictions

Pablo Mejía-Herrera & Jean-Jacques Royer (Université de Lorraine, GeoRessources-UMR 7359)

Presented at: Séminaire de annuel de l'École doctorale : « Ressources Végétales et Animales ... Quelles perspectives ? » *RP2E*-Université de Lorraine. Poster session, Janvier de 2014. Vandœuvre-les-Nancy.

Introduction

The structural complexity in a region on the earth surface directly impacts the difficulty, cost and risk associated with producing natural resources (Dromgoole and Speers, 1997 ; Trubetskoy, Galchenko and Sabyanin, 2012 ; Jolley et al., 2007). Anticipate, within a reasonable error margin, the structural complexity in a given locality could help to define better strategies to explore and exploit a natural resource placed in that locality. But, a question arises about the structural complexity: how it is possible to predict it from partial knowledge?

Smirnoff et al., (2008) showed the utility of statistical learning in the creation of 3D models representing the geology of a study area. Using sparse data obtained from several sources as training data-set, he applied support vector machine (SVM) in order to automate the creation of such models. With this method, a series of examples (called support vectors) are selected to define the classification rule to separate the different lithological units. Then, the classification rule is applied on the volume generating a cell-based 3D model. In this way, the shortest length of the example re-create the actual geology could indicate the structural complexity in a given study volume.

We built a based 3D model composed by four layered units (Fig. 1a). Later, based in that 3D model, five models are built increasing the structural tortuosity by adding deformation and faulting (fig. 14). Then, we applied the SVM predictions using the free *R* package *e1071* searching the optimal separating function between the lithological units in the first base model.

For the simplistic 3D model (fig. 15b), we estimated that 22% of the overall cells is the minimum length of a sample randomly chosen necessary to create an SVM predicting model without error (fig. 15a). But what happens when this length of sample is used to create the others "more complex" models from predictions ?

Methodology

Using partial data of the volume (22% of cells randomly chosen) as training data for each model, the geology is re-created as SVM predictions. A radial basis function, with $\gamma = 4$ and $C = 4$, was selected after finding the optimal parameters by tuning. we realized two simulations by model and then obtaining the total error (type I plus type II errors) (fig. 16a), as well as the amount of support

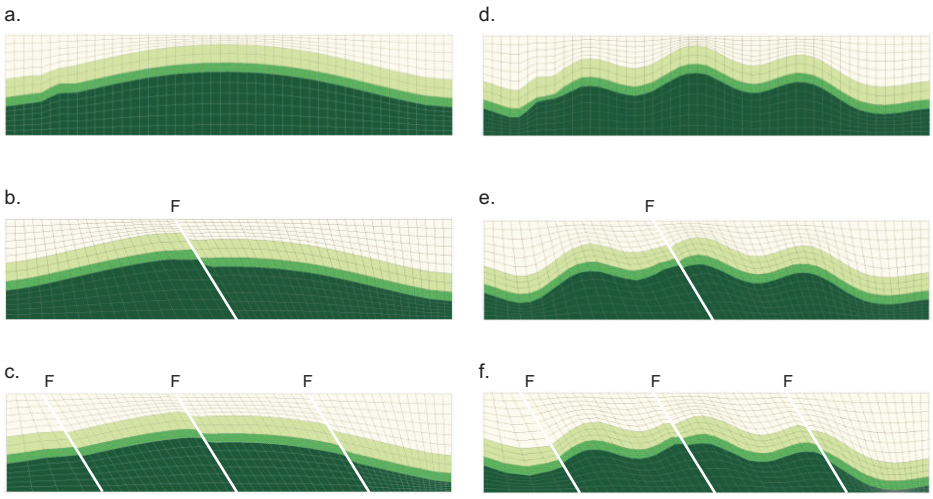

FIGURE 14 – Models with different structural complexity. a. Synthetic-simplistic 3D model. (b-f). Folded and faulted models based on the first one. The displacement in the single-fault models is bigger than the multi-fault models.

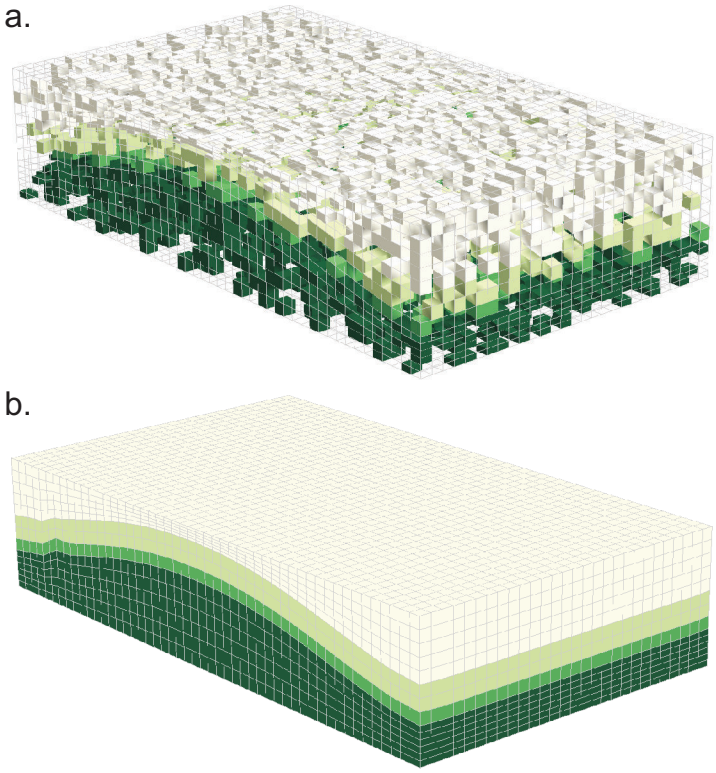

FIGURE 15 – a: Training data and b: re-created geology. SVM was used to fill the volume with the lithological units as predictions of (x,y,z). In this volume of 19600 cells, 22% of them are necessary to predict the lithology without error.

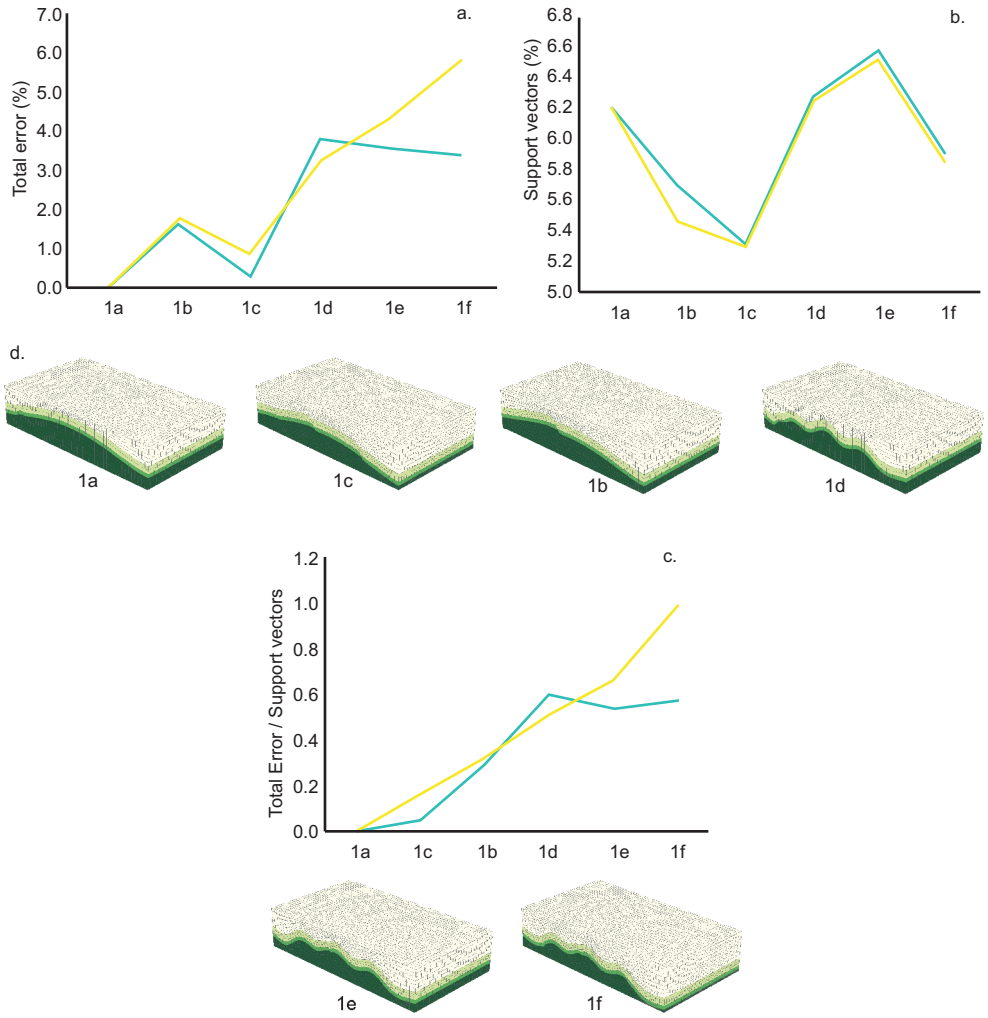

FIGURE 16 – SVM predictions estimating accuracy and error for the models. a: Total error from the error matrices in two predictions by model. b: Support vectors used by prediction on the re-created geology. c: Ratio of Total error/Support vectors (E/Sv) for the two prediction by model, ordering the models according the ratio value. d: Models arrayed by E/Sv ratio.

vectors used for the predictions (fig. 16b). The error/SV ratio (fig. 16c) may indicates what would be considered instinctively as an increase in structural complexity.

Discussion

The results show that there is a relationship between the error, the quantity of data used on a predicted geology and our perception of structural complexity. The models with folding have a higher E/Sv ratio than unfolded models. Similarly, faulted models exhibit greater E/Sv ratio than unfaulted models (except for the blue line fig. 16-1d). The impact on the prediction of the single long-dip-slip-fault in the base model is more significant than the short-dip-lip-multi-faulting, indicating the importance of fault displacement in the structural complexity estimated by this mean. This work shows the possibility to anticipate the structural complexity from partial information, being useful in cases as underground survey planning and overcoming structural uncertainty.

The above research received funding from the European Union's Seventh Framework Program under grant agreement 228559 (ProMine project).

Bibliography

P. Dromgoole and R. Speers (1997) Geoscore ; a method for quantifying uncertainty in field reserve estimates, Petroleum Geoscience. 3, 1–12.
S. Jolley, D. Barr, J. Walsh, et al. (2007) Structurally complex reservoirs : an introduction, Geological Society, London, Special Publications. 292, 1–24.
A. Smirnoff, E. Boisvert, and S.J. Paradis (2008) Support vector machine for 3D modelling from sparse geological information of various origins, Computers Geosciences. 34, 127–143.
K. Trubetskoy, Y.P. Galchenko, and G. Sabyanin (2012) Evaluation methodology for structural complexity of ore deposits as development targets, Journal of Mining Science. 48, 1006–1015.

A.3. Cu potentials in the Fore-Sudetic Monocline using 4D modeling data

Presented at: 33^{th} Gocad Meeting. September 2013. Nancy School of Geology. Vanodoeuvre-Les-Nancy.

Pablo Mejía-Herrera[1,2] & Jean-Jacques Royer[1,2]

1. Université de Lorraine, ENSG, 2 rue du doyen Marcel Roubault, TSA 70605, 54518 Vandoeuvre-lès-Nancy Cedex, France
2. Géoressources, UMR 7359, 5418 Vandoeuvre-lès-Nancy Cedex, France

abstract

This work explains a procedure to predict Cu potentials in the ore-Kupferschiefer using 4D modeling and logistic regression (LR) analysis. The predictor variables in the assessments are established from restored horizons that contain the ore-series. Applying flexural-slip to unfold/unfault the 3D model of the Fore-Sudetic Monocline (FSM), we obtained the dilatation parameter and the depth of the Zechstein base at restored times. We found that the positive dilatation outputs and the Zechstein base depth at Late Cretaceous time represent the main structural features related to the Cu mineralization. The positive dilatation outputs may reflect faulting and damaged areas in the rock mass, and hence, relating the fault-fracture systems that drove the fluid circulation from the basement and hosting the early mineralization stages. The Zechstein base depth at Late Cretaceous express the lithostatic pressure that control the hydraulic fracturing during the up-lifting at this time. In the Cu potential modeling, positive dilatation values and the depth of restored Zechstein correspond to predictor variables, and several Cu grades in binary code as targets. Then, we applied LR analysis, available in the free software ***R***, establishing the separating function between mineralized and and non-mineralized locations. The results show more accurate predictions for high Cu-grades when the positive dilatations are taken into account.

Introduction

The assessments in mineral exploration are based on relationships between a set of descriptive geological features with an expected mineral concentration [de Quadros et al., 2006]. In potential modeling, the analytical or empirical relationships between descriptive features and a mineral target express the possibility to predict a given mineral concentration in a location as function of descriptive features [Cheng, 2008]. Let evidences the set of observed features that are directly related to the mineralization process (e.g. the mineral alterations in rocks during an hydrothermal event, or the

sorting of heavy-minerals grains during a depositional state). And let geo-variables the set of features that control the system during the mineralization (e.g. pressure, temperature, pH, Eh, permeability, etc.), then in principle, it is possible to build a potential model for a given mineralization integrating evidences and geo-variables in terms of multivariate statistical analysis [Agterberg et al., 1993, Kerrich, 1993, de Araújo and Macedo, 2002]. However, during the structural evolution over the time the relationships between the evidences and geo-variables and the mineralized locations become unclear. In case of post-mineralization events, the most recent configuration obscures the precedents and the original relationships can be substantially modified. In a broad sense, the uncertainty of an assessment model is related to the structural evolution of the study area [Caumon, 2010]. One way to improve the assessment in structurally evolved terrains is restoring the starting conditions. Restoration provides partially the burial history of the rock units and the displacement field for the whole model, allowing an accurate estimation of geometry variations in the evolved terrains [Durand-Riard et al., 2011]. Eroded materials, moved blocks and volume variations can be conveniently handled during the restoration procedure. In the backward models, the relationships between the descriptive features and the mineralized locations may be easy identifiable and the uncertainty in the predictions are more constrained [Lewis and Couples, 1999]. The above approach was applied in the FSM (SW of Poland), and has given the improvement of potentials locations. That is an important step toward for predictive ore-Kupferschiefer potentials in central Europe.

Potential modeling in the FSM

Predictors and predictions

In potential modeling, the ultimate objective is to estimate the probability for a given location that a mineralization of a given type occurred [Schaeben, 2012]. It involves integration of information from diverse geoscience datasets including lithological, structural data, geochemical data, geophysical data and remote sensing data [Zuo and Carranza, 2011]. These geo-datasets express (explicitly or implicitly) the evidences and the geo-variables related to the mineralization process. The aim is to quantify indices of occurrence of mineral deposit by integrating multiple geo-datasets. Several methods have been used to accomplish this (e.g. weights of evidence-WofE [Bonham-Carter et al., 1989], fuzzy WofE [Cheng and Agterberg, 1999], LR analysis [Agterberg and Bonham-Carter, 1999], evidential belief functions [An et al., 1992], neural networks [Singer and Kouda, 1996], wildcat method [Carranza, 2010] and support vector machine-SVM [Zuo and Carranza, 2011]). However, whatever the method, the fundamental task to resolve is to assign the potential of a given location. The LR method (as others machine learning methods) is based in the construction of models that describe the system learning from the data. In this paper, mineralized and non-mineralized locations are defined from the Cu grades in the ore-series. Using different cut-off, and known potential locations, it is possible to evaluate the relevance of a predictor variable in the LR prediction model, and hence, inferring its importance during the mineralization process.

Role of fault-fractures in the ore-Kupferschiefer formation

As in several Cu ore-deposits, the role of fault-fracture systems during the mineralization is essential. In the ore-Kupferschiefer, the fault-fractures and the mineralization are linked in several aspects as : favoring the metal-bearing fluids [Muchez et al., 2005], controlling the replacement of Cu(Fe)-sulfides on former sulfides [Schmidt Mumm and Wolfgramm, 2004], allowing the interaction with the organic mater [Wagner et al., 2010], etc. Moreover, the fault-fractures systems have played a major role controlling the secondary permeability that drove the Cu-sulfides formation and the later Cu-enrichment in the FSM. Fault-fractures and permeability as factors controlling the mineralization process in the Fore-Sudetic area was appointed by Jowett [1986] in his convective flow model, and by

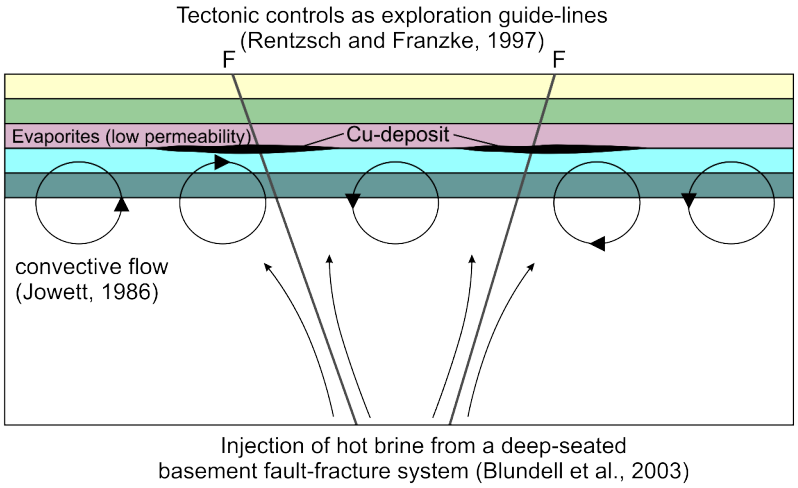

FIGURE 17 – Scheme integrating the concepts used in this work. Relation beetween fluid migration and circulation, fault-fracturing systems and tectonic exploration guide-lines on the ore-Kupferschiefer.

Blundell et al. [2003] explaining the injection of hot brine from a deep-seated basement. Rentzsch and Franzke [1997] show the presence of tectonic controls on the ore-Kupferschiefer in central Europe, suggesting the possibility to use these structural elements on the exploration of Cu-deposits at the Zechstein base in Germany. These concepts are resumed in the Figure 17.

Restoring outputs and fault-fracture systems in the Fore-Sudetic region

Following the above ideas, we consider that the structural features obtained during the restoring modeling can help in the understanding of the relationship between Cu distribution and the tectonic evolution in SW of Poland. In particular, positive dilation may reveal the most deformed locations in the mineralized layer, and therefore, the fault-fracture systems related to the presence and grades of Cu-sulfides (Figure 18). In case of several deformation events affecting the same location, the mineralization could be expressed by a major presence of Cu-sulfides or perhaps as Cu-enrichment by replacement on earlier Cu(Cu-Fe)-sulfides.

Geological aspects

Geologic settings

The Kupferschiefer is a black shale broadly spread in central Europe (from Ireland to Belarus) with very well known high Cu-grade locations in southwest Poland and central Germany [Oszczepalski and Speczik, 2011, Rentzsch and Franzke, 1997]. This layer was formed at the end of Permian times, overlaying volcanic and clastic terrestrial sequences (Rotliegendes and Wessliegendes) of Saxonian age [Karnkowski, 1999], and overlain by sediments product of the eustatic variations of the sea during the Guadalupian to Lopingian (Zechstein Formation) [Blundell et al., 2003]. The basement corresponds to a group of Early Permian sub-basins covering Paleozoic rocks affected by Caledonian and Variscan tectonism [Karnkowski, 1999]. The post-Permian sediments correspond to continental secessions and shallow marine sediments placed during the Triassic followed by a Jurassic succession of shallow marine sediments. Basin analysis shows subsidence rates in the Late Permian-Early Triassic superiors to 80 m/m.y. (Central Basin) [Karnkowski, 1999, Resak et al., 2008]. This rate decreased substantially in the Late Triassic through to the Jurassic [Karnkowski, 1999]. At the end of the Jurassic, the

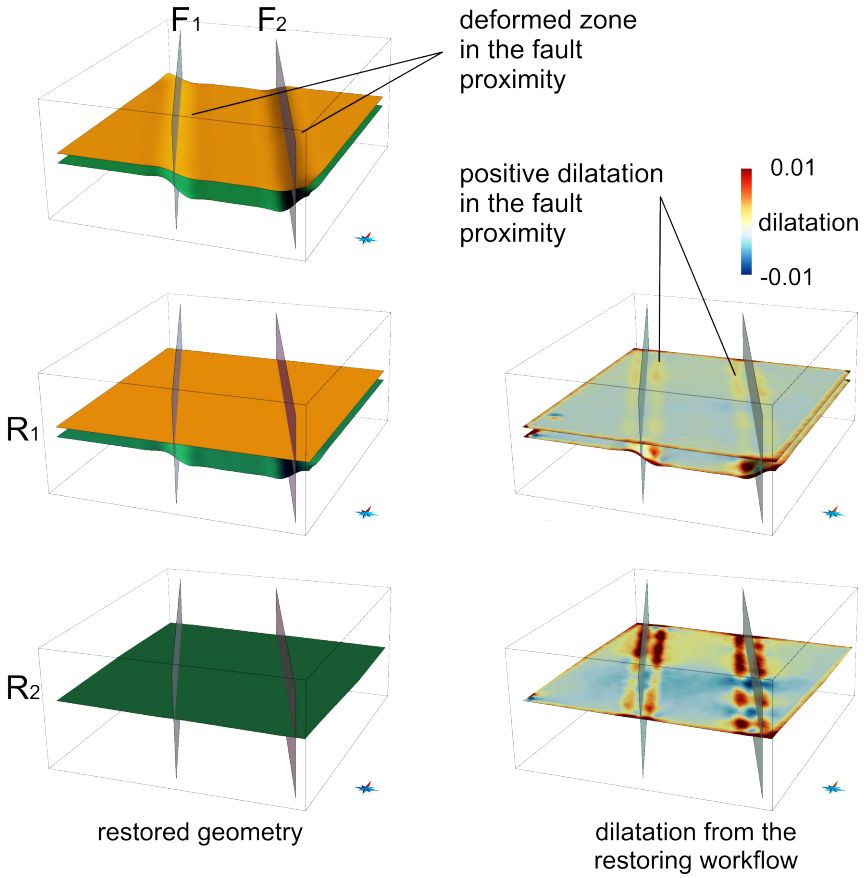

FIGURE 18 – Restoring workflow in a synthetic case. The *dilation values* highlight deformed areas in the proximity of the faults. The fault-fracture system, related to these deformed areas, would allow the fluid circulation, hosting Cu-sulfides and Cu-sulfides replacement in the ore-Kupferschiefer.

top Rotliegend surface in the Lower Silesian basin was deep up to 4 km [Blundell et al., 2003]. At the Jurassic-Cretaceous boundary, the Lower Silesian basin was inverted and uplifted, creating the Fore- Sudetic block, bounded by NW-SE trending faults extended from the basement to the post-Permian successions [Blundell et al., 2003]. During Late Cretaceous-Early Paleocene time the northern- Europe was affected by a tectonic inversion, probably linked to the Alpine orogeny. This event provoked the erosion of hundreds to thousands meters [Mazur et al., 2005, Scheck-Wenderoth and Lamarche, 2005, Resak et al., 2008, Narkiewicz et al., 2010]. In the Lubin region, the up-lift is estimated at more than 1.000 m [Stephenson et al., 2003], eroding the rocks from Triassic to Cretaceous. The pre-Cenozoic rocks were tilted 3° to 6° to the north east, probably during the Alpine orogeny. This post-Variscan cover of Permian-Mesozoic formations is subdivided into the Kimmerian stage (Permian, Triassic, Jurassic), Laramide stage (Cretaceous), and post-Laramide stage (Tertiary, Quaternary) [Oszczepalski, 1999].

Mineralization

Three main mineralized sulfide levels both as grains and veinlets can be identified within the shales : a lower dolomite level, an intermediate bituminous black shale level and an upper dolomite black shale level. The main minerals found in the polymetallic Kupferschiefer ore in Fore-Sudetic area are chalcocite, bornite, chalcopyrite, covellite, digenite, pyrite, galena, sphalerite, tennantite, native silver, stromeyerite, cobaltite and castaingite, with minor Cu, Ag, Fe, Ni, Co, Mo, Hg, Bi, Pt and Pd sulfides, arsenides, diarsenides, sulphosalts, thiosulphates, arsenates, and noble metals and alloys containing Au, Ag, Hg and Pb [Oszczepalski, 1999, Piestrzyński et al., 2002]. At least three stages are involved with the ore-Kupferschiefer formation [Vaughan et al., 1989, Speczik, 1995, Wagner et al., 2010]. These stages represent broadly the main post-Permian tectono-magmatic events in central Europe. The first mineralization stage would be associated with diagenesis process during a rifting occurred at Triassic and Early Jurassic [Ziegler, 1982]. A second stage related with the Late Jurassic extensional tectonic event that formed the nearby North German Basin, reactivating Variscan basement faults and extended them up through the overlying strata [Symons et al., 2011]. Finally, the tectonic inversion and uplifting occurred in northern Europe at the End Cretaceous-Early Paleocene, which has led to the erosion of several hundred meters of the Triassic to Cretaceous sedimentary formations [Resak et al., 2008]. This last erosion event allowed the increasing fluid/lithostatic pressure ratio, and then provoking the hydraulic fracturing required for the circulation of mineralizing fluids, the remobilization of elements and the replacement and enrichment of Cu-sulfides [Mejia and Royer, 2012].

3D modeling and restoration

Input modeling

To build the FSM 3D model, we used : (1) regional cartographic information [Pawlak et al., 2008, Dadlez et al., 2000] ; and (2) published interpreted underground information from geophysical and boreholes surveys [Krzywiec, 2006, Mazur et al., 2010]. We applied the SKUA 2011® Structure and Stratigraphy workflow (Figure 19).

Restoration

The restoration procedure consists on a series of discrete flattening surfaces deformed during the tectonic evolution. We chose the flexural slip method available in the KINE3D-2® module to obtain the recreated past geometry. The restored horizons correspond to chrono-stratigraphic makers

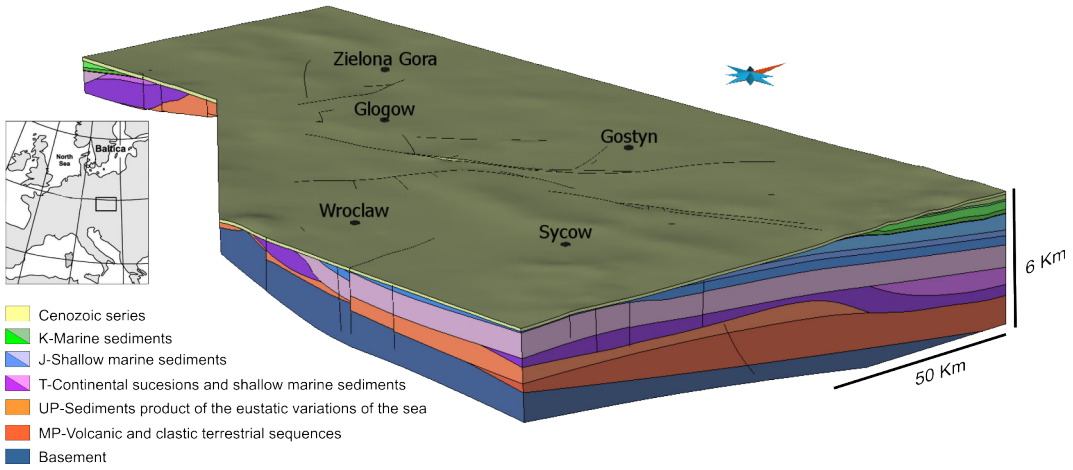

FIGURE 19 – Main sedimentary units in the FSM. The Kupferschiefer is located between the Upper Permian sediments and the Triassic successions.

Material	φ_0	dpf *10^{-4}
K	0.51	6.2
J	0.51	6.2
T	0.51	6.2
Zechstein	0.06	0.5
Rotliegend	0.51	6.2
Basement	≈0	≈0

a

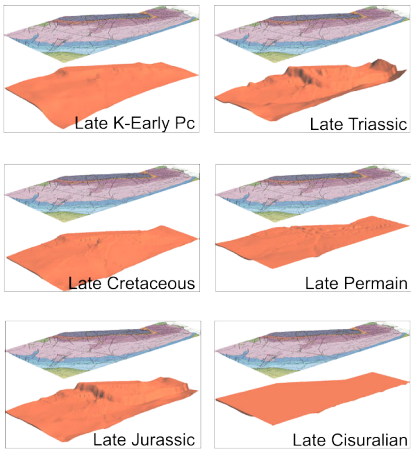

b

FIGURE 20 – (a) Decompaction parameters applied during restoration. (b) Rotliegend Formation in the FSM corresponding at restored times.

between the periods from the Upper Permian to present day. We coupled the decompaction effect during the sequential restoration using the parameters showed in Figure 20.

Cu assessment in the Fore-Sudetic region

LogCu distribution and predictors variables

We used the Cu values reported by Oszczepalski et al. [1997] in Lower Silesia to create a LogCu kriging interpolated distribution in the study area. We used also the Cu potential areas defined by Oszczepalski and Speczik [2011] for the region. In the statistical analysis between the LogCu and several structural parameters available in model (e.g. distance to faults, thickness of main sedimentary units, restored depths of the mineralized layer), the most high correlation coefficients correspond to the horizontal distance from the Fore-Sudetic Block (HFB) (0.430), and the depth of Zechstein base at late Cretaceous time (ZBK) (0.339). These two parameters are selected as continuous predictor variables in the LR analysis. We transformed the dilatation outputs on the Kupferschifer layer acquired from the multi-restoration process (Figure 21). For that, the extreme dilatation values were eliminated (they probably reflect erroneous zones in the initial geometry of surfaces), and then ne-

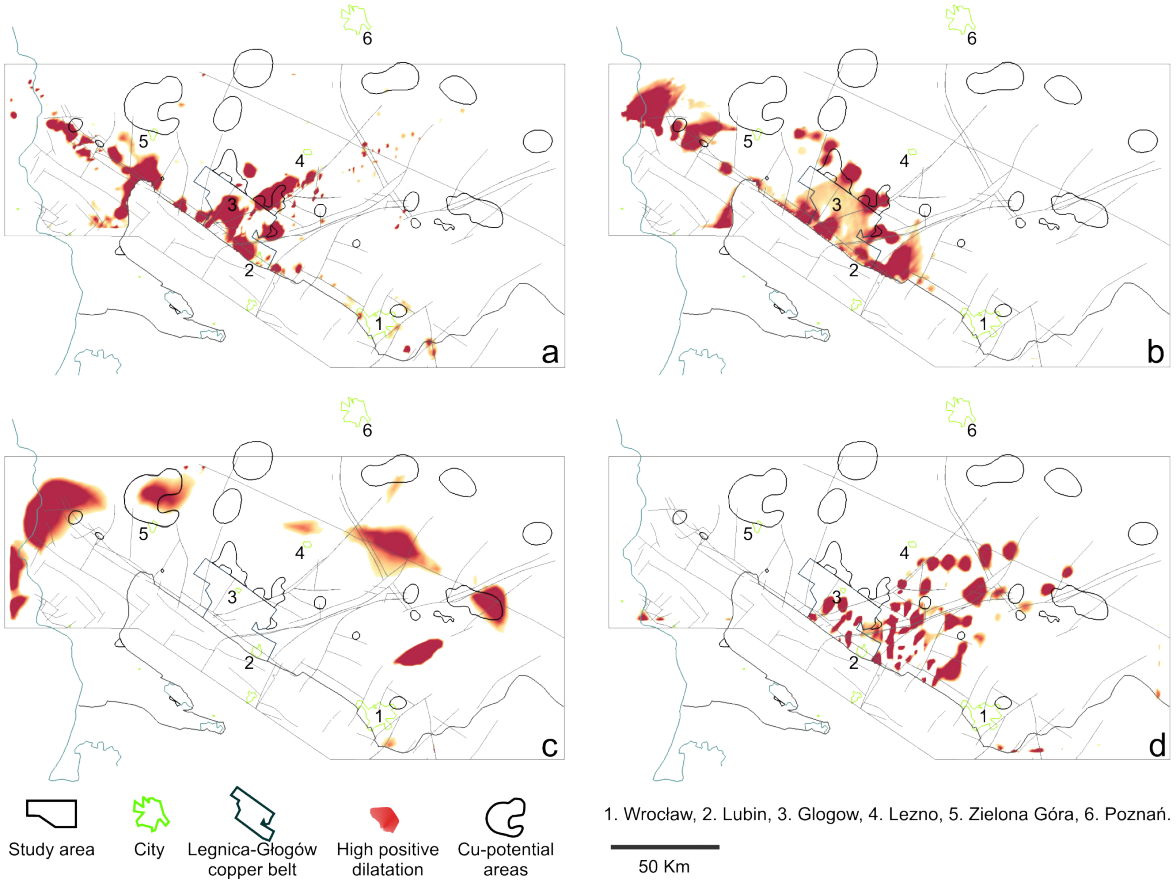

FIGURE 21 – High positive dilatation values achieved from the FSM restoring. (a) Top Rotliegend restoration, (b) Top Zechstein restoration, (c) Top Triassic series restoration, (d) Top Jurassic series restoration. Cu-potential areas from Oszczepalski and Speczik [2011].

gative and positive dilatation values are converted as binomial outputs (**0** and **1** respectively). The cumulative effect of the positive dilatation is calculated adding the terms of the binary dilatation, creating a categorical variable (PDC) of 5 elements. It means, that a location with positive dilatations in the all restoring process is labeled with **4** and, aversely, a location without dilatation in the all restoring process is labeled **0**. Finally, HFB, ZBK and PDC are used in LR analysis on $\boldsymbol{R}$ for the LogCu in binary code corresponding at 12.5, 25 and $50 Kg/m^2$ Cu-grades. Similarly, this procedure is applied for the Cu potentials areas defined by Oszczepalski and Speczik [2011] (Figure 22).

Positive dilatation on Cu potential assessments

In LR analysis the logistic function is described by a linear combination of the predictors variables (equation 5). In our case, the binomial outcomes for the LogCu grades are described by PDC (as categorical variables from 0 to 4), ZBK, HFB and the interaction term between the last two (ZBK*HFB) trying to yield the proper complete model [Schaeben, 2013].

$$\begin{gathered} log(Odds) = \beta_0 + \beta_l x_1 + \beta_2 x_2 + \beta_3 x_3 +, ..., +\beta_m x_m \\ x_{1m} = predictors \end{gathered} \tag{5}$$

The results show remarkable contrasts depending on the Cu-grades. For the $12.5 Kg/m^2$ cut-off, the relation between the Cu-potentials and the cumulative dilatation is negative. It means, that the probability of success to find a mineralized area decrease in the locations with PDC > 0. It could be

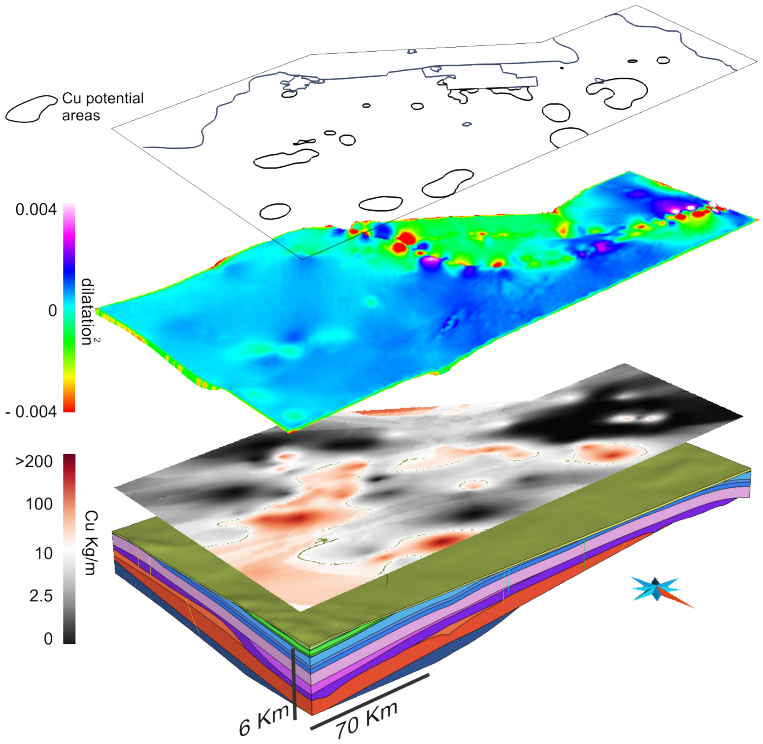

FIGURE 22 – Extracted layers from the 3D model of the FSM showing Cu distribution, Cu potentials and dilatation from 2D-restoration. With these parameters, plus HBF and ZBK, were created LR models to evaluated the influence of positive dilatation in the prediction of high Cu-grades locations.

interpreted as the Cu background in the FSM is related to non-deformed areas. However, increasing the cut-off to $25Kg/m^2$ the relation is inversed, and the probability of success improves in locations with PDC of 2 or 3. This last, could be interpreted as the expression of fault-fractures systems in the formation of medium Cu-grades deposits. For the high Cu-grades locations (cut-off $> 50Kg/m^2$), the influence of cumulative positive dilatation is more evident, increasing the probability of success almost twice on locations with PDC > 3 versus the locations with nil PDC. A similar tendency that the high Cu-grade case is obtained using the areas defined by Oszczepalski and Speczik [2011] including the LGCB mining district. These results are resumed in the Figure 23.

Discussion

The positive dilatation values obtained during the restoration show coincidences locally with well known mineralized zones. The most important corresponds to the present day exploitation area of Legnica-Glogów Copper Belt (LGCB). The PDCs also show high concentration values in the proximity of the Fore-Sudetic Block, with NW-SE sense, obeying the Odra Fault tendency. At the north of the Żary Pericline and in the proximity of Wrocław, the high PDC locations near to Cu potentials may follow this same fault system. Far of the Fore-Sudetic Block, medium to high PDC coincide with Cu potentials in the Zielona Góra depression and in the proximity of the Pogorzela elevation (Figure 24).

In relation with deformations stages and mineralization and Cu-enrichment times, the Odra Fault system may played a main role at Late Permian times in locations as the LGCB, to the north part of the Żary Pericline, and in the Wrocław proximity (Figure 21a, b). On the contrary, fault-fracture systems associated to the Pogorzela elevation, the Wolsztyn ridge and the Zielona Góra depression

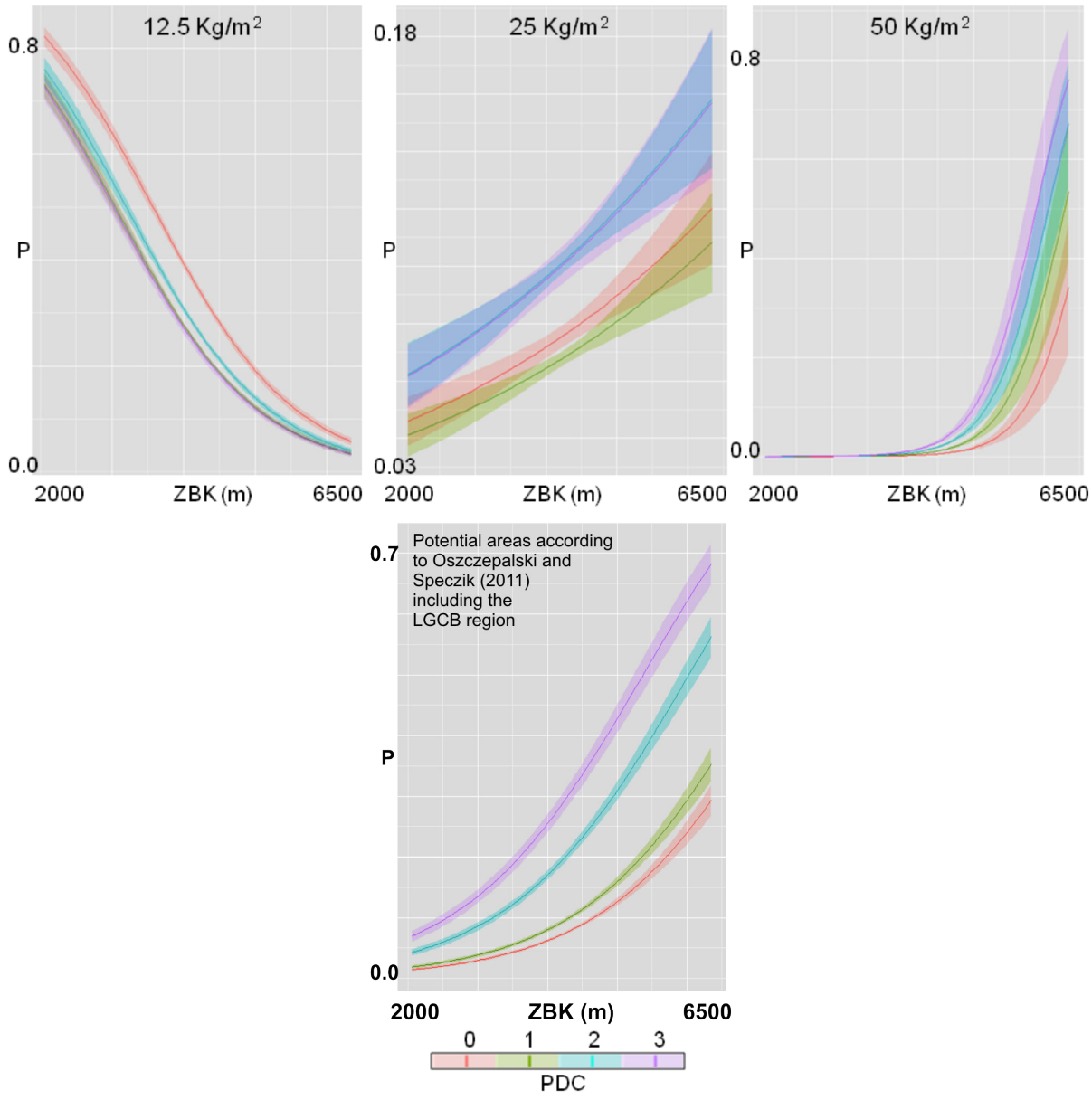

FIGURE 23 – Probabilities of Cu potentials from LR analysis applying different cut-off and mineralized zones in the predictive modeling. ZBK : depth of Zechstein base at Late Cretaceous. PDC : positive cumulative dilatation. The influence of positive dilatation predicting locations with high Cu-grades may show the activity of fault-fracture systems during mineralization stages.

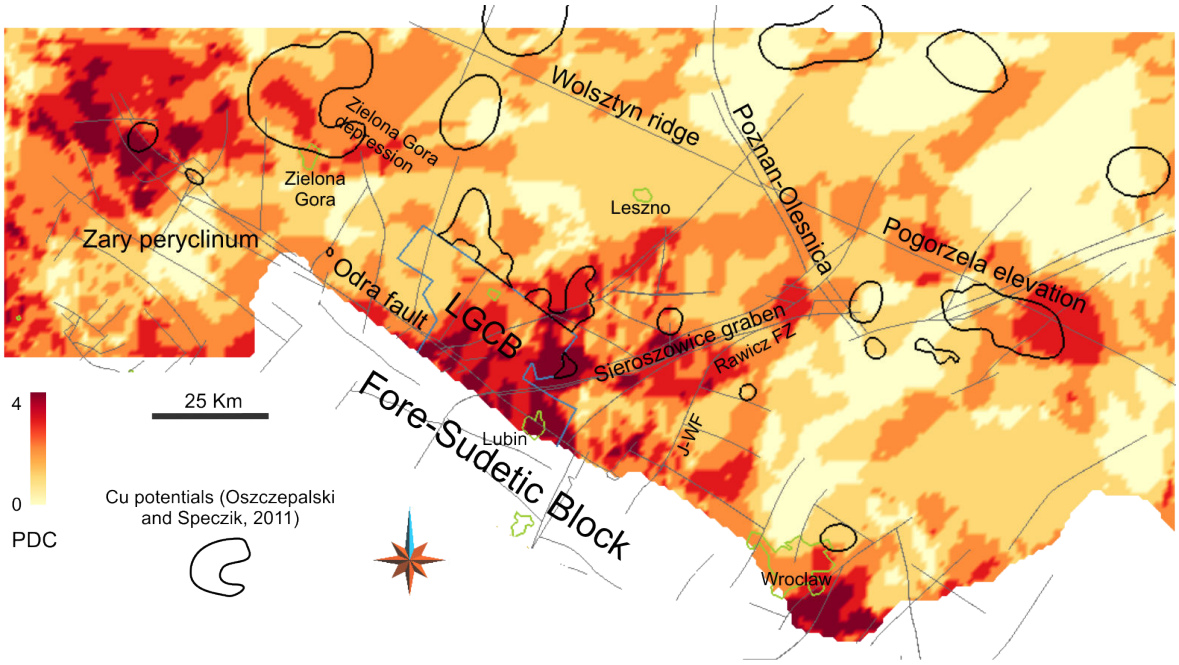

FIGURE 24 – Positive dilatations as categorical variable (PDC) in the FSM. Some main structures and Cu potentials locations are highlighted.

seems have controlled the Cu mineralization at Triassic times (Figure 21c). Finally, the Top Jurassic series restoration shows the deformation focused near to the Sieroszowice graben and in proximal fault systems. The deformation events occurred in the Jurassic probably drove also the Cu-sulfides replacement, and hence the Cu enrichment, on earlier sulfides of the LGCB (Figure 21d).

Conclusions

Dilation results obtained from the FSM restoring are related geographically to the Cu potential areas established in previous works. This relation perhaps express the impact of fault-fracture systems during the mineralization process. Upward migration of thermal fluids using deep faults and damaged areas in the rocks mass developing more high permeability allowing the effective fluid circulation, could be main factors influencing directly the Cu-sulfides formation. The Cu distribution patterns in the FSM were caused by the variation of the stress regime during the tectonic evolution from Late Permian to Late Cretaceous. The Odra fault system has controlled the mineralization at Late Permian times, but during the Triassic and Jurassic other fault-systems ruled the mineralization, in special the faults related to the Pogorzela elevation, the Sieroszowice graben and the Zielona Góra depression.

The utility of dilatation as predictor variable is evidenced from the LR analysis, completing the set of structural parameters also obtained from the restoration modeling. We believe that the above ideas and methods can be applied in similar cases where the fault-fracture system are sealed by an impermeable cap and the occurrence of hot brines expulsion events from the basement. × sectionAcknowledgements This work has been performed in the frame of the Gocad research project. We thank the industry and academic members of the Gocad Research Consortium [3] for supporting this research. We also thank Paradigm for the Gocad software and API. We appreciated the collaboration of Clementine Fourrier. We also thank Piotr Krzemiński for his comments and remarks

3. http ://www.gocad.org/w4/index.php/consortium/members

which helped improving this paper. Part of the above research received funding from the European Union's Seventh Framework Programme under grant agreement n°228559 (ProMine Project).

Bibliography

F. Agterberg and G. Bonham-Carter. Logistic regression and weights of evidence modeling in mineral exploration. In *Proceedings of the 28th International Symposium on Applications of Computer in the Mineral Industry (APCOM), Golden, Colorado*, pages 483–490, 1999.

F. Agterberg, G. Bonham-Carter, Q. Cheng, and D. Wright. Weights of evidence modeling and weighted logistic regression for mineral potential mapping. *Computers in geology*, 25 :13–32, 1993.

P. An, W. Moon, and G. Bonham-Carter. On knowledge-based approach of integrating remote sensing, geophysical and geological information. In *Geoscience and Remote Sensing Symposium, 1992. IGARSS'92. International*, pages 34–38, 1992.

D. J. Blundell, P. H. Karnkowski, D. H. M. Alderton, S. Oszczepalski, and H. Kucha. Copper mineralization of the Polish Kupferschiefer : a proposed basement fault-fracture system of fluid flow. *Economic Geology*, 98(7) :1487–1495, Nov. 2003.

G. Bonham-Carter, F. Agterberg, and D. Wright. Weights of evidence modeling : a new approach to mapping mineral potential. In *Statistical Applications in the Earth Sciences. Eds. F.P. Agterberg and G.F. Bonham-Carter*, number 9 in Paper 89, pages 171–183. Geological Survey of Canada, 1989.

E. J. M. Carranza. Improved wildcat modelling of mineral prospectivity. *Resource geology*, 60(2) : 129–149, 2010.

G. Caumon. Towards stochastic time-varying geological modeling. *Mathematical Geosciences*, 42 (5) :555–569, 2010.

Q. Cheng. Non-linear theory and power-law models for information integration and mineral resources quantitative assessments. In *Progress in Geomathematics*, pages 195–225. Springer, 2008.

Q. Cheng and F. Agterberg. Fuzzy weights of evidence method and its application in mineral potential mapping. *Natural Resources Research*, 8(1) :27–35, 1999.

R. Dadlez, S. Marek, and J. Pokorski. Geological map of Poland without Cainozoic deposits. *PIG, Warszawa*, 2000.

C. C. de Araújo and A. B. Macedo. Multicriteria geologic data analysis for mineral favorability mapping : application to a metal sulphide mineralized area, Ribeira Valley Metallogenic Province, Brazil. *Natural Resources Research*, 11(1) :29–43, 2002.

T. de Quadros, J. Koppe, A. Strieder, and J. Costa. Mineral-potential mapping : A comparison of weights-of-evidence and fuzzy methods. *Natural Resources Research*, 15(1) :49–65, 2006.

P. Durand-Riard, L. Salles, M. Ford, G. Caumon, and J. Pellerin. Understanding the evolution of synsedimentary faults : coupling decompaction and 3D sequential restoration. *Marine and Petroleum Geology*, 28(8) :1530–1539, 2011.

E. C. Jowett. Genesis of Kupferschiefer Cu-Ag deposits by convective flow of Rotliegendes brines during Triassic rifting. *Economic Geology*, 81(8) :1823–1837, 1986.

P. H. Karnkowski. Origin and evolution of the Polish Rotliegend Basin. *Polish Geological Institute Special Papers*, 3 :1–93, 1999.

R. Kerrich. Perspectives on genetic models for lode gold deposits. *Mineralium Deposita*, 28(6) : 362–365, 1993.

P. Krzywiec. Triassic−Jurassic evolution of the Pomeranian segment of the Mid-Polish Trough : Basement tectonics and subsidence patterns. *Geological Quarterly*, 50(1) :139–150, 2006.

H. Lewis and G. D. Couples. Carboniferous basin evolution of Central Ireland-simulation of structural controls on mineralization. *Geological Society, London, Special Publications*, 155(1) :277–302, 1999.

S. Mazur, M. Scheck-Wenderoth, and P. Krzywiec. Different modes of the Late Cretaceous−Early Tertiary inversion in the North German and Polish basins. *International Journal of Earth Sciences*, 94(5) :782–798, 2005.

S. Mazur, P. Aleksandrowski, K. Turniak, L. Krzemiński, K. Mastalerz, A. Górecka-Nowak, L. Kurowski, P. Krzywiec, A. Żelaźniewicz, and M. Fanning. Uplift and late orogenic deformation of the Central European Variscan belt as revealed by sediment provenance and structural record in the Carboniferous foreland basin of western Poland. *International Journal of Earth Sciences*, 99(1) : 47–64, 2010.

P. Mejia and J.-J. Royer. Explicit surface restoring-decompacting procedure to estimate the hydraulic fracturing : Case of the Kupferschiefer in the Lubin region, Poland. In *Proceedings of the 32nd gOcad Meeting*, Nancy, France, Sept. 2012. ASGA.

P. Muchez, W. Heijlen, D. Banks, D. Blundell, M. Boni, and F. Grandia. 7 : Extensional tectonics and the timing and formation of basin-hosted deposits in Europe. *Ore Geology Reviews*, 27(1) : 241–267, 2005.

M. Narkiewicz, M. Resak, R. Littke, and L. Marynowski. New constraints on the Middle Palaeozoic to Cenozoic burial and thermal history of the Holy Cross mts. Central Poland : results from numerical modelling. *Geologica Acta*, 8(2) :189–205, 2010.

S. Oszczepalski. Origin of the Kupferschiefer polymetallic mineralization in Poland. *Mineralium Deposita*, 34(5) :599–613, 1999.

S. Oszczepalski and S. Speczik. Prospectivity analysis of the polish Kupferschiefer - new insight. In *Proceedings of the 11th SGA Biennial Meeting*, Antofagasta, Chile, Sept. 2011. SGA.

S. Oszczepalski, A. Rydzewski, and I. Geologiczny. *Metallogenic atlas of Zechstein copper-bearing series in Poland*. Wydawnictwo Kartograficzne Polskiej Agencji Ekologicznej, 1997.

W. Pawlak, J. Aniol-Kwiatkowska, J. Pawlak, E. Nowak-Ferdhus, P. Migoń, A. Malicka, A. Marciniak, W. Żak, U. Wrocławski, and P. A. Nauk. *Atlas Śląska dolnego i opolskiego*. Uniwersytet Wrocławski. Pracownia Atlasu Dolnego Śląska, 2008.

A. Piestrzyński, J. Pieczonka, and A. Głuszek. Redbed-type gold mineralisation, Kupferschiefer, south-west Poland. *Mineralium Deposita*, 37(5) :512–528, June 2002.

J. Rentzsch and H. Franzke. Regional tectonic control of the Kupferschiefer mineralization in Central Europe. *Zeitschrift für Geologische Wissenschaften*, 25 :141–150, 1997.

M. Resak, M. Narkiewicz, and R. Littke. New basin modelling results from the Polish part of the Central European Basin system : implications for the late Cretaceous−Early Paleogene structural inversion. *International Journal of Earth Sciences*, 97(5) :955–972, 2008.

H. Schaeben. Comparison of mathematical methods of potential modeling. *Mathematical Geosciences*, 44(1) :101–129, 2012.

H. Schaeben. Bits of mathematics of potential modelling. In *Proceedings of the 12th Biennial SGA Meeting*, volume 2, pages 489–491, Uppsala, Aug. 2013. SGA.

M. Scheck-Wenderoth and J. Lamarche. Crustal memory and basin evolution in the Central European Basin system : new insights from a 3D structural model. *Tectonophysics*, 397(1-2) :143–165, Mar. 2005.

A. Schmidt Mumm and M. Wolfgramm. Fluid systems and mineralization in the north German and Polish basin. *Geofluids*, 4(4) :315–328, 2004.

D. A. Singer and R. Kouda. Application of a feedforward neural network in the search for Kuroko deposits in the Hokuroku district, Japan. *Mathematical Geology*, 28(8) :1017–1023, 1996.

S. Speczik. The Kupferschiefer mineralization of central europe : New aspects and major areas of future research. *Ore Geology Reviews*, 9(5) :411 – 426, 1995.

R. A. Stephenson, M. Narkiewicz, R. Dadlez, J.-D. van Wees, and P. Andriessen. Tectonic subsidence modelling of the Polish basin in the light of new data on crustal structure and magnitude of inversion. *Sedimentary Geology*, 156(1-4) :59–70, 2003.

D. Symons, K. Kawasaki, S. Walther, and G. Borg. Paleomagnetism of the Cu−Zn−Pb−bearing Kupferschiefer black shale (Upper Permian) at Sangerhausen, Germany. *Mineralium Deposita*, 46 (2) :137–152, 2011.

D. J. Vaughan, M. A. Sweeney, G. Friedrich, R. Diedel, and C. Haranczyk. The Kupferschiefer ; an overview with an appraisal of the different types of mineralization. *Economic Geology*, 84(5) :1003 –1027, 1989.

T. Wagner, M. Okrusch, S. Weyer, J. Lorenz, Y. Lahaye, H. Taubald, and R. Schmitt. The role of the Kupferschiefer in the formation of hydrothermal base metal mineralization in the Spessart ore district, Germany : insight from detailed sulfur isotope studies. *Mineralium Deposita*, 45(3) : 217–239, Mar. 2010.

P. Ziegler. *Geological atlas of Western and Central Europe*. Number vol. 1 in Geological Atlas of Western and Central Europe. Shell Internationale Petroleum Maatschappij B.V., 1982.

R. Zuo and E. J. M. Carranza. Support vector machine : A tool for mapping mineral prospectivity. *Geocomputation of Mineral Exploration Targets*, 37(12) :1967–1975, 2011.

A.4. Improving Ore Kupferschiefer Assessments with Support Vector Machine

Pablo Mejía-Herrera, Jean-Jacques Royer (Université de Lorraine, GeoRessources-UMR 7359) & Jürgen Hartsch (G.E.O.S. Ingenieurgesellschaft mbH, Freiberg)

Presented at: École Thématique CNRS : ressources minérales : défis scientifiques et sociétaux. Poster session, Février de 2013. Université de Genève. Geneva.

Introduction

The assessments in mineral exploration are based on models supported by descriptive and/or metallogenetic evidences and geo-variables. The potential maps to find an ore-deposit are expressed as a function of the posterior probabilities when the evidences are present or not (1). In other situations, the potential is the result of a linear combination of evidences and geo-variables related to the mineralization (2). However, no matter what method, the most of problems is due to small and sparse data.

With a different approach, Support Vector Machine (SVM) are supervised learning algorithms, developed on the statistical learning theory, for supervised classification. The SVM protocol search for the optimal separating hyper-plane between two classes (deposit and not-deposit) by maximizing the margin between the classes closest points (3) (fig. 25).

From published information, we defined the mineralized locations (Cu > 10-40 Kg/m) at the base of Zechstein in the Central Europe (4). The Zechstein and Rotliegendes thickness (5), pre-Cenozoic faults (6), the Rote Fäule and high Pb and Zn concentrations (4, 7)are used as evidences and geo-variables related to the Cu concentrations (fig. 26).

Methodology

We applied the free *R* package *e1071* searching the optimal SVM-separating hyperplane between deposit and not-deposit. For the training dataset we used the database in known deposit locations and then generating the potential map in the Central Europe as the response of the classification process.

To test the SVM performance, we compared the results between the SVM and logistic predictions, reducing the randomized samples (100%, 10%, 1.0% and 0.5%) in the training dataset (fig. 27). A linear kernel was applied for the SVM model. Only the predictions with odds > 9/1 are considered as potential locations for the deposits.

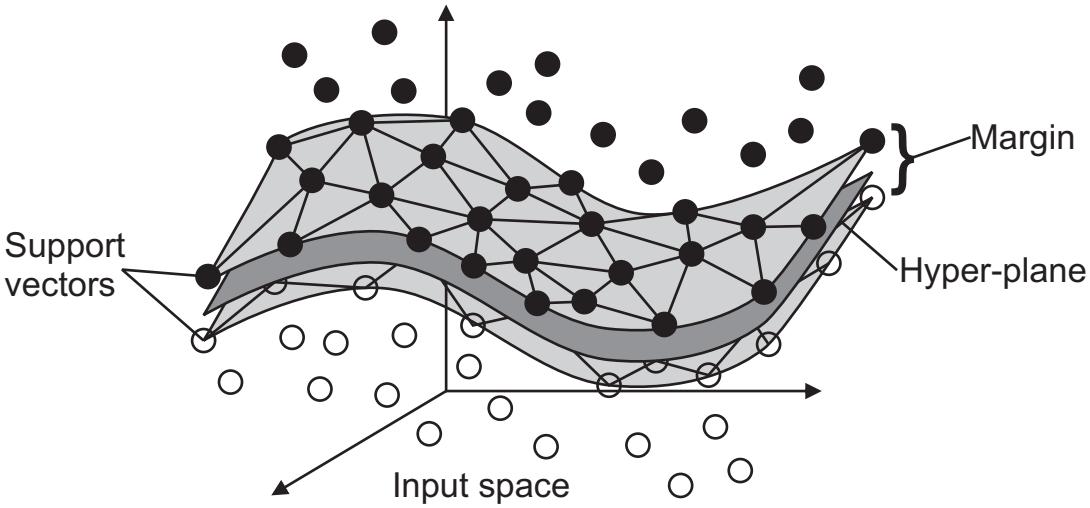

FIGURE 25 – Schematic image representing the the SVM function.

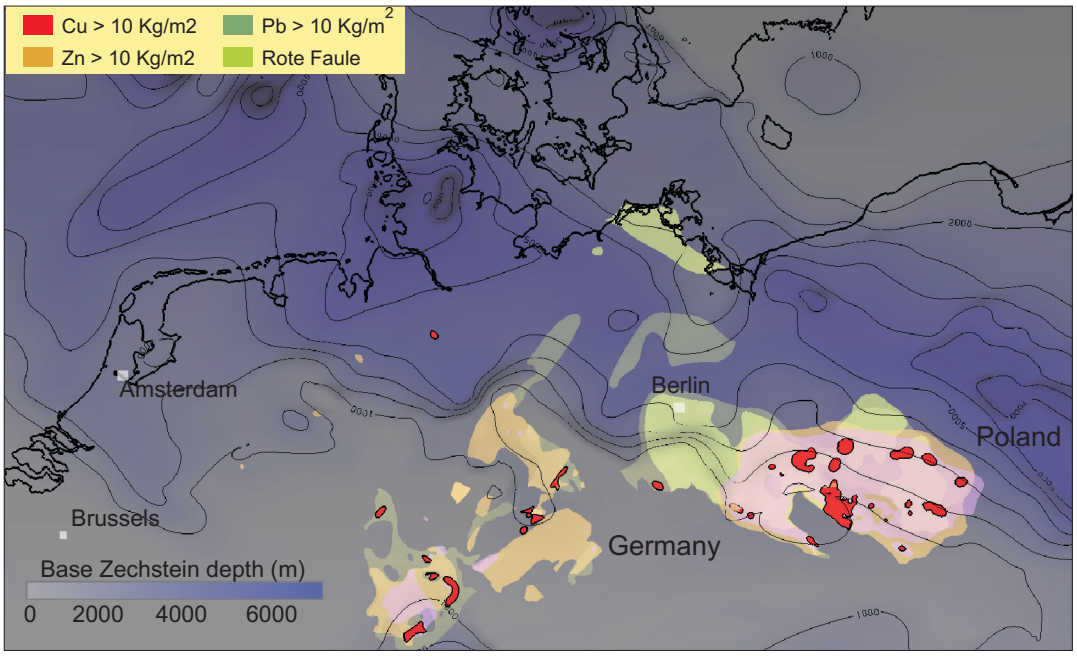

FIGURE 26 – Main *Cu Zn, Pb* occurrences in Central Europe.

Discussion

The results show that the overall performance of SVM is better than that of Logistic regression. Also the predictions rates and good generalization performance for small sample and sparse data. However, it should be pointed out that SVM has the difficult to explain the results due to nonlinearity of the method, unlike the Logistic regression where the predictions can be explained as function of the variation in the geologic data. Another disadvantage

The above research received funding from the European Union's Seventh Framework Program under grant agreement 228559 (ProMine project).

Bibliography

1. Bonham-Carter, G.F., Agterberg, F.P., Wright, D.F., 1989. Weights of evidence modelling : a new approach to mapping mineral potential. In : Agterberg, F.P., Bonham-Carter, G.F. (Eds.), Statistical Applications in the Earth Sciences.
2. Shields, D. and Todd, S. Using logistic regression to merge mineral resource databases. Nonrenewable Resources (March 1998), 7(1) :53-61.
3. Meyer D, Leisch F, Hornik K. 2003. The support vector machine under test. Neurocomputing 55 :59–71.
4. Rentzsch, J., and Franzke, H. (1997). Regional tectonic control of the Kupferschiefer mineralization in central Europe. Zeitschrift fur Geologische Wissenschaften 25, 141–150.
5. Scheck-Wenderoth, M., and Lamarche, J. (2005). Crustal memory and basin evolution in the Central European Basin System—new insights from a 3D structural model. Tectonophysics 397, 143–165.
6. Kley, J., Voigt, T., and Jaehne, F. (2008). A case of Distributed Continental Collision : Late Cretaceous Intraplate Shortening from Central Europe to North Africa. AGU Fall Meeting Abstracts C1897.
7. Oszczepalski, S., Speczik, S. 2011. Prospectivity analysis of the Polish Kupferschiefer - new insight. In Proceedings : 11th Biennial SGA Meeting. Antofagasta, Chile.

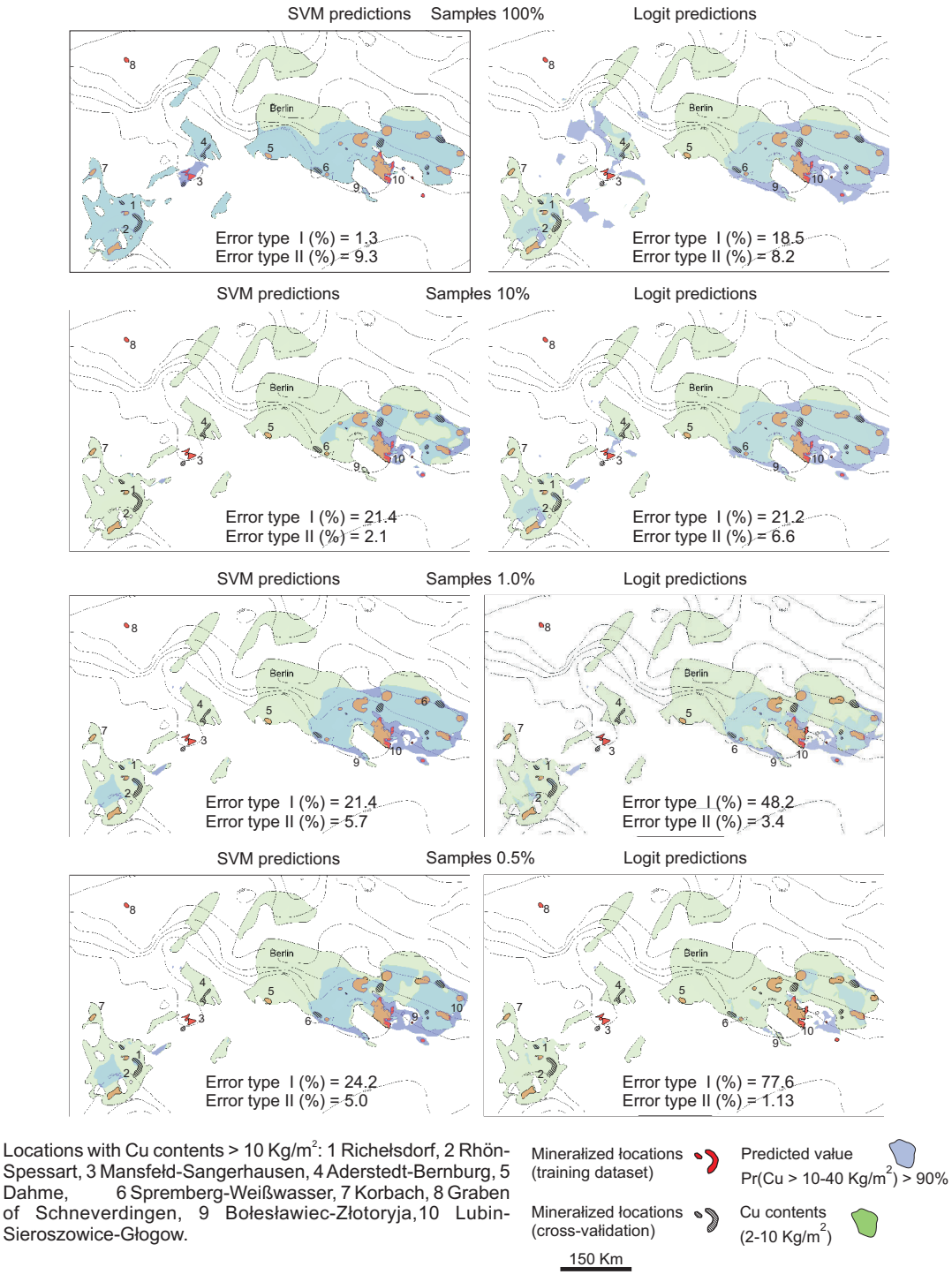

FIGURE 27 – Comparing results using SVM and LR for Cu-potentials.

A.5. Conference papers presented at: 12^{th} SGA Biennial Meeting, August 2013. Uppsala

Enhancing Copper Predictions at the Base of Zechstein with 4D Modelling

Pablo Mejía-Herrera, Jean-Jacques Royer (Université de Lorraine, GeoRessources-UMR 7359, Vandoeuvre-Lès-Nancy),
Jürgen Hartsch (G.E.O.S. Ingenieurgesellschaft mbH, Freiberg) &
Peggy Hielscher (Institut für Geophysik und Geoinformatik—TU Bergakademie, Freiberg)

Presented at: 12^{th} SGA Biennial Meeting, 2013., August 2013. Uppsala.

Abstract

3D restoration can help to better understand the history of geological formations, to identify fossil mineralizing fluid pathways, to establish the physical and chemical processes involved in ore formations and to predict the locations of potential economic mineral resources. In the case of sediment-hosted ore deposits, the unfolding and unfaulting techniques allow to visualize the impact of tectonic events during the mineralization stages and their role in the final ore-distribution. We applied a 3D restoration procedure on the German and Polish Kupferschiefer, pointing out the role played by the Late Cretaceous—Early Paleocene uplifting which affected Central Europe. On both sides of the Fore-Sudetic block, the fluids trapped beneath the Zechstein formations reached over-pressurized conditions due to the inverse up-lift phase, provoking the hydro- fracturing and the re-opening of previous discontinuities. This set of hydro-fractures was necessary in the Cu re-mobilization and later during its precipitation as enriched Cu (Cu-Fe) sulfides. A hydro-fracturing index accounting for the stress and the geomechanical constraints in the ore-series was estimated and seems to correlate with the presence of Cu-sulfides within the Kupferschiefer.

3&4D Geomodeling Applied to Mineral Exploration

Jean-Jacques Royer, Pablo Mejía-Herrera, Guillaume Caumon & Pauline Collon-Drouaillet (Université de Lorraine, GeoRessources-UMR 7359, Vandoeuvre-Lès-Nancy),

Abstract

3 & 4D geomodeling is a computer method allowing reconstitution of the deformation history of geological formations. It is common used since more than a decade as an exploration tool in oil and gas. It begins to be applied nowadays in mineral exploration. After summarizing the basic notions, concepts, and methodology of 34D geomodeling, we describe its application to mineral resources assessment and to the modeling of ore deposits comparing on limitations and recommendations. A 3&4D GeoModels cases studies of Kupferschiefers, Foresuedic Belt (Poland, Germany)., achieved during the EU FP7 ProMine research project illustrate the methodology. Perspectives and recommend-dations on applying 34 geomodeling in mineral resources appraisal are given in conclusion.

A.6. PROMINE–Nano-particle products from new mineral resources in Europe. Contributions to the WP1 & WP2

These contributions will be published as a ProMine's results book, edited by Springer.

34D Geomodeling Applied to Mineral Resources Exploration – An Introduction

J.J. Royer, P. Mejía-Herrera, G. Caumon, and P. Collon-Drouaillet

Université de Lorraine, CNRS-ENSG, Vandoeuvre-Lès-Nancy, France

Abstract

3D geomodeling, a computer method for modeling and visualizing geological structures in three spatial dimensions, is a common exploration tool used in oil and gas since more than several decades. When adding time, 4D modeling allows reproducing the dynamic evolution of geological structures, and reconstituting the past deformation history of geological formations. 3D geomodeling has been applied to mineral exploration with some successes since more than 15 years but can be considered still challenging for modeling hard rock settings. If very few 4D modeling cases studies have been investigated in mineral exploration, it begins nowadays to be applied in structural geology and mineral resources exploration. This paper describes the 3&4D geomodeling basic notions, concepts, and methodology when applied to mineral resources assessment and to modeling ore deposits. It draws the state of the art of 34D-modeling, describing advanced techniques, limitations and recommendations. The text is illustrated by several 3D GeoModels of mining explorations selected across Europe, including the Fennoscandian (Finland, Sweden), Hellenic (Greece), Iberic (Spain, Portugal) and Foresuedic (Poland, Germany), all of those case-studies have been achieved during the EU FP7 ProMine research project and recommendations on applying 3&4 geomodeling in mineral resources appraisal are given in the conclusions.

Pan-European Potential Map of Reserves associated to Kupferschiefer in Central Europe – Estimation of Copper and Base Metals Ore Resources

J.J. Royer[1], P. Mejía-Herrera[1] A. Zielińska21 & J. Hartsch[3]

1. Université de Lorraine, CNRS-ENSG, Vandoeuvre-Lès-Nancy, France
2. KGHM, Cuprum Research Development Centre, Wroclaw, Poland
3. G.E.O.S. Ingenieurgesellschaft mbH, Freiberg, Germany

Abstract

The Kupferschiefer, a thin bed of marine bituminous marl of Upper Permian (Zechstein) age, extends across north-central Europe from North Sea to Belorussia. It hosts strata-bound poly-metallic (Cu, Ag, Au, REE and PGE) sulphide deposits, which are one of the most important sources for copper and silver in the World. A pan-European potential assessment map of the Kupferschiefer formations was carried out within the framework of the ProMine European project, the final goal being to identify potential resources in copper, base metals, precious elements, PGE, REE and critical commodities. Three methods were investigated : (i) a tonnage-grade model was calibrated on the well known mining district of the Fore-Sudetic region for estimating the cumulative distributions of tonnage, size, and average copper grade of Kupferschiefer deposits. This model was further used to estimate potential resources in Central Europe in similar under-explored areas ; (ii) a prognostic model based on known deposits and geological indicators thought to be associated to their mineralization, was built for identifying possible correlations between indicators and mineralized areas. After the selection of the most pertinent indicators using weight of evidences, several predictive methods were compared including the Support Vector Machine (SVM) and the Logistic Regression Method (LRM) for estimating the probability of ore deposit occurrences. A potential resource map was then derived on the whole study areas.

4D Geomodeling: a Tool for Exploration – Case of the Kupferschiefer in the Lubin Region, Poland

P. Mejía-Herrera[1], J.J. Royer[1], J.G. Fraboulet[1] & A. Zielińska A. Zielińska[2]

1. Université de Lorraine, CNRS-ENSG, Vandoeuvre-Lès-Nancy, France
2. KGHM, Cuprum Research Development Centre, Wroclaw, Poland

Abstract

The Polish Kupferschiefer, a sediment-hosted polymetallic (Cu, Ag, Au, PGE) deposit, is one of the most important sources for copper and silver in the world. Within the framework of the ProMine European project, the Lubin region (south west of Poland), was selected for modelling in 34D the geological formations in order to better understand the distribution of the Cu-Ag mineralization, and possibly to define new potentials. The restoration – decompaction methodology available in gOcad, coupled to PetroMod 1D, were used to reconstitute the temperatures, pressures, hydraulic fracturing favourable conditions, and oil and gas maturation during the burying history of the Lubin Kupferschiefer, Southern- Western Poland basin. Conditions for hydraulic fracturing were identified within the base of the Zechstein shales, during an inversion phase at the Late Cretaceous-Early Palaeocene time. This Late Cretaceous up lifting yields the conditions for hydrothermal recirculation

of mineralizing brines explaining the location of Cu (Cu- Fe) sulphides ores in the area. The Zechstein evaporite series had played a role of impermeable cover confining the hydrothermal fluids in the lower Zechstein series. The 4D restoration-decompaction modeling allows reconstituting the burial, deformation and natural hydro- fracturing history of intra-basin sediment-hosted ore deposits. In the Lubin region, the obtained results show a good agreement between the spatial hydro-fracturing index and the emplacement of the Cu (Cu-Fe) sulphides exploited today.

Modélisation 3D et apport de la restauration structurale dans la compréhension des gisements de matières premières

Résumé : L'objectif de cette thèse est d'expliquer les avantages qu'offrent la reconstruction de l'architecture des unités géologiques, leurs déformations ainsi que leurs variations au cours du temps à l'exploration de ressources minérales, tout en appliquant des méthodes et outils de modélisation 3D et 4D. La modélisation et la restauration structurale sont utilisées ici pour estimer des attributs géologiques qui peuvent aider à la compréhension de la formation des gisements, et à l'identification des zones favorables aux minéralisations. Cette thèse est axée sur l'application de la modélisation 3D et 4D à des cas réels pour trouver le lien entre une minéralisation et des processus géologiques tel que l'exhumation des terrains, l'activité des failles et la fracturation résultant d'un évènement de déformation. Ce mémoire est organisé en trois parties : (*i*) la modélisation structurale ainsi que la restauration surfacique ont été appliquées au district minier de la Ceinture de Cuivre de Legnica-Głogów (sud-ouest de la Pologne), pour estimer les conditions favorables à la fracturation hydraulique. Cette fracturation est intervenue dans le nord de l'Europe lors d'une phase d'inversion à la fin du Crétacé et au début du Paléocène. Dans notre hypothèse de départ, la fracturation hydraulique développée au cours de cette période a joué un rôle important dans la distribution en cuivre observée aujourd'hui dans le district minier ; (*ii*) la courbure des surfaces triangulées, représentant les horizons stratigraphiques qui se trouvent dans la région des Sudètes polonaises, permet de mettre en évidence les systèmes de failles dans le socle. En particulier, des méthodes de restauration surfaciques ont été utilisées pour évaluer l'activité de des failles au cours du temps, en se basant sur la courbure des surfaces obtenues à chaque étape de la restauration. Les zones de fortes activités sont ici associées aux processus de minéralisation cuprifère de la région ; (*iii*) la restauration mécanique de la région de Mount Pleasant (Australie occidentale), a permis de simuler un évènement de raccourcissement apparu dans l'Archéen et qui est lié à un processus de minéralisation aurifère. La restauration mécanique est appliquée pour estimer le champ des déformations de la région au moment du raccourcissement. Avec ce champ de déformation, il est possible de calculer les paramètres d'endommagement de la masse rocheuse qui semblent liés aux zones aurifères situées hors des systèmes principaux de failles. Cette thèse a ainsi permis de mettre en évidence l'aspect prometteur de la modélisation et de la restauration structurale pour identifier des zones potentiellement minéralisées, mettant en valeur leur utilisation pour l'exploration des gisements et des ressources minérales.

Mots-clés : Modélisation 3D, modélisation 4D, restauration structurale, gisements, prospection, modèles prédictifs

---

Ore-deposits modeling and improving their understanding with structural restoration

Summary : The objective of this Ph.D. thesis is to apply 3D and 4D modeling methods to reconstruct the architecture and deformations over time of geological entities in a defined region. Structural restoration modeling is used here to estimate geological, physical and structural attributes for understanding the origin of ore-deposits, and for identifying potential mineralized areas. We focused this thesis on 3D and 4D modeling on real case studies with different geological contexts (e.g. uplifting, fault activity and shortening), demonstrating the advantages and drawbacks on their use for similar situations. This thesis is organized into three parts: (*i*) The application of structural modeling in the mining district of the Copper Belt of Legnica-Głogów (south-west Poland) . A surface-restoration approach was applied to estimate favorable conditions for hydraulic fracturing during an inversion, occurred in the northern part of Europe at Late Cretaceous–Early Paleocene. In our hypothesis, hydraulic fracturing developed at that time played an important role in the distribution of copper content observed in present days in the mining district. (*ii*) The curvature calculated on triangulated surfaces that represent the stratigraphic horizons in the Fore-Sudetic region (Poland), are used to highlight the fault systems in the basement as well as their activity. High curvature values reveal the fault activity which is associated with the copper mineralization process in the region. (*iii*) Mechanical restoration of the Mount Pleasant, Western Australia, simulates an Archean shortening event which occurred in the area linked to the gold mineralization process. The mechanical restoration was used to estimate the strain field in the region at the time of shortening. This deformation field was used to estimate the damage parameters of the rock mass. They show new potential gold areas located in off-fault gold systems. In conclusion, it is shown that 3D modeling and structural restoration could be used to identify potential favorable zones for the presence of mineralization, and seem promising as a tool for the exploration of ore-deposits and mineral resources.

Keywords : 3D modeling, 4D modeling, structural restoration, ore-deposits, prospectivity, predictive modeling